THE VISUALISATION OF POLARIMETRIC RADAR DATA

Dean Turner MA MSc

PhD Thesis
The University of Edinburgh
2005

Acknowledgements:

This thesis has been composed by the author named on the preceding page. The work contained herein forms part of a larger project, which examines the application of scientific visualisation to the analysis of large, multivariate datasets, which is being carried out in the computing sciences department of Brown University (Rhode Island), and is supported by the National Science Fund (Grant no. CCR0086065).

This work has not been submitted for any other degree or professional specification except as specified

Dean Turner

The author would like to thank Iain Woodhouse, whose continual support, enthusiasm and patience has been indispensable over the past four years. I would also like to thank William Mackaness for his timely and valuable insights, and John Ramage for helping in the development of the user survey. Finally, I would like to extend my gratitude to the researchers at Brown University for providing countless sources of inspiration during my visit to Rhode Island.

Abstract:
This thesis examines the application of scientific visualisation to the analysis of polarimetric radar data sets. The research contained herein forms part of a larger body of work that studies the application of scientific visualisation to the analysis of large multi-valued datasets.

Visualisation techniques have historically assumed a fundamental role in the analysis of patterns in geographic datasets. This is particularly apparent in the analysis of remotely sensed data, which, since the advent of aerial photography, has utilised the intensity of visible (and invisible) electromagnetic energy as a means of producing synoptic map-like images.

Progress in remote sensing technology, however, has led to the development of systems which measure very large numbers of intensity 'channels', or require the analysis of variables other than intensity values. Current visualisation strategies are insufficient to adequately represent such datasets, whilst retaining the synoptic perspective.

In response to this, two new visualisation techniques are presented for the analysis of polarimetric radar data. Both techniques demonstrate how it is possible to produce synoptic image suitable for the analysis of spatial patterns without relying on pixel-based intensity images. This allows a large number of variables to be ascribed to a single geographic location, and thus encourages the rapid identification of patterns and anomalies within datasets. The value of applying the principals of scientific visualisation to exploratory data analysis is subsequently demonstrated with reference to a number of case studies that highlight the potential of the newly developed techniques.

CONTENTS:

List of Figures:

CHAPTER 1 – INTRODUCTION

This thesis is concerned with the development of new visualisation techniques for the analysis of polarimetric radar data. The work contained herein forms a separate, but subsiduary part of a larger project examining the application of scientific visualisation to the analysis of large, multivariate datasets. This larger project is being carried out in the computing sciences department of Brown University (Rhode Island).

Research into the visual analysis of polarimetric radar data has particular relevance to the work carried out at Brown for a number of reasons. Polarimetric radar systems are capable of generating large amounts of data that contain valuable and unique sources of information for environmental studies. Visualisation strategies associated with the analysis of remote sensing data, however, only allow a small subset of this data to be analysed at any one time using conventional pixel-based intensity images. It is the aim of this thesis, therefore, is to develop new techniques that will allow a larger set of variables to be analysed in a manner that encourages the identification of spatial patterns. The benefits of developing such techniques, in the context of exploratory data analysis and research development, will also be demonstrated using these techniques to both observe and explain patterns in real datasets.

In order to achieve this aim, this thesis is split into two sections. The first section consists of a literature review, and covers chapters 2 and 3. In chapter 2, the key concepts and approaches to scientific visualisation are identified, and applied to current visualisation strategies for the analysis of remotely sensed datasets. This leads into a more in-depth discussion, in chapter 3 of current visualisation techniques used for the analysis of polarimetric radar data. Through this, it is demonstrated that the images most commonly associated with the representation of polarimetric radar do not function adequately as tools for exploratory analysis.

The second section of this thesis, therefore, goes on to provide two novel approaches to visualising polarimetric radar data, the rationale for which is outlined in chapter 4. In chapter 5, a relatively simple visualisation technique is proposed for the analysis of variables derived from the widely-used entropy/α decomposition. Using techniques similar to those developed at Brown University, data variables are mapped to the visual parameters of elliptical icons, which are then used to produce synoptic images. Using this technique, five separate variables can be mapped to a single geographic location. Examples of the benefits of this approach are then given, with reference to real polarimetric datasets.

The following chapters then go on to describe a more involved visualisation strategy for the synoptic analysis of polarimetric response patterns. The polarimetric response graph, at present, represents the most complete description of polarised backscatter, and uses a single graphic to represent hundreds of individual intensity values. A limitation of the polarimetric response graph, however, is that it is typically used to

represent single resolution elements or areal averages, and cannot be used to analyse spatial patterns in polarimetric response. In chapter 6, it is demonstrated that the main cause of this limitation is the form of the graphic most commonly used to represent polarimetric response patterns. This graphic is subsequently redesigned in order to produce an iconic representation that is more suitable for synoptic analysis. This technique is then used as a basis for the development of a software application that, for the first time, allows spatial patterns in polarimetric response patterns to be examined.

Chapter 7 then assesses the newly designed graphic and technique, both in terms of its visual qualities, and its application to scientific problem solving. The first of these aims is achieved using a web-based questionnaire survey, which asks non-experts to identify patterns in different representations of polarimetric response. The latter applies the synoptic visualisation technique to the analysis of a region of unusual response patterns observed over an area of reed beds. The characteristics of the observed response, when visualised using the new technique, are subsequently used to develop and verify a model that defines the nature of the polarimetric interactions in this region.

The aim of this thesis, as a whole, therefore is to promote and encourage the idea of visual thinking through the medium of scientific visualisation techniques. Using the example of radar polarimetry, it is shown that, by using imagery, it is possible not only to develop an understanding of the key concepts of this field, but also to develop tools that identify potential research avenues. Whilst the field of remote

sensing has a long history of using visual output to understand various aspects of the earth's surface, the techniques that have been developed to achieve this have not kept pace with the increasing complexity of new remote sensing platforms. The establishment of spatial patterns and relationships is a core concept at the heart of both remote sensing and geography as a whole. In the following chapters it is demonstrated that the application of scientific visualisation strategies allows this method of enquiry to be retained, even as datasets become more and more complex.

CHAPTER 2 – SCIENTIFIC VISUALISATION

2.1 – Introduction

"..meaning follows the lines drawn by natural organisation."

Dr. Wolfgang Kohler

Scientific visualisation can be very broadly defined as the process of making images out of data sets that allow patterns and relationships between variables to be visually explored. This simple description belies the complex, multi-disciplinary nature of the field, which draws on subjects as diverse as art history, perceptual psychology, graphic design and computing science. The concept of visualisation as an aid to problem-solving, however, should not be restricted to the production of images. The term visualisation itself refers not only to the act of making and analysing images, but also to the ability of humans to be able to 'picture' the relationship between objects (both concrete and abstract) in order to better understand aspects of the world around us. The benefit of this ability as a means of scientific discovery is easily illustrated with reference to the 'thought experiments' conducted by Einstein whilst formulating the theory of relativity (Schwartz, 1979). The concepts of stationary and moving observers, for example requires an abstraction that is most effectively rendered in the visual domain. In this respect, it is notable that the concepts behind key scientific discoveries in the modern era are most effectively communicated using

visual analogies. Examples of these analogies are shown in figure 2.1, which are commonly recognised visual metaphors for the concepts of general relativity, black holes and DNA structure.

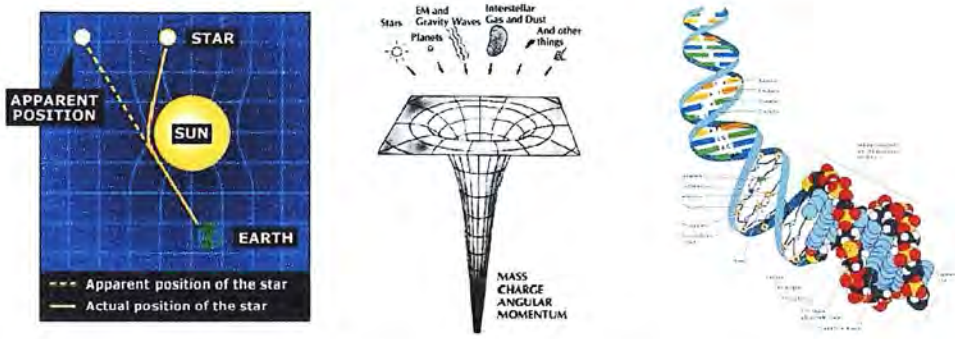

figure 2.1 - Images which have become synonomous with the scientific discoveries that they represent: general relativity, black holes and DNA structure (sources, respectively: Doyle, 2002, Gearhart, 1979 and Ussery, 1998).

The development of scientific visualisation as a research discipline, however, makes explicit the link between visual representation and scientific analysis. In doing this, it is possible to develop approaches to the visual representation of data that exploit and maximise the considerable advantages the human visual system still holds over even the most advanced computers.

This chapter aims to produce an overview of current work in the field of scientific visualisation, and to develop a new framework that can be applied to the analysis of remotely sensed data. To this end, the following chapter is composed of three sections, each of which examines different aspects of scientific visualisation as a research discipline, and how these areas can be used to analyse the types of image commonly created by earth scientists when using remotely sensed data.

In the first section, the main definitions and concepts of scientific visualisation are discussed. The links between scientific visualisation, cartographic visualisation and the use of map-like images in remote sensing are presented in order to provide a framework in which allows for the development of a critical approach to different forms of visual representation. Particular attention is given to the work of Alan MacEachren, and the role of images in exploratory data analysis. Through this, it is possible to define a set of goals with which new visualisation techniques can be assessed.

The second section deals with the semantics of visualisation, or how images can be deconstructed into a number of visual elements. The relationships between these different elements can subsequently be used to inform an approach to visualisation that exploits the power of the human visual system in the recognition of patterns and anomalies within datasets. This section thus examines the work of the Gestalt psychologists, and their influence on the development of codes of graphical representation, such as the visual variables developed by Jacques Bertin. The occurrence of these codes in different forms of art is also discussed, illustrating how the study of paintings and designs by famous artists can be used to guide the development of visualisation techniques.

The use of these visual variables in the representation of remotely sensed data is then considered. It is shown that the majority of visualisation strategies in remote sensing use only a limited set of the possible visual variables. This is largely a result of the dominance of the RGB colour composite in remote sensing visualisation. The

reasons for this reliance are discussed, alongside the limitations this approach imposes. Finally, the benefit of developing alternative modes of representation is discussed in relation to the visualisation of radar data, with particular reference to SAR interferometry.

The third and final section examines the development of visualisation software. A brief review of different types of visualisation software is presented, identifying the means by which users have been given a greater degree of control over the visual components defined in the previous section. The role of three-dimensional graphics and animation is also discussed, with reference to the challenges this poses for both the delivery of and interaction with different forms of visualisation.

Finally, attention is given to the development of bespoke visualisation strategies. In this section, the work of the Computing Sciences department at Brown University is reviewed, emphasising the importance of collaboration between scientists from different fields and visualisation specialists. Particular attention is thus given to increasing the awareness of the value of visual representations of large multi-valued dataset in the preliminary stages of data analysis, and the means by which applications can be built that encourage their further development. As such, this section serves as an introduction to the types of visualisation 'tools' which are currently available, and those which are currently being developed at Brown University. The focus of later chapters, and the purpose of this study, will therefore be to investigate how these tools can be applied to the analysis of polarimetric datasets.

2.2 – Defining Scientific Visualisation

The field of scientific visualisation is a complex, multi-faceted field that hinders simple categorisation. Different authors and research groups approach the subjects of visualisation in different ways. In this chapter, the work of a number of different research groups will be analysed in order to extract examples of 'good practice', which will subsequently go on to inform the research sections of this thesis. In order to develop a framework for the analysis of different visualisation techniques, however, it is first necessary to define exactly what is meant by 'scientific visualisation'.

Scientific visualisation can be very broadly defined as the process of making images out of data sets that allows patterns and relationships between variables to be visually explored. In recent history, the study of visualisation has tended to focus on the digital manipulation of data, and the development of multi-media, interactive tools for data analysis (van Dam et al., 2002, MacEachren and Kraak, 1997). Such developments can be viewed as a response to the exponential increase in the size of digitally-stored datasets, which itself is a consequence of scientific progress in the 20th century. Today, we are faced with what has been termed a 'firehose' of data (van Dam et al., 2000), which are being collected at a rate that far exceeds our ability to process, analyse and use the information contained therein.

It is important to remember, however, that the practice of visualising data has a history far more elongated even than that of the written word (Tufte, 1983). The

discovery of cave paintings with 'proto-cartographic' qualities for example (Dorling and Fairbairn, 1997, p.4), show that as long ago as 30 000 BC, humans have used images not only to celebrate, but also to understand the nature of the world around them.

Such an analysis of visualisation thus places cartography as the main source of inspiration for modern graphical techniques. Indeed, in discussing the cartographic sophistication of a 1546 edition of Cosmographia by Petrus Apianus, E.R. Tufte notes:

> *"..according to historical record, no-one had yet made the quantitative abstraction of placing a measured quantity on the map's surface, instead of the name of a city, let alone the more difficult abstraction of replacing latitude and longitude with some other dimensions, such as time and money.'*
>
> (Tufte, 1983)

Effective cartography, therefore, was perhaps the first form of graphical representation to develop into a means of data analysis. Even today, map-making remains a basic and powerful visualisation technique, and plays an important role in the development of spatial relationships and in problem solving. A classic, and much-used example of the use of cartography to analyse data patterns is Dr. John Snow's dot map of cholera deaths in London in September 1854, which used the resulting patterns to locate an infected water pump. The map used to do this, when stripped of all the location detail (i.e. streets and buildings) is essentially a bivariate

scatterplot with two categories represented by different symbols; water pumps (squares) and deaths (dots).

The importance of cartography as a visualisation technique is also inherent in the analysis of remotely sensed data, which relies heavily on the use of map-like images for the analysis of data, and dissemination of results. The importance in visual representation of data in this field stems from its origins in aerial photography, which was first used in the early part of the 19th century. The first remotely-sensed images are believed to be photographs taken from tethered balloons over the city of Paris by a photographer known as 'Nadar' in 1858, although similar experiments were also being carried out over Boston around the same time (see figure 2.2) (Lillesand and Kiefer, 1994, pp.51). Despite the oblique perspective of these images, their map-like qualities are readily apparent, and allowed, for the first time, a synoptic overview of patterns of urban development. The subsequent development of aerial photography thus provided a unique and fascinating means of observing patterns in both natural and anthropogenic environments

During the following century, the use of aerial photography as an aid to cartography became more prevalent, spurred on in no small part by the two World Wars of the 20^{th} century. It was during the Second World War that another remote sensing technique, namely radar, became operational as an aid to navigation. Whilst the initial development of radar depending on the analysis of non-image data, and the use of plan position indicators (PPIs), it was later found that crude greyscale image-maps could be produced from backscatter intensity measurements that allowed

bombers to delineate geographical features such as coastlines and urban environments during air-raids (Boerner et al., 1998).

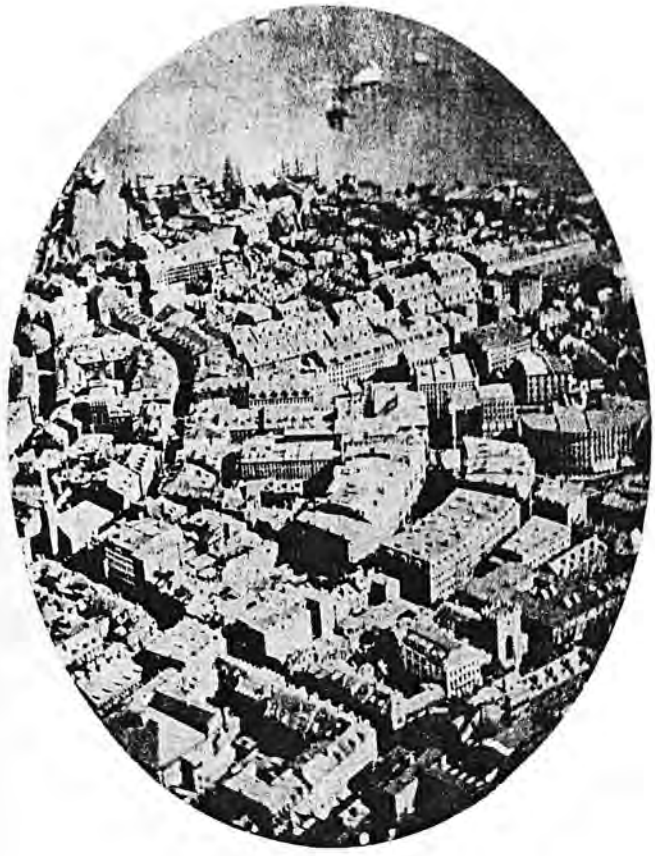

Figure 2.2 – An example of an early aerial photograph, taken over the streets of Boston in 1860 by James Wallace Black (Lillesand and Keifer, 1994).

In the latter half of the twentieth century, the technological developments that had been achieved during wartime in radar technology were adopted and developed for scientific applications. Whilst aerial photography (now predominantly in colour) remained popular for topographic mapping (Lillesand and Keifer, 1994, pp.338),

scientists became more interested in the use of electromagnetic frequencies outside of the visible spectrum. The late seventies and early eighties thus saw the development of a wide range of multi-spectral scanners, which, due to the developments in space technology, were mounted on satellite platforms such as Landsat and SPOT (Schowengerdt, 1997, pp.3). Such platforms presented users with a number of different spectral bands, such as the near and thermal infra-red, which allowed scientists to 'see' the planet in an entirely different 'light'.

The images produced by such platforms, however, bore many of the same characteristics of the first aerial photographs, as intensity values of 'invisible' spectral bands were simply transferred to the visible spectrum. Just as colour photography had allowed the visible spectrum to be split into three spectral bands (namely, red, green and blue light), the predominance on the RGB colour composite in image-processing software facilitated comparisons between different spectral bands outside of the visible spectrum. The conceptual ease by which different 'bands' of spatial information can be represented using this technique have led to the application of RGB colour composites in the analysis of other types of data, such as the interpretation of astronomical imagery (Whitehouse, 2004).

The nature and potential drawbacks of the RGB colour composite as a visualisation technique are developed further in the following section. For now, however, it is sufficient to observe that the majority of remote sensing images (i.e. representations of 'raw' data) contain many similar characteristics to aerial photographs, which themselves can be considered as 'map-like' objects.

It is fitting, therefore, to analyse the visualisation of remotely sensed data within a framework developed by Alan MacEachren for cartographic visualisation. This approach, based on the work of DiBiase, and detailed in (MacEachren, 1994), is particularly useful as it begins to encourage a critical appreciation of the types of images that are commonly employed by scientists in published papers and presentations. In particular, the approach developed by MacEachren allows us distinguish between images which encourage the exploration of datasets, and those which attempt to impose a particular interpretation or understanding.

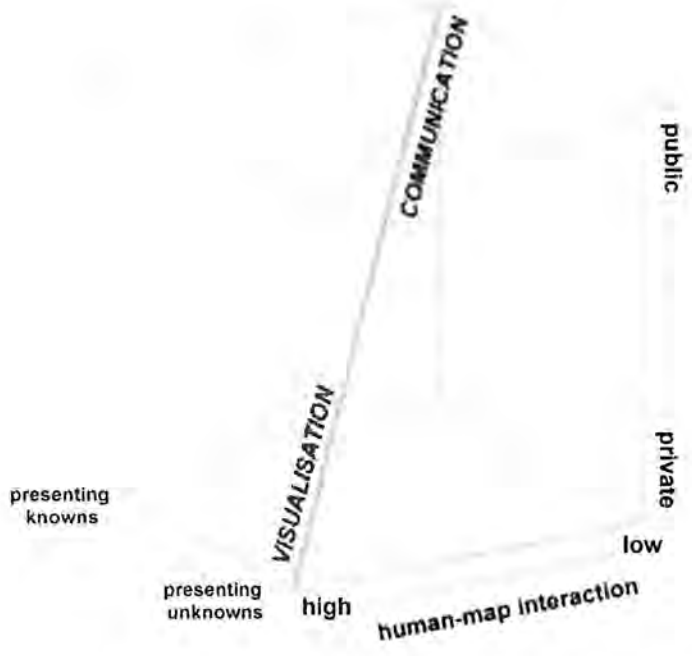

figure 2.3 - Maceachrens comparison of visualisation and communication, which occupy different poles of a cube defined by three axes: human-map interaction. intended audience and data type.

Using the graphical framework of a cube, MacEachren presents three variables that separate the fields of cartographic visualisation and communication. The first is the

intended audience: is the map (image) design for public or private use? Secondly, he defines the level of interaction, from low to high: is the user able to manipulate the parameters which control the appearance and content of the visual representation? Thirdly, the purpose of the map (image) is discussed: is the map intended to present knowns or to reveal unknowns? By using these three continua as axes of a cube, the fields of communication and visualisation are shown to exist at separate ends of the diagonal component, as shown in figure 2.3

One of the most useful aspects of this framework is that it encourages us to analyse the nature of graphical representations, and to assess the quality of different types of visualisation as research tools. An oft-quoted adage in the field of visualisation is that 'a picture paints a thousand words'. Whilst this is undoubtedly true, it does suggest that every image based on collected data can be viewed as an example of visualisation. In many cases, however, the use of imagery to represent data is a means of validating a particular viewpoint in a manner that encourages the viewer to accept the proposed theory as self-evident. In some cases, images may be used to represent false or amplified relationships, to mask weaknesses in the underlying research, or to simply attract attention. Numerous examples of such images can be found in the popular media, where quasi-scientific graphics are routinely used to promote products and opinions. For examples of how such images are also common in academia, the reader is directed towards 'How to Lie with Maps', by Mark Monmonier (1991), and the works of E.R. Tufte (1983, 1990).

In remote sensing, a similar reliance on images as a form of scientific validation can be found in the proliferation of classification maps in research literature and presentations. Whilst such images are a useful means of assessing and redeveloping classification algorithms, there is an inherent danger when the goal of a research project is to produce an image with well-defined boundaries between different landscape components. The natural variability and 'fuzziness' of boundaries in the natural environment, which in turn leads to the problem of 'mixed pixels' in remote sensing data is typically viewed as a constraint (Fisher, 1997). The use of classification maps effectively removes this problem by assigning individual pixels to singular classes, rather than continuous scales. However, the resulting images seldom retain information relating to the certainty with which each pixel has been classified, which in turn reduces the level of enquiry that can be applied to the final image as a tool of data exploration. Whilst the visualisation of uncertainty in remote sensing data products is an ongoing field of research (Wittenbrink et al., 1996, Van der Wel et al, 1998), it remains that the majority of classification maps in remote sensing research are designed as tools of coercion, rather than investigation.

In order to produce effective visualisations, both in remote sensing and in other disciplines, it is necessary to create pictures which 'pose a thousand questions', rather than seek to impose a particular interpretation or theory. The fundamental quality of an effective visualisation technique is that it will encourage the user to establish links between the different variables that are represented, which can subsequently be used to direct further research.

A further important detail inherent in MacEachren's cube is the use of a continuous axis to represent the difference between visualisation and communication. In viewing figure 2.3, it is tempting to think that each example image would occupy a singular point within the cube. In reality, however, a single image may occupy several different positions at different stages in a research project, and be used by a range of different people. In (MacEachren and Kraak, 1997), four goals are identified which occupy different points on the line between visualisation and communication. The first goal is data exploration, whereby unknown or raw data is visualised in a creative manner in order to find variables that produce patterns. These patterns in turn can suggest preliminary relationships, and lead to the second stage of data analysis. Creating a series of different images, and comparing the resulting patterns in each may achieve the third stage of data synthesis. The same images can then be used as a means of explaining and presenting the course of the research to others, and describing how conclusions have been reached.

The concepts embodied by figure 2.3, whilst developed specifically for cartography, also provide a means of assessing the different types of image product used in remote sensing. In particular, the diagonal 'path' between visualisation is clearly evident in many remote sensing journal papers which follow a similar structure, as described below:

1) The area of interest, and its main features, are described, often accompanied by an intensity image or RGB colour composite that shows the 'raw' data.

2) The characteristics of areas of known landcover are located and examined within the dataset, using the image as a guide.
3) A technique is described which allows the characteristics of these landscape components (such as crop type, soil moisture etc.) to be extracted and contrasted with other features.
4) The technique is applied to the whole image, resulting in a classification map, which segments, or decomposes, the original dataset into a number of discrete categories.

The use of classification algorithms and the production of classification maps, as discussed earlier, is a characteristic feature of remote sensing research, and one which dominates both textbooks and research literature. The two types of image that 'book-end' this approach correspond to MacEachren's two extremes of visualisation and communication. Images created from 'raw' datasets are often examined in private on desktop computers, using image processing software which affords the user a high degree of interactivity. Such analysis is typically used in the preliminary stages of research, and allows the user to examine both the geographical coverage, and potential information content of new datasets, and, as such, can be said to be 'revealing unknowns'.

The standard classification map, however, is more aligned with the characteristics of communicative images. Firstly, such images are designed to provide a map-like representation of the effectiveness of a particular approach, and are thus inherently intended for public, rather than private consumption. Likewise, the degree of

interactivity is minimal, with options for changing the colour of individual classes performing an aesthetic, rather than exploratory function. Finally, the fact that a classified image represents an interpretation of a dataset means that, even if it does not 'reveal knowns', it at least encourages the viewer to accept the classification boundaries as factual. It is interesting to note at this point that while classified images have an inherent uncertainty value for each pixel, there are few efforts to represent this uncertainty on the image itself, with such information often relegated to subsidiary tables and figures. The inclusion of visual representations of these uncertainty variables, however, would means that classified images could once more become tools of visualisation, and would allow users to more effectively assess the validity of different approaches to classification. Whilst the visualisation of uncertainty in remote sensing is an ongoing field of research (Dungan et al., 2002, Johnson, 2002), it remains that the majority of classification maps in remote sensing research are designed as tools of coercion, rather than investigation.

In summary, however, it is enough to state at this point that the field of remote sensing has relied on the principles of scientific and cartographic visualisation in the initial stages of data exploration. Just as John Snow used cartography to examine spatial relationships relating to cholera deaths, remote sensing scientists have used map-like images to establish similar 'eureka moments', such as the observation of the Nazca lines in aerial photography over Peru (Kosok, 1965), or the observation of buried archaeological remains in radar data (Blom et al., 1984). The use of intensity-image based visualisation, therefore, is so embedded in the historical and

technological development of remote sensing that alternative visualisation strategies are rarely considered.

As remote sensing technology becomes more advanced, however, the types of data become more difficult to visualise. As multi-spectral sensors and hyper-spectral sensors increase the number of spectral channels obtainable from remote sensing platforms, the effective visualisation of multiple intensity channels becomes a problem for conventional techniques. These problems are compounded further by instruments, such as Synthetic Aperture Radar, which measure variables other than simple intensity values.

The field of remote sensing, however, is over-reliant on a limited set of visualisation techniques that are based on a prevalent optical analogy that has persisted since the advent of aerial photography. The reasons for, and implications of this limitation are discussed in more detail in the following section, which examines the practical theory of scientific visualisation in more detail.

2.3 – Visualisation Theory and Techniques

In the previous section, the concepts of scientific visualisation were defined relative to the manner in which images can be used as tools of investigative data exploration, and was applied to the types of images commonly used to visualise remotely sensed data. A subsidiary branch of research in scientific visualisation examines the practical means by which effective visualisations can be created, using graphical symbols and structures. In order to achieve this, however, it is important to examine

the means by which the human visual system recognises and processes patterns, and how this ability can be harnessed and manipulated through the development of visual semantics.

All images are the result of reflected light which reacts with the light sensitive cells which cover the retina to form electrical signals which are subsequently processed by the brain (Medin et al., 2001, pp81). In sighted humans, the visual pathway is by far the most important sense in terms of information collection, with over 50 percent of neurons dedicated to this ability (van Dam et al., 2000). Through this pathway, patterns of light are translated into complex three-dimensional scenes with discrete, recognisable objects. The fact that this translation is carried out without any obvious effort belies the complexity of processes that lie behind the human visual experience. The extraction of information from images in this manner is an example of a common adage used in cognitive psychology: humans can perform certain functions very easily which computers find very difficult (Medin et al., 2001) (pp.80). When confronted with any image, the human visual system will always attempt to impose some kind of structure that will allow the scene to be understood as a number of separate, but interlinked components.

The nature and analysis of these scene components is the basis of a branch of perceptual psychology known as *Gestalt Psychology* which was developed by Max Wertheimer, Kurt Koffka and Wolfgang Kohler in the early part of the 20th century (Kohler, 1930). The literal translation of *gestalt* is form, or shape, and thus Gestalt

psychology is concerned with the means by which humans are able to automatically process 2D images into organised objects.

Research by the Gestalt psychologists, and others, have shown that humans are particularly adept at recognising patterns and anomalies within images (Bruce and Green. 1987). The development of visualisation strategies must therefore seek to understand the manner in which information is encoded in images, so that it is possible to manipulate different visual components to represent patterns that would be otherwise invisible to the naked eye.

The development of scientific visualisation thus requires the use of a visual 'language', or semantics, which can be used to describe the graphical qualities of visual objects. One well-known example of such a language is the graphical technique developed by Jacques Bertin in his seminal text, 'Graphics and Graphic Information Processing' (Bertin, 1980). In this, he describes a set of visual variables (shown in figure 2.4), which are described as 'the means at the disposal of graphics'. Bertin subsequently goes on to describe a series of rules that can be used to govern the effective use of these variables.

Since this time, other authors have sought to refine and re-apply these rules, particularly as the advent of computer-aided visualisation strategies have become more prevalent in graphic design (for examples, see Brewer, 1996, Wang and Ormeling, 1996). The means by which modern software packages allow this refinement is discussed in more detail in the final section of this chapter.

The concepts of gestalt psychology, and the deconstruction of images using visual variables, however, is a useful means of analysing the types of imagery commonly used in remote sensing. In the previous section, the dominance of intensity images and RGB colour composites in the visualisation of remotely sensed data was discussed. It was demonstrated that this dominance had it roots in the historical basis of remote sensing in aerial photography, and the synoptic viewpoint this afforded of the earths surface.

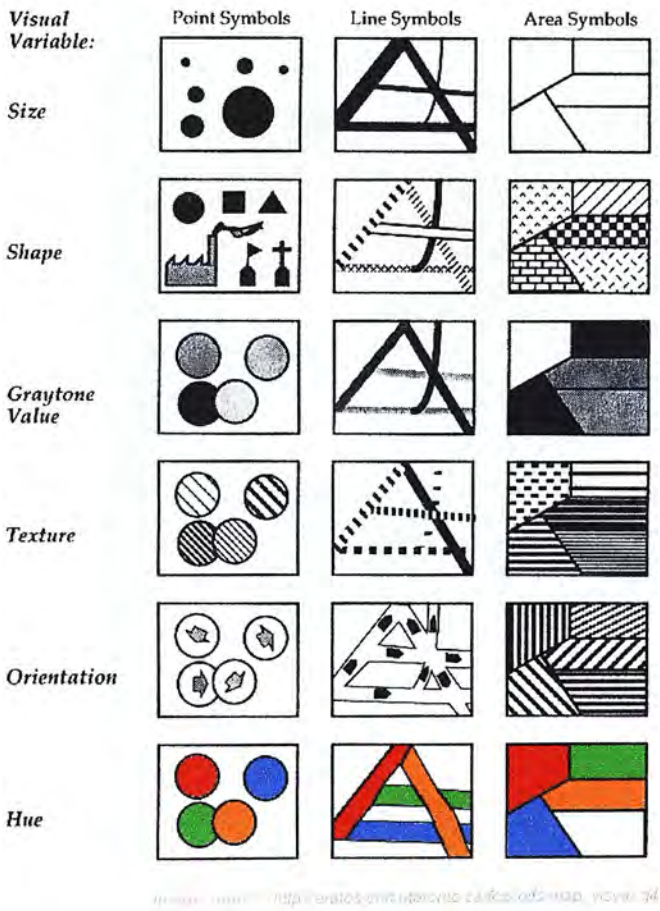

Figure 2.4 – The visual variables, as defined by Bertin.

The visual analogy which dominates passive remote sensing thus stems from the similarity between the old aerial photographs used for cartographic purposes in the early part of the century, and the digital data provided by the airborne and satellite multi-spectral scanners. Leaving aside the exact nature of the photographic process, a black and white aerial photograph can be considered as a record of the reflected and emitted energy over a range of frequencies that covers the optical spectrum. The various shades of grey, and their spatial organisation, presents the viewer with a complex scene which can be understood via a combination of the gestalt principles outlined previously, and the physical, cultural and social knowledge of the viewer.

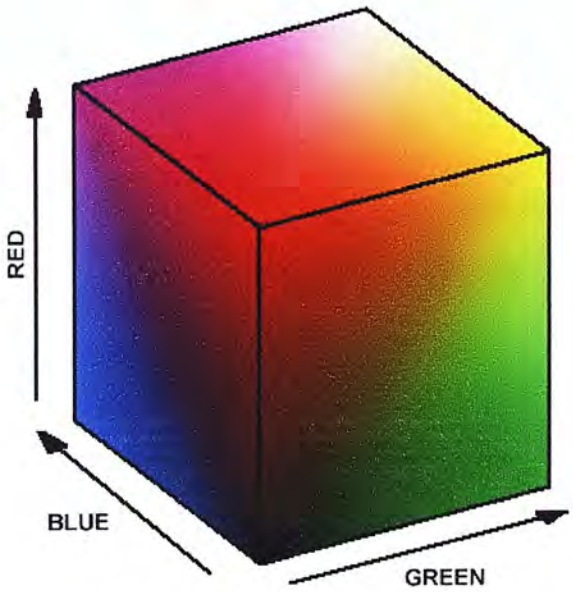

Figure 2.5 – RGB colour space: Any colour can be defined by the relative intensities of red, green and blue light, which can be represented as the axes of a cube. The diagonal path traced for equal values in each channel thus represents the greyscale transition from black to white.

Colour photography uses the same principles as black-and-white photography, but uses a series of filters to split the electromagnetic spectrum into `bands' which

represent blue, green and red light. During processing, the intensities for each band are combined to form a single colour, which can be represented as a single point in the RGB colour cube, as shown in figure 2.5. The resulting image retains the *gestalt* qualities of a black and white print, but contains extra information encoded in the visual variable of colour.

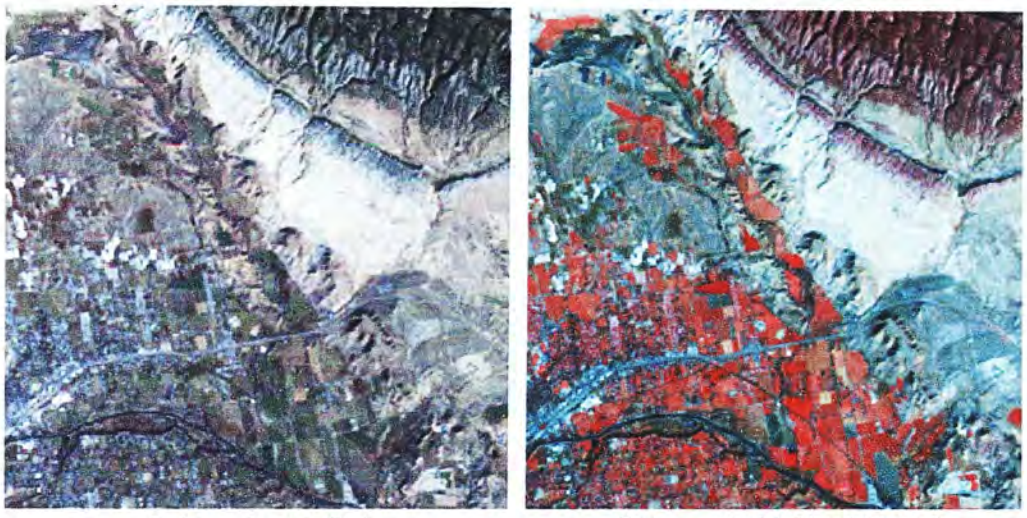

Figure 2.6 - RGB composites for a LANDSAT image over Canon City.
(left) RGB = Bands 3,2,1 (Optical Bands)
(right) RGB = Bands 4,3,2 (Near Infra-Red, Red and Green)
Note that the infra-red image contains information relating to vegetation health and species which is not visible in the image based on optical bands (image taken from ENVI sample files).

The visualisation of multispectral data uses the same visualisation structure as colour photography, but substitutes intensity values recorded over 'invisible' bands of the electromagnetic spectrum for one or more of the visible colour bands. The resulting images thus retain the structural, *gestalt* characteristics of aerial photography, allowing viewers to use the geographical distribution of known objects to interpret

the information contained in the colour channels. Figure 2.6 shows an example of two images created from Landsat data using different spectral bands. The patterns of fields, road networks and topography are clearly identifiable in both images, but the rightmost image contains extra information relating to different crop characteristics, which primarily affect the data values recorded in the infra-red channel.

Images similar to those shown in figure 2.6 are often used as tools of exploratory visualisation, and form the basis of supervised classification procedures through the identification of training sets and regions of interest. An inherent limitation of such images, however, is the constraint that only three bands of information can be represented at any one time. In terms of the visual variables discussed by Bertin, therefore, the RGB colour composite is inherently limited to the representation of 5 variables (namely, the red, green and blue colour intensity, and an x-y location).

This poses a problem for sensors the use multiple wavebands, from the 11 bands measured by LANDSAT-5 to over one hundred bands, as measured by hyperspectral scanners such as AVIRIS (Campbell, 1996). The analysis of information contained in more than three bands thus requires the use of different visualisation techniques. Spectral line graphs, for example, can be used to assess the variance of a single pixel or areal average over a wide range of wavebands, but lose the spatial information encoded in the synoptic image representation. Even combinations of spectral lines graphs and synoptic images, such as the image cubes used to represent hyperspectral data (Schowengerdt, 1997), are restricted in that only a single column (or row) of an image can be analysed at any one time.

Other approaches attempt to condense, or decompose, the information contained into multi-channel datasets into a smaller number of dimensions. Principal Components Analysis (PCA) is an example of this approach, and uses eigenvector analysis to compress the variance in a multi-dimensional dataset into a smaller number of channels, which can subsequently be represented as grey-scale intensity images and RGB composites (Jensen, 1994). Whilst such techniques can be an effective means of reducing datasets, there is also the danger that potentially useful anomalies within the dataset will be removed that could have been analysed through visual interpretation.

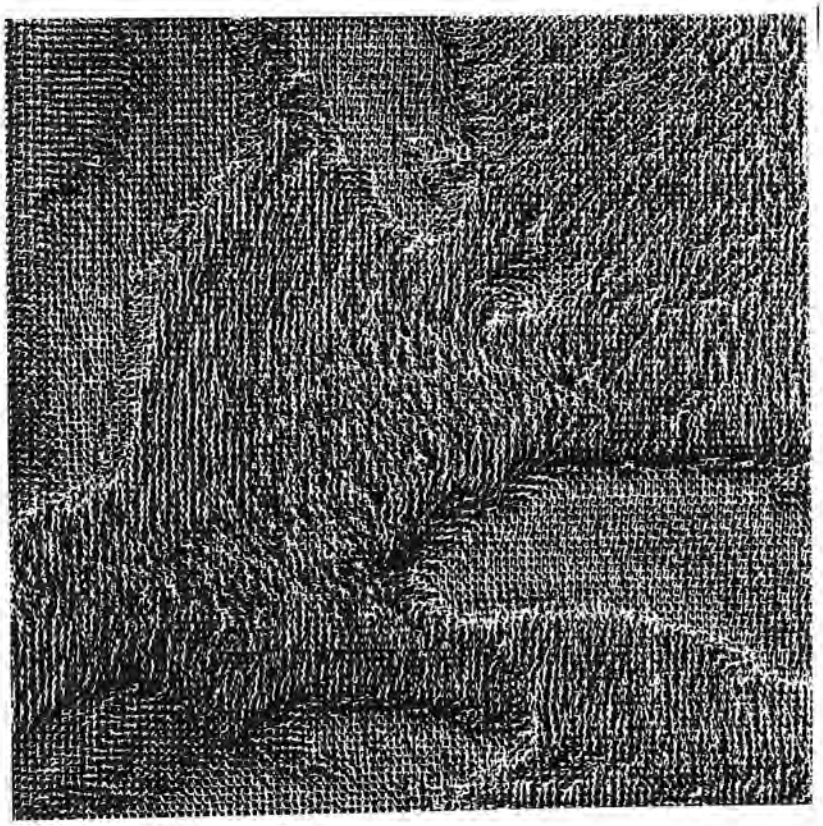

Figure 2.7 - An example of multi-dimensional visualisation developed using the EXVIS system (Smith, 1991).

The development of alternative models of representation for multi-dimensional datasets in remote sensing has been investigated, but have yet to be integrated into image processing packages or otherwise adopted in the remote sensing community. One example of such a technique is the EXVIS system which uses oriented line segments to represent five channels of Landsat data per resolution element (Smith, 1991). The resulting images have a carpet-like texture (as shown in figure 2.7), which can be used as a basis for area segmentation, and for the observation of data anomalies.

The dominance of the RGB composite as a means of image analysis, however, seems set to continue due to the convenience and appeal of pixel based images with map-like qualities. However, the benefits of developing new visualisation strategies should not be overlooked, as they can often perform an important role in the dissemination of new techniques and applications.

A good example of this can be found by studying the visualisation strategies employed in the analysis of radar data, and, in particular, interferometric radar data. The historical development of visualisation in radar remote sensing differs from that of passive remote sensing in that it has its roots in military navigation, rather than reconnaissance. Radar instruments was used during bombing raids, where the backscattered intensity of microwaves was used to form crude, low resolution images which outlined major geographical features, such as coastlines and towns, in 'real-time'. The development of radar was therefore predominantly driven by the need to identify hard targets, with the surrounding non-target areas considered as 'clutter'.

Since the end of WWII, however, it was realised that the information contained in this clutter could be used to identify different landscape components, such as surfaces, vegetated areas and urban environments, each of which had different backscattering properties (Boerner et al., 1998). The development of synthetic aperture radar (SAR) and the launch of the first satellite based radar system (Seasat-1) in 1978 (Lillesand and Keifer, 1994) led to the development of a dedicated research field examining the application of radar data to environmental studies.

In the wider remote sensing community, however, data from radar platforms has the reputation of being more 'difficult' to handle than data from passive sources. It is contended that this reputation is due in part to the nature in which radar data is typically visualised. As the widespread adoption of radar data in the remote sensing community post-dated the boom in remote sensing brought about by the Landsat program, the means by which radar data is typically analysed uses many of the same tools used to view data from passive sources.

The validity of the optical analogy used to describe passive data, however, breaks down when applied to radar data. In Woodhouse (2000), the characteristics of radar systems are shown to be more akin to human aural perception than to visual perception, and the process of making images out of radar data likened to imaging how a bat would 'see' the world.

In practice, this means that images formed from radar data require a degree of abstraction that is not required for other forms of remote sensing imagery. For example, image 'artefacts' such as radar layover and foreshortening require an understanding of the imaging properties of radar systems, and the requirement for an off-nadir image track to avoid range ambiguity. It is telling that in some remote sensing textbooks, the process of radar remote sensing is often (incorrectly) compared to oblique flash-photography, underlining the pervasive influence of optical analogies in the early stages of remote sensing education (for example, see Lillesand and Keifer, 1994, pp.9).

Alongside the geometric structure, the mode of collection also affects the radiometric nature of radar images. Within a single time bin (which represents a resolution element in the final radar image), a radar antenna may receive backscatter from several different features in the imaged scene (for example, individual branches and trees). Each pixel in a radar image, therefore, has a radiometric intensity that is affected by the combination of many different waves of varying amplitude and phase. This variation results in the characteristic salt-and-pepper appearance of radar images, that is commonly termed 'speckle'. When applying analysis techniques developed for optical sensors, the presence of speckle has a deleterious effect on image quality, and greatly inhibits the effectiveness of classification algorithms unless carefully removed, or filtered (Lee et al., 1999).

An understanding of the characteristics of speckle, and in particular the understanding of variation in phase, however, have been instrumental in the

development of techniques in radar remote sensing which have allowed the extraction of unique and valuable types of data. Both interferometry and polarimetry are based around the understanding and manipulation of phase values in order to characterise the nature of wave interactions in greater detail.

With respect to scientific visualisation, however, the analysis of phase values requires the development of visualisation techniques that provide information on a variable which has no direct visual analogue. The difficulties this poses for the visualisation of polarimetric radar data forms the basis of the remainder of this thesis, and is not discussed further here. It is however, instructive to examine the means by which interferometric data has been visualised, as this provides an excellent example of how the development of novel visualisation techniques can greatly enhance the adoption of new technologies.

Radar interferometry is a technique that allows the precise measurement of topography and relief displacement to sub-centimetre accuracies through the comparison of complex images recoded by antennas at different locations or times (Madsen, 1998). The technique was first applied to the topographic mapping of Venus in 1969, and was later used to map the moon in 1972. Although the first airborne interferometer was developed for military purposes, and tested in 1974, it was not until 1986 that Zebker and Goldstein presented the first application of interferometry for the topographic mapping of terrain surface (Madsen, 1998). Since this time, the field of radar interferometry has developed into a standard remote sensing tool for the analysis of topography and surface displacement. Application

areas include the mapping of earthquake deformations (Massonet, 1993), ice sheet motion (Goldstein, 1993) and vegetation (Wegmuller, 1997).

The field of radar interferometry is of particular relevance to the current research due to the visualisation techniques used for the representation of interferometric datasets. Both repeat-pass and single-pass interferometry record two complex images of a radar scene, each representing both the amplitudes and phases of coherently added waves within a resolution element.

By analysing the *phase difference* between two complex images, it is possible to extract information relating to the topography or to surface displacements, depending on various system parameters (Madsen, 1998).

The visualisation of interferometric data, therefore, is not as straightforward as for systems where intensity is the only variable of interest. The development and application of the interferogram, therefore, represents a unique remote sensing product, which allows the visualisation of three variables with dissimilar data structures. This is achieved using the HSV (Hue, Saturation, Value) colour space. In discussing multi-spectral passive sensors, the RGB colour cube was introduced as a means of visualising three linear variables. The HSV colour decomposition is similar to the RGB colour space in that it provides a means of uniquely identifying any colour. It is different to the RGB colour space, however, as each of the three variables used to describe a particular colour have different qualities, which makes

the HSV decomposition unsuitable for the representation of continuous, linear datasets.

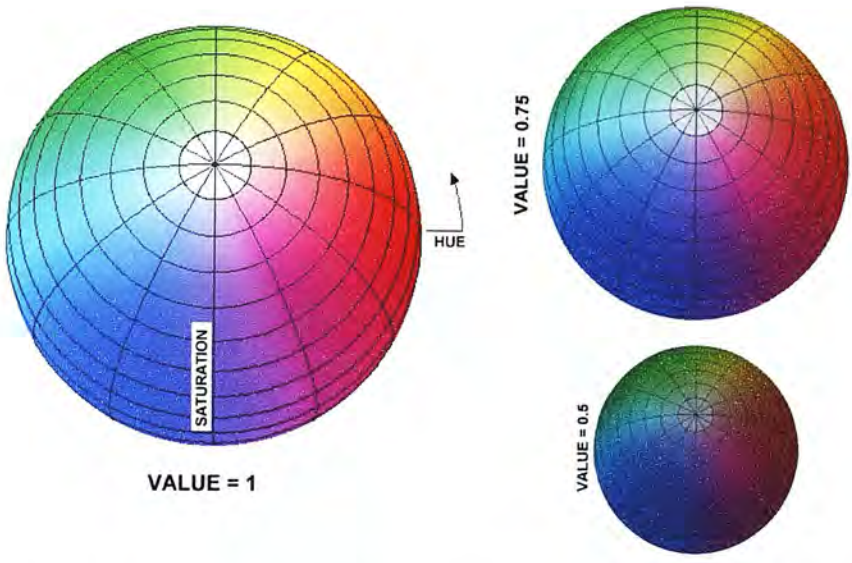

Figure 2.8 - HSV colour space, represented as a hemisphere, where longitude represents hue, latitude represents saturation (ranging from 0 to 1 from pole to equator) and the size of the sphere represents value. Note that black is represented by a sphere with a radius of 0, which is invariant to changes in hue or saturation.

In figure 2.8, the HSV colour space is represented as a sphere. From this, it is clear that the hue parameter is a cyclical value that can be represented as a value between 0 and 2π radians. This quality can subsequently be used to illustrate the key concepts of interferometry. In figure 2.9, variations in phase difference for two simple elevation models are represented using the hue parameter. In the case of the flat earth scenario, simple trigonometry shows that phase difference values will increase as a function of range distance, leading to cyclical bands of colour termed fringes. The addition of topography to the imaged scene leads to a distortion of these linear bands, as shown to the right of figure 2.9. By subtracting the measured phase from the flat earth value, the resulting fringes in the phase difference image appear similar to

contour lines. The phase difference image can subsequently be used to derive a digital elevation model through a process known as phase unwrapping, using the operational parameters of the radar system (wavelength) and at least one point of known elevation (Madsen, 1998).

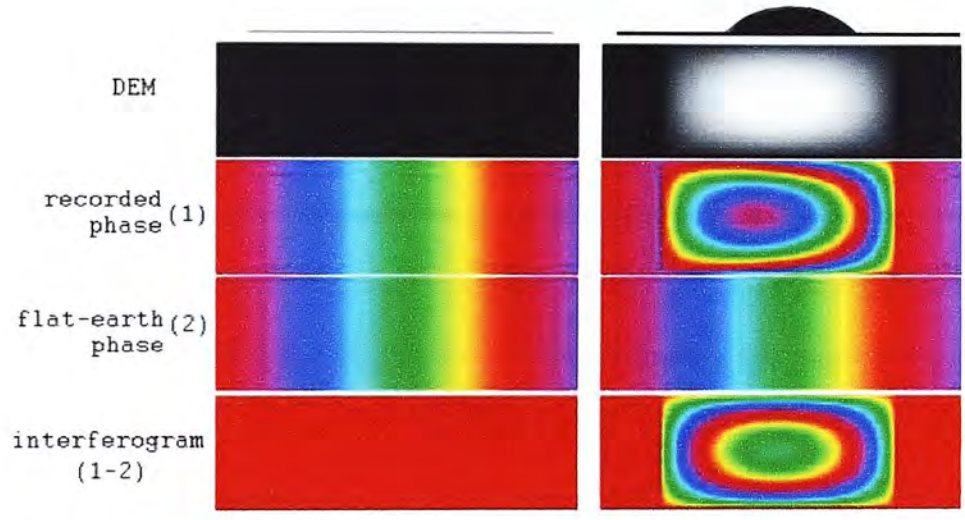

Figure 2.9 - Representation of phase difference using hue in an interferogram. For flat terrain (left) phase difference values increase with range, giving predictable 'fringes' of colour. The addition of topography (right) distorts these fringes

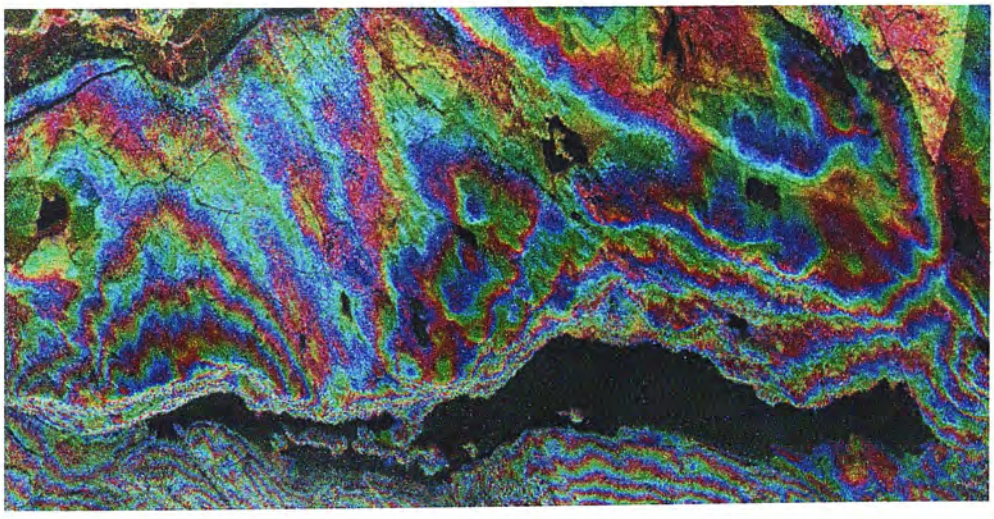

Figure 2.10 – An Interferogram constructed from L-band data collected over Glen Affric.

The remaining two parameters of the HSV colour space can also be used to represent different aspects of interferometric data. The value parameter is analogous to grey-scale intensity and can thus be used to represent the backscatter intensity for each resolution element, providing locational detail in a manner similar to that described for passive remote sensing images. The saturation parameter is used to represent the coherence of the recorded wave. Areas of high coherence (represented by saturated colours) indicate areas where phase values measured by each antenna are well correlated, and are associated with areas where there is a single dominant scattering mechanism, such as over bare surfaces. Areas of low coherence, in contrast, occur where phase values between antennas are uncorrelated, and are associated with areas with multiple scatterers of random size and distribution, such as over vegetated areas. By assigning this parameter to the saturation channel, the phase information contained in the hue channel is only evident where it is of potential use i.e. areas of high coherence. Figure 2.10 shows an interferogram constructed from L-band data collected over Glen Affric, in the northwest of Scotland (Cloude et al., 2001). Note that the fringes appear similar to contour lines in areas of high coherence, but lose their definition over forested areas.

It should be noted that the interferogram is an example of a visualisation technique in remote sensing which does not rely on the visual analogy that is so pervasive in other application areas. Nevertheless, the interferogram does achieve effective perceptual analogies. As phase difference is a cyclical value, it is most effectively mapped to a cyclical visual variable. Similarly, the use of saturation to map coherence is an effective means of representing uncertainty. The resulting image thus not only acts as

an effective means of analytical visualisation, but also provides an easily recognisable and straightforward means of explaining the fundamental concepts of interferometry.

By way of illustrating the value of effective visualisation in the dissemination of new ideas in science, it is interesting to note that the results of an early paper examining the application of interferometry to earthquake mapping were presented in 1993 on the front cover of 'Nature' magazine (Massonet, 1993). Since this time, the interferogram has become a standard means of both analysing and presenting interferometric data in academic journals and presentations (Zebker, 2000).

The study of polarimetric radar data, as will be detailed in chapter 5, has not benefited from the development of an effective visualisation technique akin to the interferogram, and still remains dominated by images that perpetuate the optical analogy discussed earlier. The development of dedicated visualisation software packages in recent years, however, has greatly extended the range of visual variables which can be controlled and used in the design of visualisation strategies. The final section of this chapter thus examines recent developments in computer hardware and visualisation software, and provides examples of how these have been combined to produce innovative and powerful exploratory environments.

2.4– Development of Tools for Scientific Visualisation

In the final section of this chapter, the 'tools' which are available for creating visual representations of visual datasets. This is followed by a number of examples of visualisation produced by scientists in the Computing Sciences department at Brown University, who specialise in the development of visualisation techniques and environments.

In previous sections, the technological development of remote sensing has been described. The latter half of the twentieth century has seen an explosion in the amount of digital data collected by airborne and satellite platforms. This flood of data, however, is by no means unique to remote sensing, and poses a number of challenges for those charged with transforming this data into useable, effective information. Scientific visualisation, it is believed, can play a valuable role in stemming what has been described as the 'firehose of data' (Van Dam et al., 2000).

It is possible to identify two general sources of this data. Firstly, there are data generated by automated recording devices, which provide information for a vast range of disciplines at a wide range of scales. The development of recording and monitoring technology over the last half of the 20th century means that many of these disciplines are now characterised by large volumes of data, from the analysis of sub-microscopic particles, through medical imaging, up to the study of global circulation patterns, and indeed beyond to the analysis of continuous data sets from the furthest reaches of space.

Secondly, the analysis of recorded datasets have provided information which can be used in the development of mathematical models which predict the effects of changing key variables in system which, again, operate within a wide variety of scales and disciplines. Thus modelled data may be used to predict the effects of a newly developed drug, or to predict future variations in climate patterns. These models are also capable of generating large volumes of data, often measured in terabytes or even petabytes (Van Dam et al, 2000).

Scientific progress, however, not only affects the amount of information we are able to collect, but also the means by which we can store, access and represent data types. Since the development of the first real-time data plotters for oscilloscopes developed in the 1950's, the development of new recording technologies have depended on some form of visual output for the validation, analysis and presentation of scientific data (Van Dam et al., 2000). Since the 1970's, the advent of desktop computing, and increasing availability of digital datasets has led to the development of software packages which allow users convert data into representative images. By analysing the development of visualisation strategies in widely available software packages it is possible to demonstrate how the range and control of visual variables for the analysis of datasets has increased, and widened the scope for the development of innovative, tailor-made visualisation strategies.

At the most simple level, spreadsheet packages such as Microsoft Excel and Minitab allow graphics to be generated from grouped datasets. The visualisation provided are restricted to a set of predefined choices including line graphs, bar charts and pie

charts, alongside values derived from statistical analysis techniques, such as polynomial regression lines and error bars. Although limited in comparison with more dedicated visualisation packages, this type of software nevertheless allows data to be presented in a manner that allows the identification of trends and anomalies in a manner that cannot be achieved using a table of numbers. The disadvantage of these packages, however, is that the level of user interaction with the structure of visualisation techniques is generally limited. For example, in Microsoft Excel, the types of graphics that can be produced must be chosen from a set of predefined chart types, all of which require data to be properly formatted. Subsequent changes to the structure of the visualisation are restricted to largely cosmetic changes, such as the colouring of individual chart elements and text formatting for axes. More recent editions of the package also allow the addition of effects which needlessly complicate the design of the graphic, such as the addition of relief shading to bar charts, and unnecessary 3D projections. Such embellishments can often detract from the quality of a graphical representation by distracting the viewer from the true information content, and should thus be avoided (Tufte, 1990).

Image processing packages represent a second generic type of software which can be used from data visualisation, and one which has particular relevance to the visualisation of remote sensing datasets. Image processing software requires that the dataset used is arranged in a regular grid structure, whereby each data value can be used to generate a pixel intensity value. The collection of pixel values thus generates a grey-scale image that acts as a map of data values. Colour images can also be

generated by assigning three co-located datasets to the red, green and blue colour guns of a conventional monitor screen.

A wide variety of image processing packages exist, which are suitable for different applications. Packages such as Paint Shop Pro and Adobe Photoshop, for example, are designed mainly for artistic purposes, although many contain mathematical functions which are used for image filtering and edge detection (Jensen, 1994). A major disadvantage of these packages for scientific analysis, however, is that they are limited to common computer graphic formats (such as bitmaps, jpegs and tiffs) as sources of data input.

More useful in terms of scientific visualisation, therefore, are image processing packages which are designed specifically for the scientific community, such as ERDAS Imagine and ENVI. The development of such packages was a response to the increasing availability of datasets from remote sensing platforms such as Landsat in the 1970's, but the same software can also be used for other continuous, cell-based datasets, such as those derived from medical imaging techniques. Scientific image processing packages combine the visual representation techniques used by standard image processing software with powerful mathematical functions, such as interactive histogram adjustment, boxcar filtering, principal components analysis and ortho-rectification. Other functions allow the sorting of datasets into discrete categories using classification algorithms.

Despite the power and widespread usage of image processing packages, there are a number of problems inherent in their usage with respect to the development of visualisation strategies. In the previous section, it was demonstrated how the reliance on pixel based images limited the number of visual variables which could be manipulated and assigned to data values.

A further disadvantage of the pixel-based approach to data visualisation in remote sensing is that it encourages the assumption that an area covered by a pixel (at whatever resolution) is made up of one, consistent landcover type. Although the problems of mixed pixels are widely recognised and covered in remote sensing textbooks (Campbell, 1996, Lillesand and Keifer, 1994), very little attention is paid to this problem in a research context, where classification strategies often focus on features which are smaller than the nominal resolution of the platforms used (particularly in the case of satellite remote sensing) (Fisher, 1997).

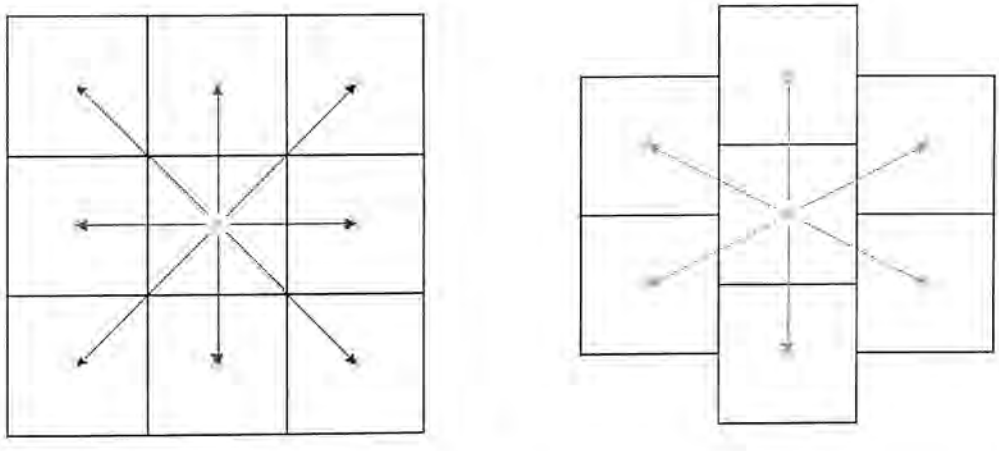

figure 2.11 – Comparison of nearest neighbour analysis using a rectilinear (left) and hexagonal gridding system (right). Distances are measured from the centre point of each pixel.

In addition, even where pixels are composed of similar landcover elements, their reflectance values may be influenced by reflectance values from neighbouring cells (Fisher, 1997). The reflectance characteristics of surfaces are commonly described in remote sensing using the bi-directional reflectance function (BDRF), which can be used to classify surfaces between the two extremes of specular or diffuse. In the case of a totally specular reflection, all incident radiation is reflected at an angle equal to that of the incident ray. For diffuse surfaces, the incident radiation will be scattered equal in all directions. In practice, the concept of diffuse scattering is often depicted as a radial, circular pattern (Campbell, 1996, pp41.). Therefore, if we imagine a large area covered by a diffuse surface, it can be assumed that each pixel will have an equal contribution from each of its immediate neighbours, and vice versa.

The use if a rectilinear grid, however, does not support this assumption. In figure 2.11, it can be seen that the distance between the centre point for a pixel and its neighbours varies depending on whether or not the neighbour lies on a diagonal axis. An alternative mode of representation, therefore, would be to use a hexagonal tessellation for the arrangement of pixels, which, as shown in figure 2.11, would ensure that neighbouring pixels are equidistant. The benefits of adopting such an approach are detailed further in (Staunton, 1989) and (Middleton and Sivaswamy, 2001), where it is demonstrated that the use of a hexagonal grid can improve certain image processing functions, such as boxcar filtering.

It is realised, however, that the rectilinear grid structure still has a number of advantages, not least of which is the fact that traditional display devices, such as monitors and TV screen are also made of rectilinear grid structures (Staunton, 1989). The use of a rectilinear grid, therefore, ensures the highest resolution, whilst the use of a hexagonal grid, as shown in figure 2.11, would require each data pixel to be composed of at least four image pixels. It is therefore unsurprising that the rectilinear grid has become the standard means of presenting data in digital image processing packages.

The examination and consideration of alternative modes of visualisation, even at the theoretical level, however, allows the scientist to reflect on the assumptions that are imposed by traditional and ingrained visualisation practices. The adoption of alternative visualisation practices, where required, can also be achieved through the development of 'bespoke' visualisation approaches and environments. The development of such approaches, whilst still more time-consuming than using the 'off the shelf' solutions described above, have nevertheless become much easier to achieve using software packages which are specifically designed to allow the development of novel visualisation strategies.

Examples of such packages include IDL and AVS, and are characterised by a greater degree of freedom for users in terms of both data input and visual output. These packages are characterised by a modular approach, whereby different subroutines are used for data input, manipulation and representation. The user subsequently

constructs visualisation strategies from these individual components. This is achieved using either written programs (as in IDL) or by connecting components in a graphical interface (as in AVS). The use of these and similar packages thus requires a greater degree of expertise and training than other menu-based visualisation packages. The advantage of using these packages, however, is that the individual subroutines can be combined and manipulated in a manner which allows a far greater degree of control over the types of visualisation which are produced. In addition, users can create applications that are designed specifically for the visualisation of a particular dataset, allowing the development of 'bespoke' visualisation strategies.

A further advantage of dedicated visualisation packages is that they allow a larger number of variables to be represented in a single image. Visualisation strategies discussed so far have been limited to static representations of data restricted to a two dimensional plane. Modern visualisation packages, however, allow for the generation of three dimensional surfaces and volumetric representations that increase the spatial dimensionality of representations. Animated sequences can also be generated, allowing for an assessment of temporal patterns and anomalies, and have become a popular means of representing cartographic data (Slocum, 2004).

Finally, the number of variables which can be represented at a single (three dimensional) location can be increased through the use of data icons, or glyphs, which allow a greater degree of control over the visual variables outlined earlier in this chapter.

As an example of how this increased range of visual variables can be applied to the visualisation of multi-variate datasets, the following example details work carried out by a visualisation group in the computing sciences department of Brown University. Within this research group, scientists have looked to famous works of art as a means of developing novel approaches to the construction of images. In (Laidlaw et al., 1998), for example, the intricate layers of brushstrokes used in the paintings of Van Gogh have been used as a source of inspiration for the development of visualisation techniques based on the layering of different levels of information, each of which convey qualities of datasets which can be read at different scales.

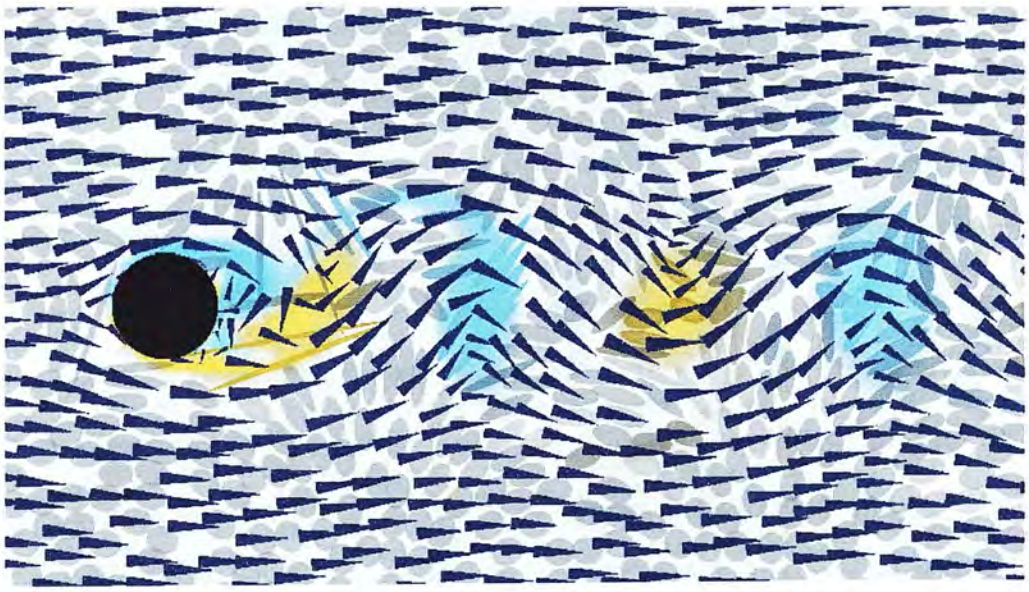

Figure 2.12 The use of 'layers' of visual variables in the construction of exploratory visualisations. In this image, various aspects of fluid flow are encoded on five separate layers, using a combination of colour, transparency and shape to represent up to nine variables at a single location (Kirby et al., 1999).

In figure 2.12, an example image is shown which represents fluid flow around an obstacle. The image is composed of five layers, which mimic the manner in which oil paintings are typically constructed. The first layer is a primer, which is shaded

grey in order to accentuate the transparency of subsequent layers. The second layer uses colour to represent the direction of vorticity of the flowing liquid, with blue representing clockwise and yellow representing counter-clockwise vorticity. The magnitude of the vorticity is also represented in the opacity of this layer, so that the layer becomes almost transparent where the vorticity is zero. The use of opacity as a visual variable demonstrates how the advent of computer-aided visualisation has allowed the application of new visual variables that were not considered by Bertin.

The subsequent layers in figure 2.12 use a series of icons to define other variables associated with fluid flow: ellipses are used to represent the rate of strain tensor, while arrows are used to encode velocity, using the size and orientation of the arrows to encode the vector magnitude and direction, respectively.

The resulting image thus operates at a number of different scales. As with an oil painting, and overall understanding of the structure of the composition is first achieved by viewing the image from a distance, but additional detail is revealed to the viewer depending on their proximity to the image. In addition, through careful selection of visual variables, the inherent properties of different variables are clearly embedded in the image. For example, the use of two contrasting colours to represent the binary relationship between clockwise and anti-clockwise flow effective allows the image to be divided into regions at the small scale. The use of icons at the large scale, in contrast, allows the variables of size, shape and orientation to provide detail to the pattern which as already been established.

The above example demonstrates the importance of good design principles in the construction of visualisation strategies. The effective use of visual variables is dependant on two requirements. Firstly, the user must be able to encode different data variables to the most suitable visual variable. Secondly, the user must have an awareness of how these visual variables interact with each other, and construct the image so that each element can be read separately, as well as in combination.

2.5 - Chapter Summary

In this chapter, a structure for the assessment of visualisation strategies has been introduced, which will be applied to other examples of existing and developed approaches to visualising data throughout the rest of this thesis.

The role and value of visualisation in data analysis has also been examined in an age which is characterised by ever-increasing volumes of data, with particular attention paid to the field of remote sensing. It has been shown that, historically, visualisation has played a fundamental role in the analysis of remotely sensed data. It has also been shown, however, that due to this history, the means by which data are represented use only a limited set of the visual variables which are at the disposal of graphic designers.

The field of Synthetic Aperture Radar, and in particular SAR interferometry, was then used to illustrate the tangible benefits of developing new approaches to

visualisation, both in terms of developing a conceptual understanding of new types of data, and in disseminating this understanding into the wider scientific community.

Finally, the development of visualisation software was reviewed, illustrating that the means at the disposal of current graphic designers in the scientific community permits the development of powerful and imaginative representations of large, multi-variate datasets.

In the following chapter, the aspects of scientific visualisation discussed here will be applied to current strategies for the visual analysis of polarimetric datasets, in order to identify areas for potential improvement.

CHAPTER 3 – POLARIMETRIC RADAR DATA: APPLICATION AND VISUALISATION

3.1 – Introduction

This chapter aims to provide a brief overview of the field of radar polarimetry, which will allow those unfamiliar with the subject to comprehend the concepts embedded in the visualisation strategies developed in later chapters. To this end, the first section of this chapter examines the fundamental properties of polarised waves and how their polarisation is altered through interactions with different objects. This is followed by a description of how radar polarimeters measure these interactions, and how they can be applied to environmental research.

The latter half of the chapter then goes on to examine the different ways in which polarimetric radar data are visualised. Whilst a variety of techniques have been employed to visualise polarimetric datasets, it is shown that two distinctive scales of enquiry exist; namely, the synoptic and the site-specific. The different types of information that can be extracted from each form of representation are thus compared in order to identify possible areas of improvement. These areas will subsequently go on both to justify, and to inform the work carried out in the following chapters.

3.2 – Conceptual Basis of Radar Polarimetry

Polarisation is a feature of all waves in the electromagnetic spectrum, and describes the path traced by the electrical component of the electromagnetic vector as it propagates through space. This path is affected by the refractive index and dielectric properties of different objects and atmospheric layers.

At radar wavelengths, polarisation is altered by interactions with surfaces and with objects that are of similar size to microwaves (5-30cm). The utility of radar polarimetry in the context of earth observation thus stems from the fact that many features of interest in the natural environment consist of objects of similar dimensions to these wavelengths. In particular, vegetation elements associated with both forest and agricultural structure, such as trunks, branches and stalks can all affect the polarisation of a propagating microwave (Durden et al., 1989, Fortuny-Guasch et al, 2003). Other application areas, such as geological mapping and sea-ice studies, exploit the sensitivity of polarised waves to surface roughness and dielectric properties (Dall et al., 1995, Skriver and Pedersen, 1995).

In order to understand the nature of radar polarimetry, and the information that can be derived from polarimetric datasets, it is first necessary to understand how polarised waves are produced. All radar systems use antennas to both transmit and receive electromagnetic waves at microwave frequencies. Using a single dipole antenna, the path traced by the electromagnetic vector is restricted to a plane parallel to the orientation of the antenna, and thus a linearly polarised wave is produced. Any linearly polarised wave can be described using two variables: amplitude (A) and

phase (θ). As shown in figure 3.1, these variables can be represented using either a simple sine wave, or as a rotating pointer.

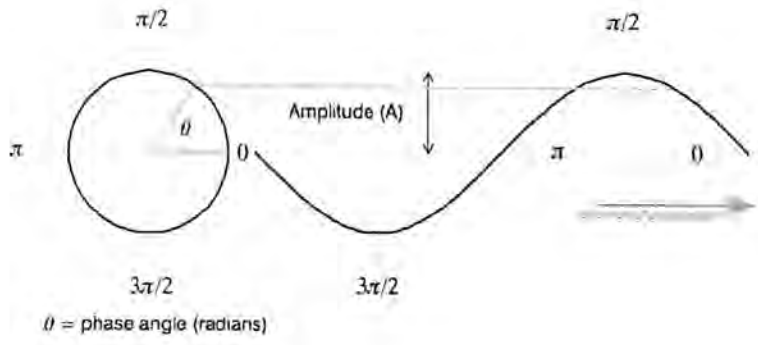

figure 3.1: Representing phase an amplitude, either as a rotating pointer (left) or as a simple sine wave (right).

Linearly polarised waves represent a subset of the total set of polarisations that can be achieved. In order to achieve the full set of polarisations, it is necessary to use two orthogonally aligned antennas, which are typically chosen as h (horizontal) and v (vertical). If both antennas are used to generate microwaves of equal frequency, but variable phase, then the full set of polarisations can be obtained. Using two antennas, the path traced by the electromagnetic vector is equal to the projection of the sine values for each antenna in the plane defined by the axis of propagation. A fully polarised wave can therefore be uniquely defined using three parameters: two amplitude values (A_h and A_v) and a phase difference (θ_{h_v}), usually measured in radians. From this, it is possible to identify three characteristic polarization states, which can be used to describe the full set of polarisations.

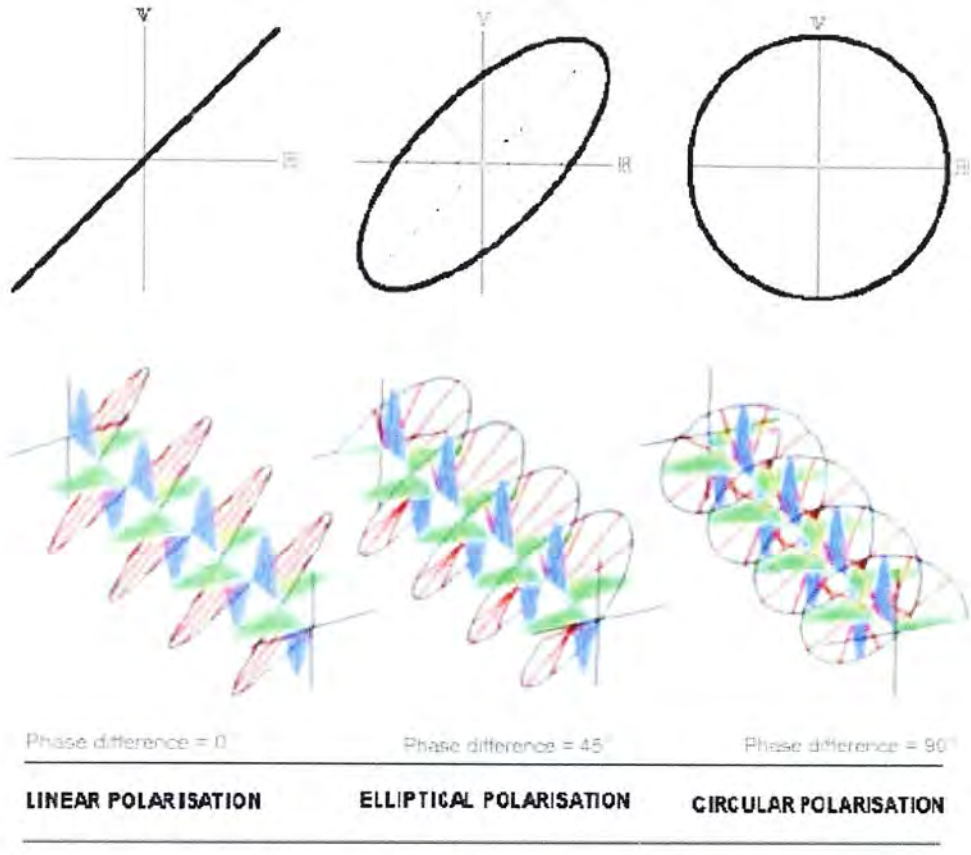

figure 3.2: Illustration of the three major polarization types, which occur as a function of the phase difference between the horizontal (green) and vertical (blue) wave components

Figure 3.2 gives examples of the different forms of wave polarisation, which are described in more detail below:

- Linear Polarisations: Linear polarisations occur when the phase difference (θ_{h_v}) is equal to 0 or π (or integers multiples thereof). In this case, the magnitudes of the relative amplitudes for both the horizontal and vertical wave components are equal with respect to time, and the wave traces a linear path as it propagates through space. When the absolute amplitudes

of both the wave components are equal, the resulting wave is oriented at 45° or 135° for phase differences of 0 or π, respectively. By varying the amplitude of either component, waves of any orientation can be generated.

- Circular Polarisations: When phase difference (θ_{h_v}) is equal to odd integer multiples of $\pi/2$, the path traced by the electromagnetic vector forms a circle when projected onto the plane defined by the orthogonal antennas. Varying the amplitudes of either wave component will result in an elliptical waveform, whose major axis lies parallel to the wave component with the greatest amplitude.
- Elliptical Polarisations: Elliptical polarisations represent a general case of wave polarisation, and occur for all other phase difference values not yet described.

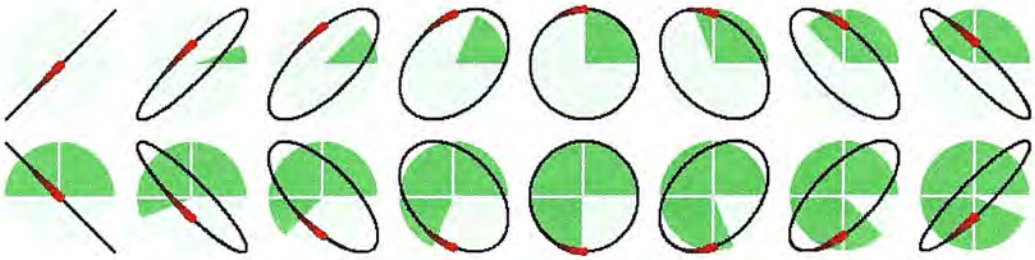

figure 3.3: Diagram illustrating the cyclical nature of phase difference. For each sequential image, the phase difference increases by $\pi/8$ (represented by the shaded portion of the background circle). Note that for phase differences greater than π, the direction of rotation (or handedness) of the propagating wave is reversed.

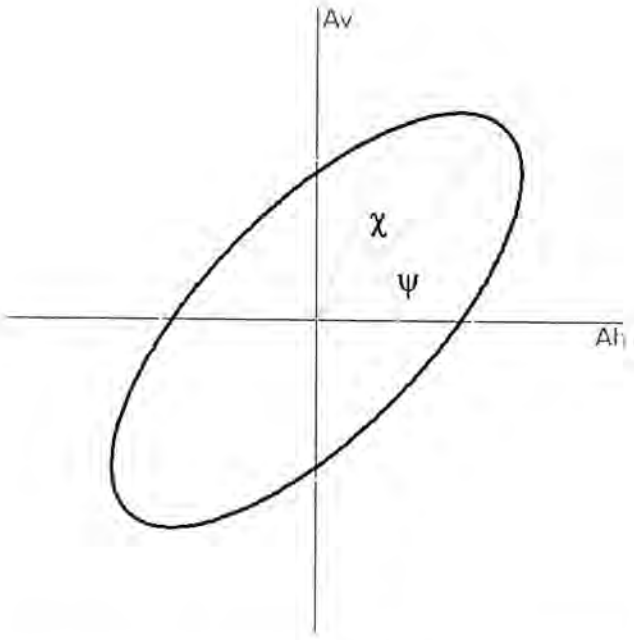

figure 3.4: The polarization ellipse, which can be defined using two parameters; namely, the orientation angle (ψ) and ellipticity angle(χ).

Figure 3.3 demonstrates the relationship between phase difference and waveform. Note that for phase differences between π and 2π the direction in which the wave rotates as it propagates through space is reversed. The direction of rotation is termed the handedness, and is defined as being either left-handed (anti-clockwise) or right-handed (clockwise), using the screw rule, and when viewing the wave from behind the transmitting antennas.

By projecting the path traced by the electromagnetic vector onto a 2D plane, it is possible to represent polarisation states using a polarisation ellipse as shown in figure 3.4. From this representation, it is possible to describe wave polarisation using two further parameters, namely the orientation angle (ψ) and the ellipticity angle (χ). These parameters can be related to E_h, E_v and θ_{h_v} as follows:

$$\begin{aligned} \tan 2\psi &= (\tan 2\alpha)\cos\theta_{h-v} \\ \sin 2\chi &= (\sin 2\alpha)\sin\theta_{h-v} \end{aligned} \tag{3.1}$$

where α is an auxiliary angle defined as follows:

$$\tan\alpha = \frac{A_h}{A_v} \tag{3.2}$$

The value of ψ ranges between $-\pi/2$ and $\pi/2$ whilst the value of χ ranges from $-\pi/4$ and $\pi/4$. Positive (negative) orientation angles thus represent left-handed (right-handed) polarisations.

As can be deduced from figure 3.3, both the orientation angle and ellipticity angle are continuous variables (i.e., they are cyclical, rather than having a definite start and end point). Subsequently, it is possible to represent 2ψ and 2π and longitude and latitude coordinates, respectively, of the so-called Poincaré sphere. From this, it is possible to represent any polarisation as a point on a sphere, where the radius is equal to the total power of the wave (I_o), defined as the square of the total amplitude:

$$I_o = A_h^2 + A_v^2 \tag{3.3}$$

Figure 3.5 shows the Poincaré sphere, parameterised by the aforementioned spherical coordinates (2ψ. 2χ and I_o). Note that the left- and right-handed polarisations are mapped to the upper and lower halves of the globe, respectively.

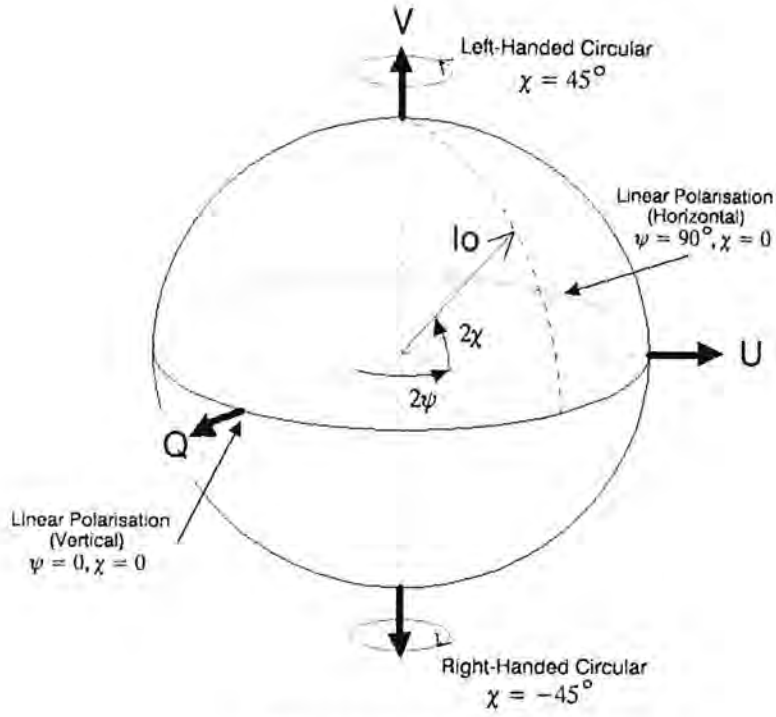

figure 3.5: The Poincaré Sphere

Each point on the sphere can also be referenced by Cartesian coordinates (I_o, Q, U and V in figure 3.5). This final set of coordinates relates to another means of representing wave polarisation known as the Stoke's vector, first introduced in 1852 (Ulaby and Elachi, 1990). The parameters of the Stoke's vector have the distinction of having the same physical dimensions, and thus represent a useful means of representing wave polarisation parameters, as will be explored further in following sections. For now, however, it is important to be aware of the mathematical relationships between the parameters discussed so far:

The Stokes vector can be related to previous wave parameters as follows:

$$\vec{S} = \begin{bmatrix} I \\ Q \\ U \\ V \end{bmatrix} = \begin{bmatrix} A_h^2 + A_v^2 \\ A_h^2 - A_v^2 \\ 2A_hA_v\cos\theta_{h-v} \\ 2A_hA_v\cos\theta_{h-v} \end{bmatrix} = \begin{bmatrix} I_o \\ I_o\cos 2\psi\cos 2\chi \\ I_o\sin 2\psi\cos 2\chi \\ I_o\sin 2\chi \end{bmatrix} \quad (3.4)$$

The various descriptions of polarisation are all utilized at different points in the following sections. The reason for including them here is to illustrate how all of these descriptions can be represented visually, and to demonstrate how all of the mathematical formulations are interchangeable. In the following section, these representations will be used to explain the nature of radar polarimetry.

3.3 – Polarisation Synthesis.

In the previous section, it was shown that the complete set of wave polarisation states could be produced using two orthogonally aligned antennas. In radar polarimetry, this quality is exploited in order to derive backscatter response patterns for all possible combinations of transmit and receive polarisations.

In order to achieve this, a polarimetric radar system (a "polarimeter") uses the equivalent of two orthogonal antennas to transmit microwaves of equal frequency. The backscattered response for each wave is then recorded by both antennas, leading to storage of four separate, complex values for a single resolution element. These values form the base data product from which all other vectors and matrices used in radar polarimetry can be derived, and can be represented using the scattering matrix (S):

$$\bar{S} = \begin{bmatrix} S_{hh} & S_{hv} \\ S_{vh} & S_{vv} \end{bmatrix}, \tag{3.5}$$

Using the scattering matrix, it is possible to derive a secondary matrix, termed the Stokes' matrix (K), which is formed as follows:

$$\bar{K} = 2\bar{R}^{-1T}\bar{W}\bar{R}^{-1},$$

where $\bar{W}$ and $\bar{R}$ are defined as follows:

$$\bar{W} = \bar{S} \otimes \bar{S}^* = \begin{bmatrix} S_{hh}S_{hh}^* & S_{hh}S_{hv}^* & S_{hv}S_{hh}^* & S_{hv}S_{hv}^* \\ S_{hh}S_{vh}^* & S_{hh}S_{vv}^* & S_{hv}S_{vh}^* & S_{hv}S_{vv}^* \\ S_{vh}S_{hh}^* & S_{vh}S_{hv}^* & S_{vv}S_{hh}^* & S_{vv}S_{hv}^* \\ S_{vh}S_{vh}^* & S_{vh}S_{vv}^* & S_{vv}S_{vh}^* & S_{vv}S_{vv}^* \end{bmatrix} \tag{3.6}$$

$$\bar{R} = \begin{bmatrix} 1 & 0 & 0 & 1 \\ 1 & 0 & 0 & -1 \\ 0 & 1 & 1 & 0 \\ 0 & i & -i & 0 \end{bmatrix}$$

*(note that in the above equations, and in others later in this thesis, the subscript * refers to the complex conjugate of a value, while the subscripts –1 and T refer to the inverse and transpose of a matrix, respectively. The above derivation is one of many means of extracting the Stokes' matrix, and is based on the method proposed in (Guissard, 1994))*

The Stoke's matrix allows the backscattered intensity for any combination of transmit and receive polarisations to be derived, through a procedure termed

polarisation synthesis. In this, two Stokes Vectors (as described in the previous section) are constructed using ψ and χ values which represent the transmit and receive polarisations. Theses vectors are termed S_t and S_r, respectively. The required intensity value can thus be found using the following equation:

$$P_{S_t,S_r} = \vec{S}_r \bar{K} \vec{S}_t \tag{3.7}$$

The process of polarisation synthesis leads to a practically infinite set of polarisation combinations. In practice, therefore, a smaller, but representative sample of polarisation states is used, which are termed the co-polarised (co-pol) and cross-polarised (cross-pol, or x-pol) responses.

The co-pol response set is defined as the polarisation combinations where S_t and S_r, are equal. The cross-pol response set uses values for S_t and S_r which represent antipodal opposites when plotted on the Poincaré sphere (figure 3.5). In practice, for a given polarisation, the cross-pol value can be found by adding π (i.e. 90°) to the orientation angle, and changing the sign of the ellipticity angle.

Even when using this subset, the number of values generated for a single pixel using polarisation synthesis is considerable. Using a 5° increment for ψ and χ, for example, a total of 648 individual intensity values must be considered.

The visualisation of these values therefore is not straightforward. In the following section, one common mode of representation, the polarimetric response graph, is

introduced, and used to illustrate the types of information contained in polarimetric radar data.

3.4 – Interaction Types

In previous sections, discussion on the nature of radar polarimetry has been largely restricted to the means by which polarised waves can be produced, recorded and synthesised. In this section, the information content of polarimetric datasets is examined more closely.

The practical basis of radar polarimetry is the measurement of how, and why, different landscape elements change the polarimetric properties of microwaves. Early papers on the possible environmental applications of radar polarimetry were based around the concept of dominant interaction types (Zebker et al, 1987, van Zyl, 1989). An understanding of these interaction types is fundamental to an understanding of radar polarimetry in general, as much of the terminology used in these early papers continues to dominate research literature to the present day (Fortuny-Guasch et al., 2003, Qong, 2002).

The nature of the interaction types discussed in these early papers relate to the geometric alignment of scattering objects in a resolution element, and the effects these alignments have on the polarisation of propagating waves. In figure 3.6, a number of different interaction types are described with respect to forested environments. Two of these interaction types, namely the surface and dihedral scattering, are defined by the number of times the incident wave is reflected off

different objects, before returning to the sensor. As a result, these interactions are often termed single and double bounce interactions, respectively. Such interaction types, when considered in isolation have well-defined polarimetric response patterns, which are considered in more detail in the following section.

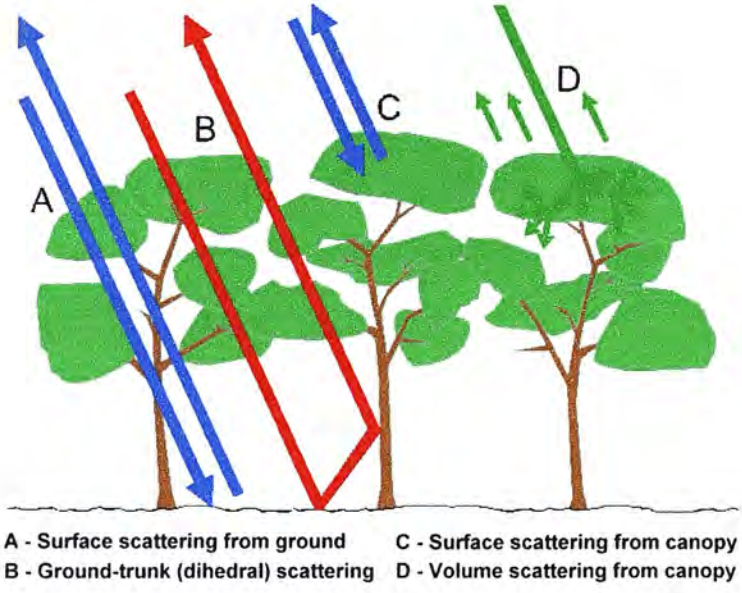

figure 3.6 – Polarimetric interaction types, illustrated with reference to forested environments.

The third interaction type (D in figure 3.6) is a more general case, where multiple interactions lead to a more random backscattered response pattern known as volume scattering. The distinction between these three types of scattering has dominated the study of radar polarimetry, and is a recurrent theme in further descriptions of polarimetric radar data. In the following section, the means by which these interactions, and others, are evident in visual representations of polarimetric datasets is considered in more detail.

3.5 – Polarimetric Response Graphs

The polarimetric response graph is a standard visualisation technique used in radar polarimetry to examine backscatter values for the co- and cross-polarised response channels. The graphs were first presented in (Zebker et al., 1987), where they were used to illustrate the calibration of polarimetric datasets, and to characterise the response patterns over different landscape components. Since this time, the polarimetric response graph has been used to examine response patterns over forests (Durden et al., 1989), agricultural areas (Skriver et al., 1999, Lemoine, 1992), and geomorphological landscape units (Dall et al., 1995), and has also been used in estimating slope angles (Schuler et al, 1995).

The polarimetric response graph is typically represented as a pair of isometric surfaces, where the base axes describe the orientation (ψ) and ellipticity (χ) angles defining the polarisation of the transmitted wave. The height of the surface at any point, therefore describes the normalised backscattered intensity (σ) for a given polarisation combination.

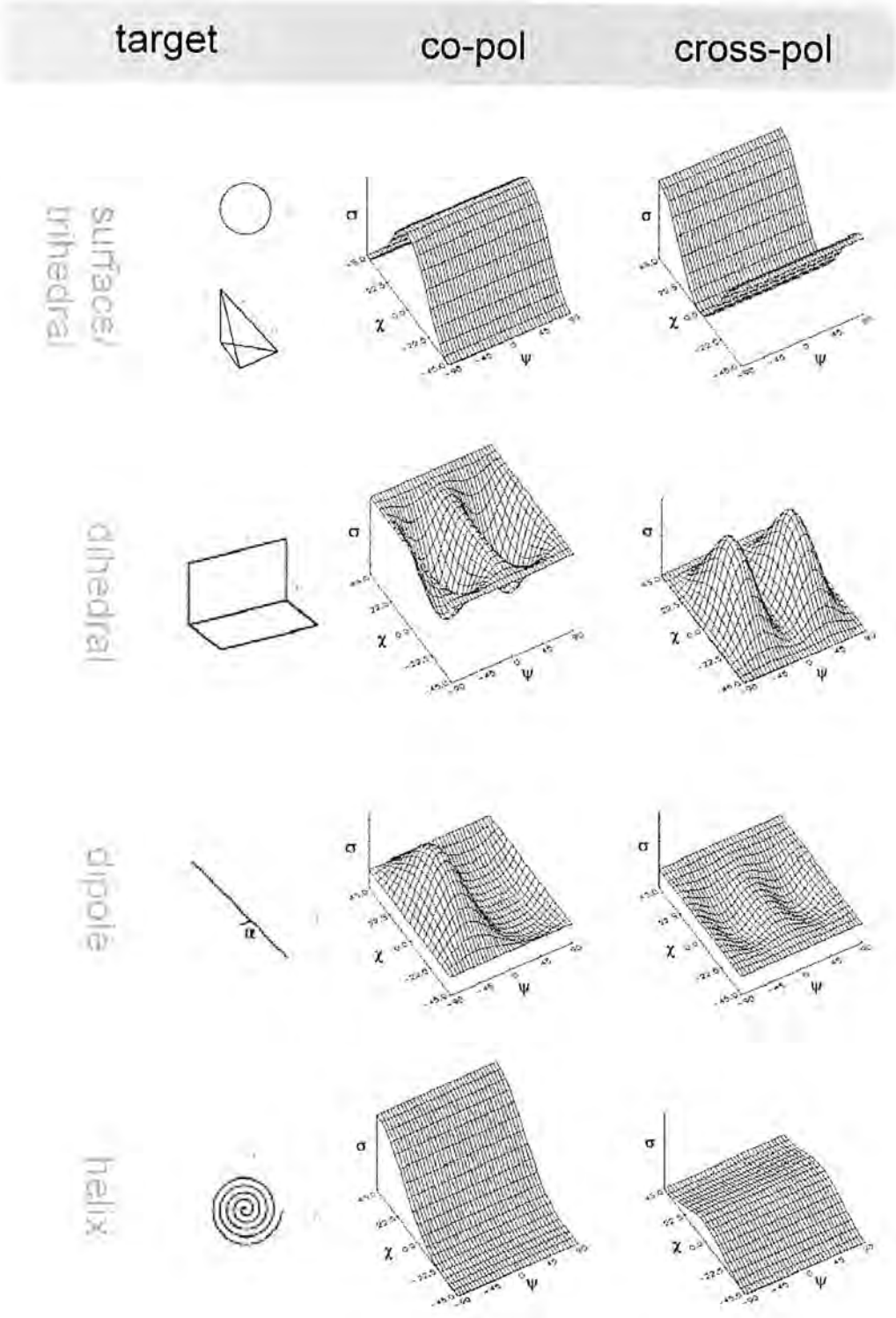

figure 3.7: Polarimetric response graphs for idealized scattering objects.

In Ulaby and Elachi (1990), a number of response graphs are presented for idealised scattering objects. Some of these objects (i.e. the sphere and dihedral) are closely correlated with the interaction types described in the previous section. The other patterns (i.e. the dipole and helix), are less common in phenomenological response patterns, but are nevertheless useful in understanding the nature of polarimetric interactions.

The top row of figure 3.7 shows the polarimetric response graph scattered from a sphere with a radius greater than the wavelength of the incident wave. The scattering properties of a sphere were first described by Mie (from Ulaby and Elachi, 1990) and is conceptually the most simple interaction to describe, and thus forms a useful introduction to polarimetric scattering. A sphere, or a flat surface that is large in relation to the radar wavelength will reflect incident energy in much the same way that a mirror would reflect light. In practice, this means that the reflected energy will have an opposite sense of rotation (when seen from the point of view of the radar instrument), but will be otherwise identical. This is clearly evident in the response graphs, which have minima in the co-pol response for the circular polarisations as a result of this change in handedness. The maxima, in contrast, occurs along the linear polarisations, where $\chi = 0$ and no handedness can be defined. On the cross-pol graph, this pattern is reversed, with maxima for the circular polarisations again reflecting the apparent change in handedness.

The observation of this type of response pattern in recorded data is often linked to the presence of surface interactions, as represented in figure 3.6. The total power returned from such a surface is primarily a function of both the properties of the surface, and the angle of inclination relative to the incidence angle of the radar wave. As such, high responses are expected for smooth reflective surfaces that are inclined normal to the incident wavefront. These variations in total received power, however, cannot be deduced by viewing the response graph alone, however, as the graphs are usually normalized to accommodate the variation of total intensity caused by viewing geometry. This ensures that the emphasis is placed on the polarimetric response alone, rather than intensity.

The second row of figure 3.7 shows the polarimetric response pattern associated with dihedral interactions. A perfect dihedral reflector (also known as a "corner reflector" or "double-bounce" interaction) can be thought of as two mirrors that are aligned orthogonally. A radar wave that strikes either surface perpendicular to the bisecting line of the two surfaces will undergo two reflections, and return in the direction from which it came. The response pattern of a dihedral, as shown in figure 3.7, is an extension of the surface interaction, in that it describes the interaction of a wave with two surfaces. Just as a single surface will reverse the direction of wave propagation, a dihedral will cause the wave to revert back to its original handedness, hence the maxima for the co-pol response in the case of circular polarisations.

The response patterns for the linear polarisations is more interesting, as it exhibits two clear minima in the co-pol response pattern at +/-45°. The cross-pol response pattern is, again, the inverse of the co-pol. This pattern is the result of a phase shift of 180° between the horizontal and vertical wave components. For the horizontal and vertical linear polarisations, this has no effect as the incident wave has no vertical or horizontal component, in each respective case. As a result the co-pol response for these polarisations remains high. Where ψ= +/-45°, however, the phase shift results in a rotation of the incident wave by 90° (see figure 3.3 for visual confirmation of this), leading the minima in the co-pol and maxima in the cross-pol response patterns.

The occurrence of dihedral response patterns in observed data is very useful as it allows an assessment of the geometrical structure of scatterers with a resolution element. Many features of the natural and anthropogenic environment, such as tree trunks and buildings, act as dihedral-type reflectors. Note also that the addition of a third reflective surface results in a trihedral reflector. The addition of an extra surface once more reverses the direction of rotation, and causes a phase shift of 180°, resulting in a response pattern that is identical to that of a sphere. Trihedral corner reflectors are often deployed in radar scenes to act as calibration targets (for example, see Cloude et al, 2001), as the geometrical configuration of surface results in high backscatter values with a well-defined polarimetric structure within a wide range of viewing directions.

The two remaining response pattern structures define backscatter for a dipole and a helix. These patterns are useful in that they demonstrate how the geometrical configuration of scatterers can affect backscatter response. In the case of the single dipole scatterer, a peak response occurs in the co-pol response where the orientation angle of the incident wave matches the orientation of the dipole. Similarly, a helical scatterer will produce high responses in the co-pol cases where the handedness of the helix matches the handedness of the incident wave and a null response occurs where the handednesses differ.

Dipole structures are commonly used in the mathematical modeling of crops and forests (for examples, see Ferrazolli and Guerriero, 1994 or Woodhouse and Hoekman, 2000). Some level of helical scattering is sometimes observed in actual data sets but there is very little evidence for this being a consequence of physical helicity within the vegetation (Cloude, 2002). The observation of such well-defined polarimetric response patterns in phenomenological radar data is rare, however, as resolution elements containing such structures typically consist of large numbers of different scatterers that may not have any particular orientation. This in turn leads to the depolarization of the backscattered signal, which is evident in the polarimetric response graph as a pedestal, or minimum level of backscattered response which is independent of polarisation (Van Zyl, 1989). In terms of interaction types, the presence of a pedestal, or shoulder, in the polarimetric response graph is indicative of volume, or multiple, scattering.

In summary, the polarimetric response graph represents a visualisation technique that attempts to convey a large number of backscatter intensities in order to represent the interactions of polarised waves with landscape objects. An inherent disadvantage of this technique, however, is that, by choosing to represent a large number of polarisations with such an elaborate visualization method, it is necessary to sacrifice the spatial relationships that are an important aspect of remotely sensed data. In the following sections, visualisation techniques which attempt to represent these spatial variations are considered in more detail.

3.6 – Synoptic Intensity Images

Ever since the advent of aerial photography, the use of intensity imaging has been a fundamental visualisation technique in the analysis of remotely sensed data (see chapter 2). It is unsurprising, therefore, that this technique has also been applied to the visual analysis of polarimetric radar datasets. The benefits of using intensity images, as outlined in chapter 2, is that they allow for an analysis of the spatial relationships which may exist within datasets. The application of traditional intensity imaging to polarimetric data, however, is problematic, as the number of intensity channels available inhibits effective and representative visualization.

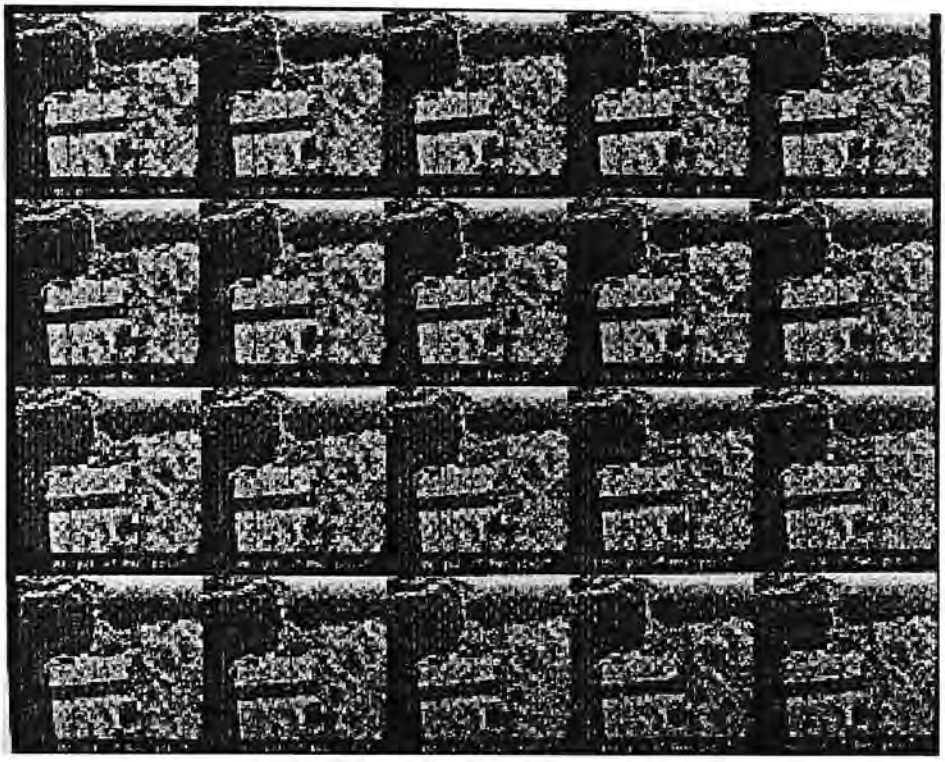

figure 3.8: Small multiples showing backscattered intensity over San Francisco at multiple L-band polarisations. Each images represents a rotation of the orientation angle by 2.5° (from Van Zyl et al., 1987).

As an example of this, figure 3.8 shows an early attempt at visualizing polarimetric radar data using small multiples (Tufte, 1983) representing sequential changes in ψ (Van Zyl et al., 1987). The resulting reduction in scale required for each image, however, reduces the effectiveness of the graphic, as the low resolution inhibits the observation of patterns or differences between individual images. In addition, the incremental changes in polarisation parameters lead to only minor differences between individual image frames, and thus it is unlikely that any patterns will be observable.

The use of RGB colour composites for representing polarimetric datasets is also problematic. In practice, any combination of polarisation channels can be used to

form an RGB composite. However, the choice of polarisation combinations used requires a priori knowledge of the scattering properties of features that are likely to be of interest. This, in effect, reduces the utility of the RGB composite in terms of exploratory visualisation of data sets where the types of relevant polarimetric response cannot be assumed beforehand.

It is also common to see RGB composites formed from the channels that are most easily extracted from the original scattering matrix. Figure 3.9, for example, shows an RGB colour composite formed using values extracted from the covariance matrix. The covariance matrix (C) is a transformation of the scattering matrix that allows direct access to intensity values:

$$\vec{S}_l = \begin{bmatrix} S_{hh} & \sqrt{2}S_{hv} & S_{vv} \end{bmatrix}^T \tag{3.8}$$

$$C = \vec{S}_l \vec{S}_l^{*T} = \begin{bmatrix} |S_{hh}|^2 & \sqrt{2}S_{hh}S_{hv}^* & S_{hh}S_{vv}^* \\ \sqrt{2}S_{hv}S_{hh}^* & 2|S_{hv}|^2 & \sqrt{2}S_{hv}S_{vv}^* \\ S_{vv}S_{hh}^* & \sqrt{2}S_{vv}S_{hv}^* & |S_{vv}|^2 \end{bmatrix}$$

Note that the diagonal elements of this matrix are real number that represent the backscatter intensity for two co-polarised channels (hh and vv) and one co-polarised channel (hv). The trace of this matrix (i.e. the sum of the diagonal elements) thus represents the total power received by the sensor.

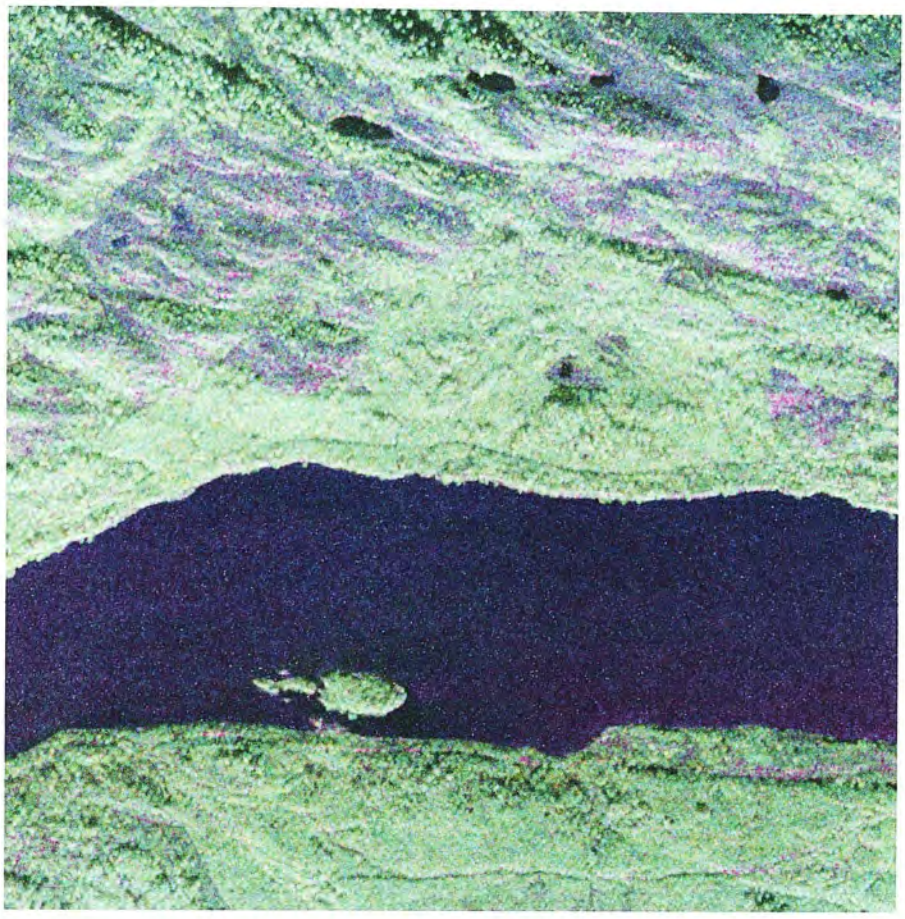

Figure 3.9: RGB colour composite of Glen Affric formed using total power variables from the covariance matrix.
hh = Red, hv = Green, vv = Blue

The resulting RGB composite appears similar to RGB composite formed from passive multi-spectral sensors, or multi-frequency SAR instruments. However, the optical analogy is weakened by the fact that the different channels represent polarisation states that do not act as colour analogues in the same way as spectral bands or discrete frequencies. By assigning the cross-pol channel to the green colour gun, the presence of vegetation (which has a high cross-polarised response due to the volume scattering of the canopy) is clearly evident. The difference between the hh and vv channels, (assigned to the red and blue channels, respectively) is less clear,

In figure 3.10, an RGB composite is thus formed which represents surfaces in blue, dihedrals in red and volume scattering in green. Whilst similar in appearance to the image shown in figure 3.9, this image is easier to interpret as each colour channel is now ascribed to a particular type of scattering mechanisms. Both techniques, however, have a disadvantage in that the reliance on these three scattering types may lead to problems in interpreting areas with well-defined scattering regimes which exist outside of this simple trichotomy.

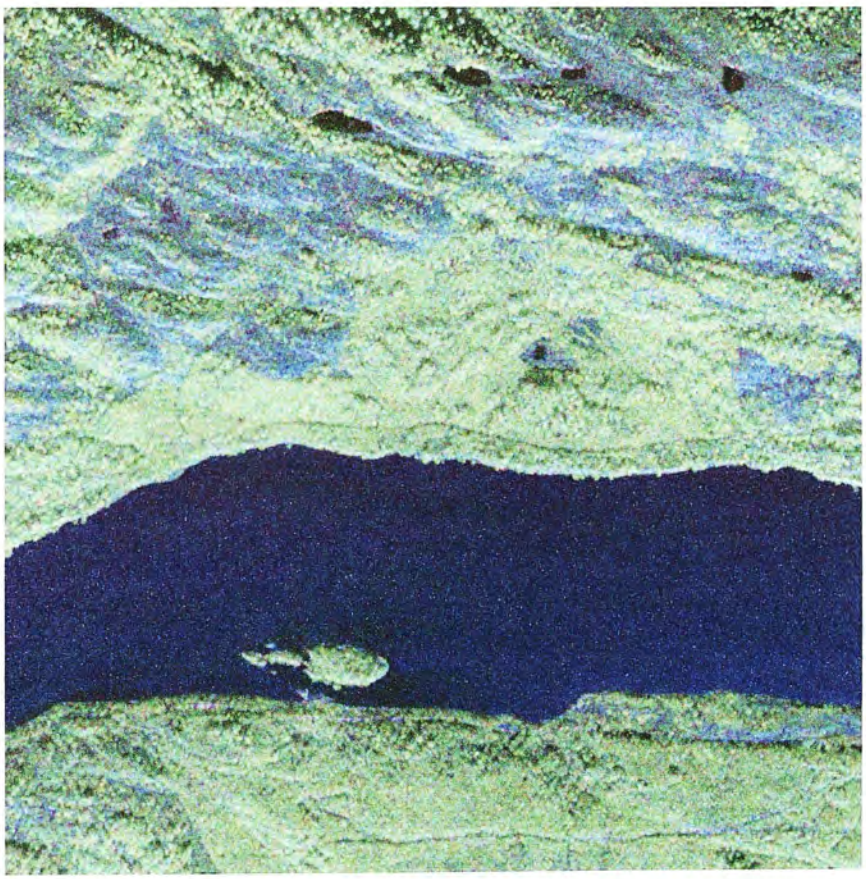

Figure 3.10: RGB composite for the same area as in figure 3.9, formed using intensities from the Coherency matrix.
hh-vv = red, 2hv = green, hh+vv = blue

due to a lack of any cognitive link between the data variable, which is determined by orientation, and the visual variable, which defines colour.

A more useful representation, in this respect, is to use intensity values derived from the coherency matrix, T. This is formed in a manner similar to the covariance matrix, but uses an initial vector which is formed through the application of the Pauli spin matrices to the original scattering matrix (Cloude and Pottier, 1996)

$$\vec{S}_p = \frac{1}{\sqrt{2}} \begin{bmatrix} S_{hh} + S_{vv} & S_{hh} - S_{vv} & 2s_{hv} \end{bmatrix}^T \tag{3.9}$$

$$\begin{aligned} T &= \vec{S}_p \vec{S}_p^{*T} \\ &= \begin{bmatrix} |S_{hh} + S_{vv}|^2 & (S_{hh} + S_{vv})(S_{hh} - S_{vv})^* & 2(S_{hh} + S_{vv})S_{hv}^* \\ (S_{hh} - S_{vv})(S_{hh} + S_{vv})^* & |S_{hh} - S_{vv}|^2 & 2(S_{hh} - S_{vv})S_{hv}^* \\ 2S_{hv}(S_{hh} + S_{vv})^* & 2S_{hv}(S_{hh} + S_{vv})^* & |4S_{hv}|^2 \end{bmatrix} \end{aligned}$$

The advantage of this approach is that the individual intensity values defined by the diagonal matrix component can be more easily related to the interactions types, as shown in figure 3.6, because now the relative phase difference between the co- and cross-pol channels is accounted for. The hh+vv channel thus produces high values for surface interactions, and low values for dihedrals. This pattern is reversed for the hh-vv channel, whilst the presence of volume scattering leads remains encoded in the hv response. Note also that, as with the covariance matrix, the sum of the diagonal elements of the coherency matrix is equal to the total power received by the antenna array.

3.7 – Polarimetric Phase Difference and Coherence

The Covariance Matrix, introduced in the previous section, is additionally useful as it can be used to derive two further variables; namely, the polarimetric coherence and phase difference. Both of these variables can be defined from the off-diagonal components of the coherency matrix, which defines the complex coherence between any two antenna configurations (i.e. hh-vv, hh-hv and hv-vv). In practice, the complex coherence for the hh-vv channel is most commonly used in research.

The polarimetric coherence describes the correlation in phase differences between the hh and vv channels, and thus defines the 'randomness' of scattering. It can be estimated as follows:

$$\gamma_{hh-vv} = \frac{S_{hh}S_{vv}^{*}}{\sqrt{S_{hh}S_{hh}^{*\,2} + S_{vv}S_{vv}^{*\,2}}} \tag{3.10}$$

This results in a complex number, the magnitude of which can be used to assess the number of scatters in a single resolution element. High values of the coherence magnitude suggests the presence of a single, well defined scattering regime over the area of interest, whereas low values are indicative of volume scattering. This relationship is illustrated in figure 3.11, which inversely maps coherence to the saturation of a green hue overlain on a background intensity image. The resulting image allows a clear distinction between forested and non-forested regions.

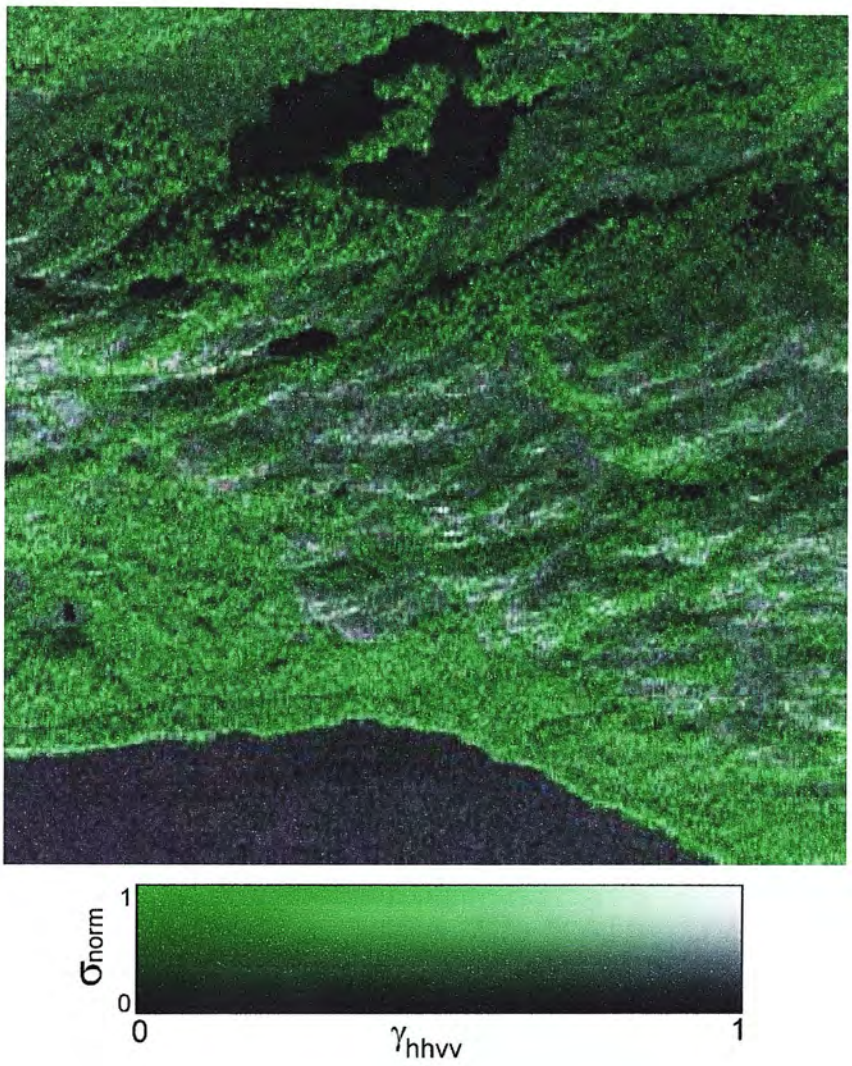

figure 3.11 – Visualisation of polarimetric coherence. The coherence is inversely mapped to a green saturation channel, and overlain on a greyscale intensity image.

The polarimetric phase difference measures the difference in phase between the hh and vv channels, and can be derived as follows:

$$ppd_{hh-vv} = \tan^{-1}\frac{\Im(S_{hh}S_{vv}^{*})}{\Re(S_{hh}S_{vv}^{*})} \tag{3.11}$$

This results in a value between 0° and 180°, which can be related back to the interaction types and polarimetric response graphs discussed in sections 3.3 and 3.4. From this, it can be deduced that a polarimetric phase difference close to zero are indicative of surface scattering, whilst values close to 180° indicate dihedral interactions. Volume scattering, in contrast produces random phase difference values across the entire range.

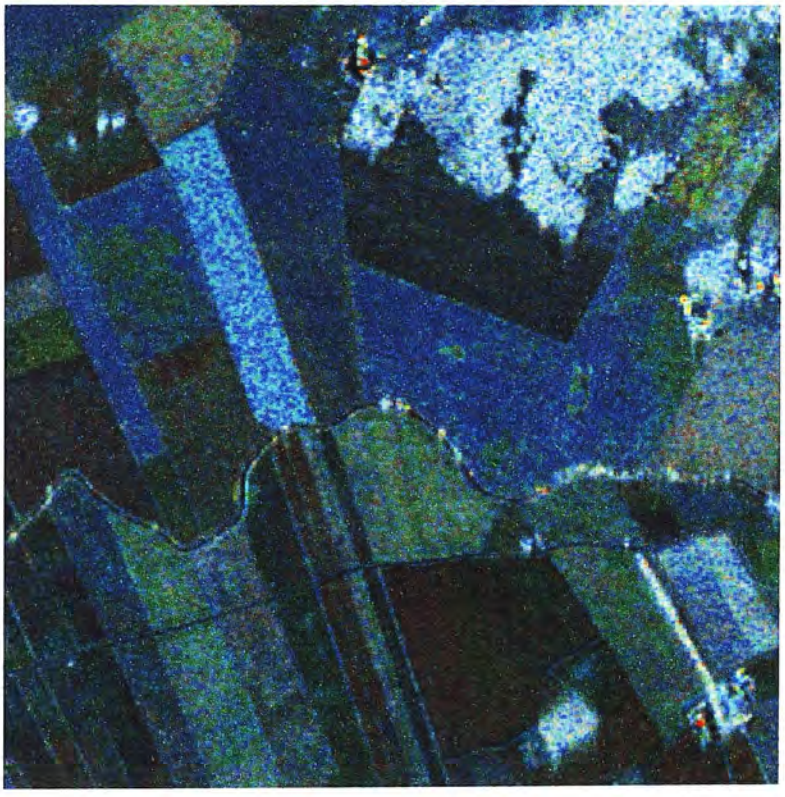

Figure 3.12 – An HSV composite showing polarimetric phase difference, coherence and total power. Phase difference values ranging between 0° and 180° are inverted and re-scaled to occupy the hue range between 0° (red) and 240° (blue).

The polarimetric phase difference and coherence are similar in structure to the phase difference and coherence variables used in radar interferometry – the former examines the similarity of waves of different polarisation, whereas the latter examines the similarity of waves from different locations, or times. For this reason, it is possible to represent these values using an HSV composite, producing an image with similar qualities to an Interferogram (cf. chapter 2). Such a visualisation was proposed by (Imbo and Souryis, 1999) and applied to variables with similar characteristics which can be derived from the Entropy/α decomposition (which will be discussed in detail later in this chapter).

Figure 3.12 shows the application of an HSV composite to an L-band polarimetric dataset over an agricultural area in Sweden. The value, or intensity channel is composed of the total power, or span image for the region, providing important structural and contextual detail. The polarimetric phase difference is inversely mapped to the hue channel so that values from 0° to 240° in hue (i.e. from red through green to blue) represent phase difference values between 180° and 0° (dihedral to surface interactions, respectively). The polarimetric coherence is then mapped to the saturation channel, so that areas of low coherence are represented by grey scale values, whilst areas of high coherence have a well-defined hue.

From the image shown in figure 3.12, it is readily apparent that the nature of the polarimetric phase difference has qualities that are distinctive from interferometric phase differences, which render the visualisation structure less powerful. For an

interferogram, the predictable relationship between phase and topography results in a regular pattern of fringes of colour over areas of high coherence (as shown in chapter 4). In polarimetric datasets, however, the patterns of phase values are less predictable due to large-scale variations in interaction types. While some authors have observed areas of relatively continuous (i.e. stable) phase difference values over agricultural areas (Ulaby et al., 1987, Boerner et al, 1987), these tend to occur in isolated patches within otherwise highly variable areas. This variability is clearly evident in figure 3.12, where few areas of continuous phase difference values are present even in areas of (relatively) high coherence. The primary benefit of such images, in terms of visualisation, therefore, is in the identification of hard targets with well-defined scattering characteristics, such as the yellow/red pixels indicating buildings (and thus, dihedral interactions) in figure 3.12.

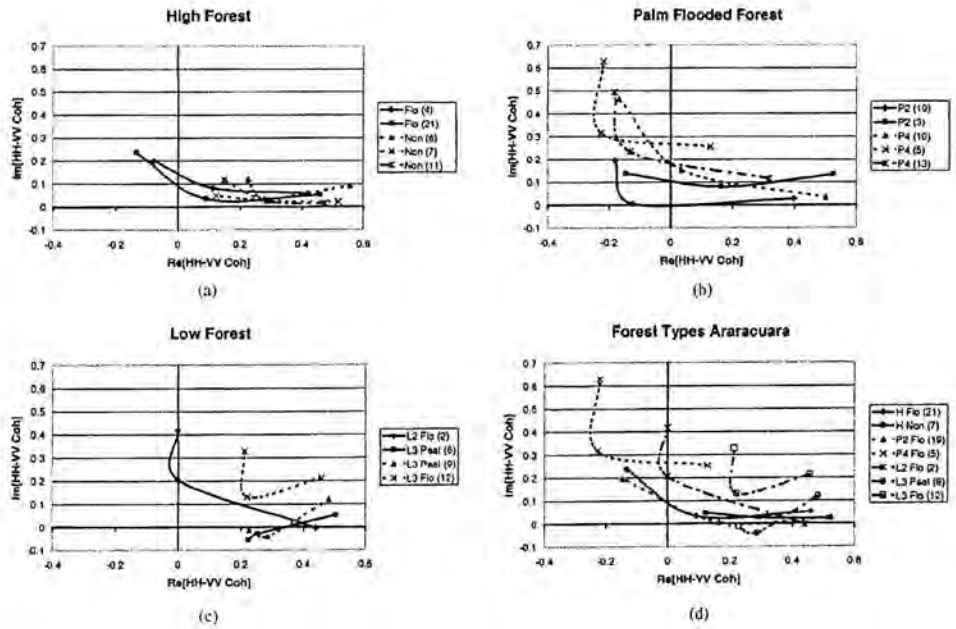

Figure 3.13: Scatterplots showing the polarimetric phase difference and coherence for forested areas at different frequencies (from Hoekman and Quinones, 2001)

As with the polarimetric response graph, however, it is possible to examine the nature of polarimetric phase difference and coherence at a more specific level. In (Hoekman and Quinones, 2001), for example, polarimetric phase differences and coherence values were examined for multiple polarisations over forested areas. The results of this analysis were presented as scatterplots, using the real and imaginary components of the hhvv channel of the covariance matrix (examples of which are shown in figure 3.13). These graphs essentially represent polar plots, where the argument and magnitude of each point represents the phase difference and coherence, respectively. By joining points representing these values for different frequencies over different forest types, information can be derived on the nature of polarimetric scattering. In general, it is shown that as frequency increases (from C- through L- to P-band), phase differences values will migrate from surface to volume or dihedral scattering, whilst coherence generally increases. Such a relationship is indicative of greater canopy penetration at longer wavelengths, and variations in these patterns can be used to infer canopy and stand density within areas of homogenous species. Such inferences can subsequently be used, alongside backscatter intensity as a basis for classification (Hoekman and Quinones, 2003).

The visualisation of such patterns at the synoptic scale, however, is inhibited by the need to represent three pairs of values (i.e. phase and coherence) at each pixel. The benefit of developing a synoptic approach, would be to allow patterns in multi-frequency data such as those proposed by Hoekman and Quinones, to be correlated with spatial patterns in a more effective and straightforward manner.

3.8 – Decomposition Techniques

In mathematics, the definition of decomposition is 'the expression of a given object or quantity in a number of simpler components' (Borowski and Borwein, 1989). In terms of radar polarimetry, the process of decomposition is typically used to condense the scattering matrix (or permutations thereof) into a small number of characteristic variables. A concise review of the many decomposition techniques used in radar polarimetry was published by Cloude and Potter (1996). The wide scope of this article, however, is outwith the current aims of this thesis so that only two of the most commonly used techniques; namely, the Freeman decomposition and the Entropy/α Eigenvalue decomposition (also known as the H/α decomposition), will be considered.

The so-called "Freeman decomposition" was developed by Freeman and Durden (1998). It attempts to decompose the covariance matrix into three separate matrices representing surface, volume and dihedral interactions. In previous sections, it was shown that these interactions are a commonly used means of describing polarimetric datasets. Indeed, early papers in radar polarimetry such as Van Zyl (1989) uses the dominance of one of these interaction types as a basis for classification. The Freeman decomposition, however, goes one stage further by allowing three separate intensity values to be extracted which give the relative proportions of each type of scattering for a single resolution element. The approach used in this decomposition assumes that the backscatter from individual scattering elements is additive. Put simply, this assumes that each resolution element consists of three scattering elements

representing the volume, surface and dihedral components, and that the polarised backscatter from each of these components does not interact (i.e. change the polarisation) of the others.

As the Freeman decomposition results in the output of three intensity channels, it is ideally suited to visualisation using an RGB colour composite. By assigning the red, green and blue channels to dihedral, volume and surface scattering, respectively, an image can be created which presents the results of the decomposition in a straightforward manner, particularly in the context of forest research.

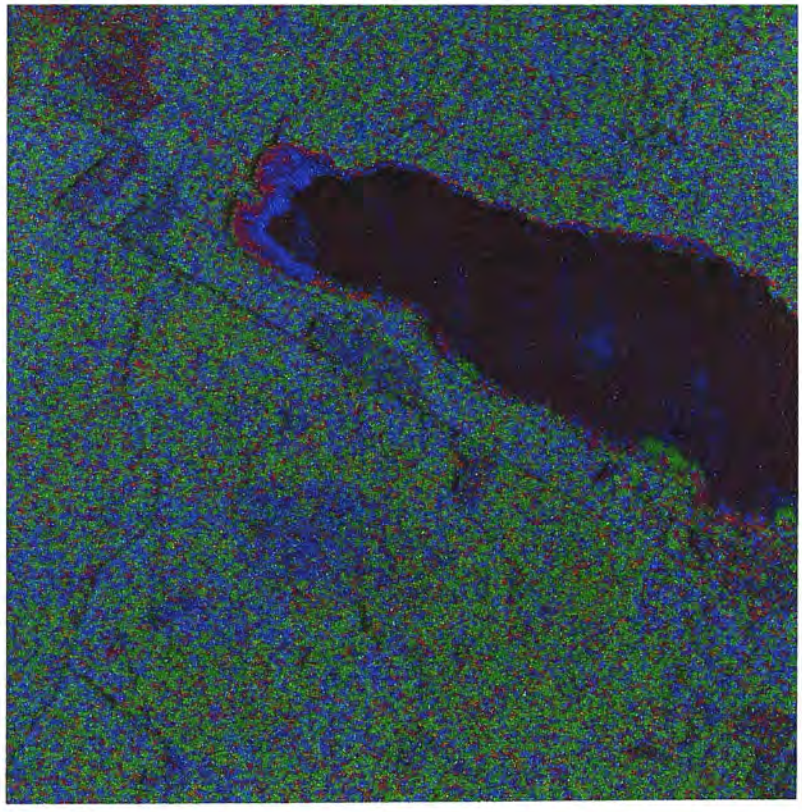

Figure 3.14: Application of the Freeman decomposition to a forested area in Sweden. An RGB colour composite is used to reflect the relative intensities of the double (red), volume (green) and surface (blue) scattering components.

In figure 3.14, the results of the Freeman decomposition are applied to a L-band dataset taken over an area of boreal forest in Sweden. The resulting image clearly shows varying patterns of canopy density over the region, which is evident in the relative proportions of blue and green. The occurrence of dihedral interactions (i.e. red pixels), however, occurs only in isolated cases, and they are more likely to be found in areas of young or recently felled trees, where trunks and snags are more exposed.

The Freeman decomposition, whilst widely used in polarimetric radar literature as a basis for classification (for example, in Lee at al., 2004), has the disadvantage of applying a prescriptive approach to the analysis of polarimetric datasets. This approach relies on the validity of using three scattering mechanisms to define all types of polarimetric interaction, and thus runs the risk of either ignoring or misrepresenting polarimetric interactions that fall outside of this classification scheme. The application of the Freeman decomposition therefore, does not aim to describe unusual response patterns, such as those described by both (Boerner et al., 1987) and (Ulaby et al., 1987), which are related to transmission effects caused by vertical dipoles in agricultural areas.

Images derived from the Freeman decomposition (such as the one shown in figure 3.14), therefore, do not fulfil the requirements of scientific visualisation, as they represent an interpretation of polarimetric radar data that is based on a number of assumptions. Areas or pixels that contain response patterns that deviate from these assumptions, such as those described in (Boerner et al., 1987) and (Ulaby et al.,

1987) are therefore likely to be misinterpreted or ignored in the visual representation, just as they are in the mathematical structure of the decomposition.

A second decomposition approach, developed by Shane Cloude and Eric Pottier (1996), uses an eigenvector-based decomposition of the coherency matrix to derive a number of variables which characterise the scattering properties of resolution elements. This approach has a number of advantages: firstly, the eigenvalue decomposition results in variables which are *basis invariant*: that is, they are independent of the antenna configuration used to collect the data. Secondly, the decomposition results in single-value variables which can be used as a basis for classification (Cloude and Pottier, 1997). A final advantage is that, unlike the Freeman decomposition, the variables produced by this approach are abstract, and do not attempt to directly describe physical features in the landscape. The user is therefore able to interpret the values based on patterns in the datasets, rather than the assumptions of the decomposition approach.

The two most commonly used variables used are the entropy (H), and the alpha angle (α). These two variables can be considered as basis invariant version of the coherence and phase difference values explored in section 3.6. The advantage of using basis-invariant parameters is that they provide singular values describing different scattering properties that, unlike the polarimetric phase difference and coherence values, are invariant with respect to the choice of polarisation chosen.

As with the phase difference and coherence, the entropy and alpha angle are inter-related variables: as entropy increases it becomes less possible to distinguish different scattering mechanisms. This can be illustrated by producing a scatter plot of entropy versus alpha, as shown in figure 3.15. All points within this graph fall within limits set by upper and lower curves, which progressively reduce the range of obtainable alpha angle values as entropy increases, leading to a singularity when $H = 1$, where the only obtainable value for $\alpha = 60°$ (Cloude and Pottier, 1997).

Using the Entropy-Alpha space defined above, it is possible to perform a classification on polarimetric images using different 'zones' of the bounded space, an example of which is also shown in figure 3.15. Using this technique, Cloude was able to illustrate differences in scattering regimes which act as a function of wavelength over forested areas (Cloude and Pottier, 1997), and has since become a widely adopted treatment for polarimetric datasets.

Despite the interesting results achieved by this classification procedure, the images which are commonly presented do not function adequately as a data visualisations. The use of fixed boundaries in H-α space render such images as presentation devices, designed to illustrate the effectiveness of the classification technique, rather than tools to encourage data exploration. In order for this mode of presentation to achieve the goals of visualisation, an interactive version would need to be produced, where users are encouraged to shift the prescribed boundaries in order to observe the changes in classification.

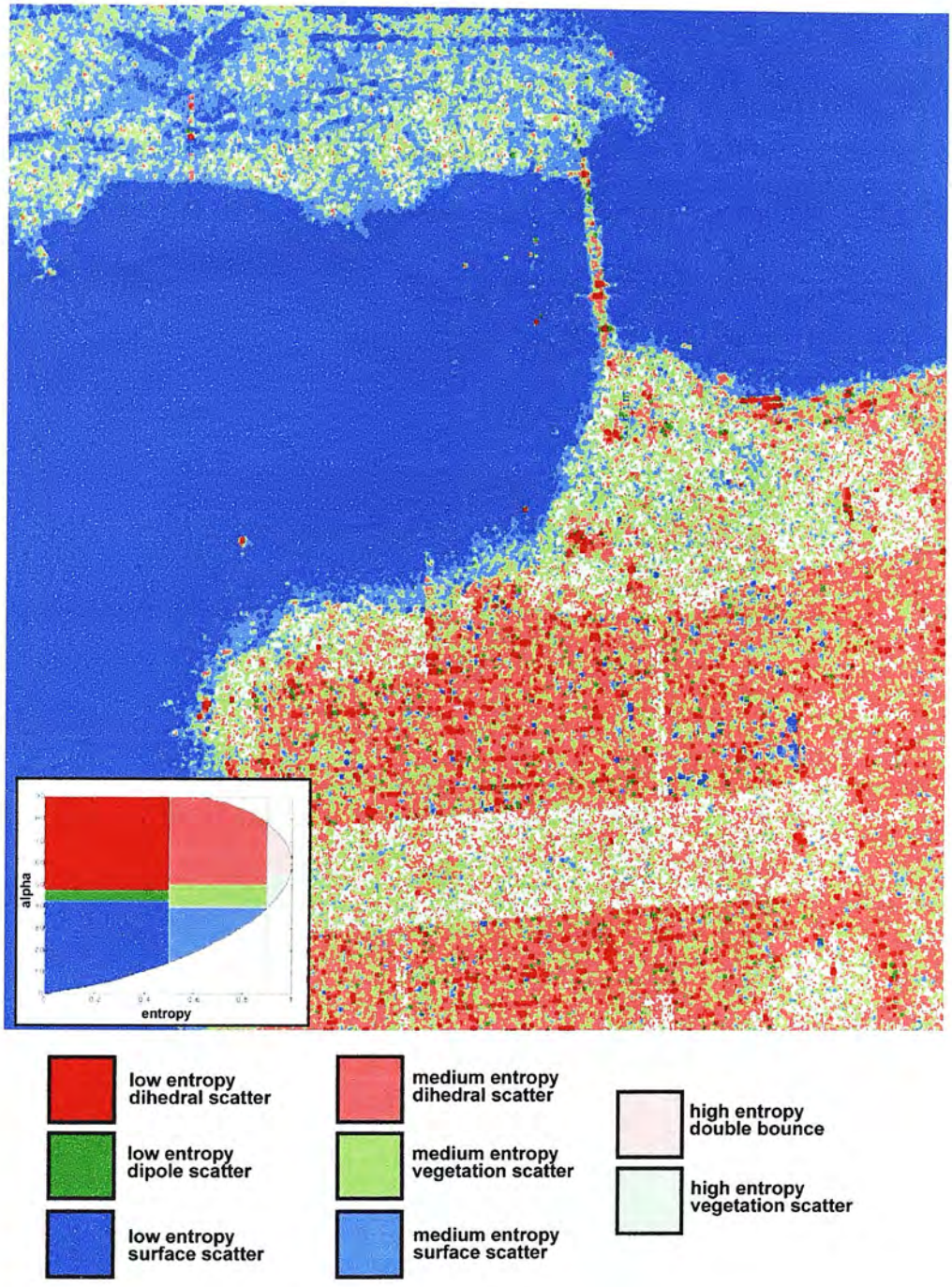

figure 3.15 – Classification of L-band data over San Francisco based on the subdivision of α-H (alpha-entropy) space. The graph to the left of the image shows the feasible range of α and H values divided into colour coded regions representing different scattering types. Note that this classification effectively distinguishes between urban, ocean and vegetated areas in the San Francisco image.

As was briefly mentioned in section 3.6, however, it is possible, however, to produce a visualisation of these parameters that does not attempt to classify the data prior to visualisation. The HSV visualisation technique defined by Imbo et al. (1999) and described in section 3.6 was originally designed to visualise the entropy and alpha angle parameters, in conjunction with the total power variable.

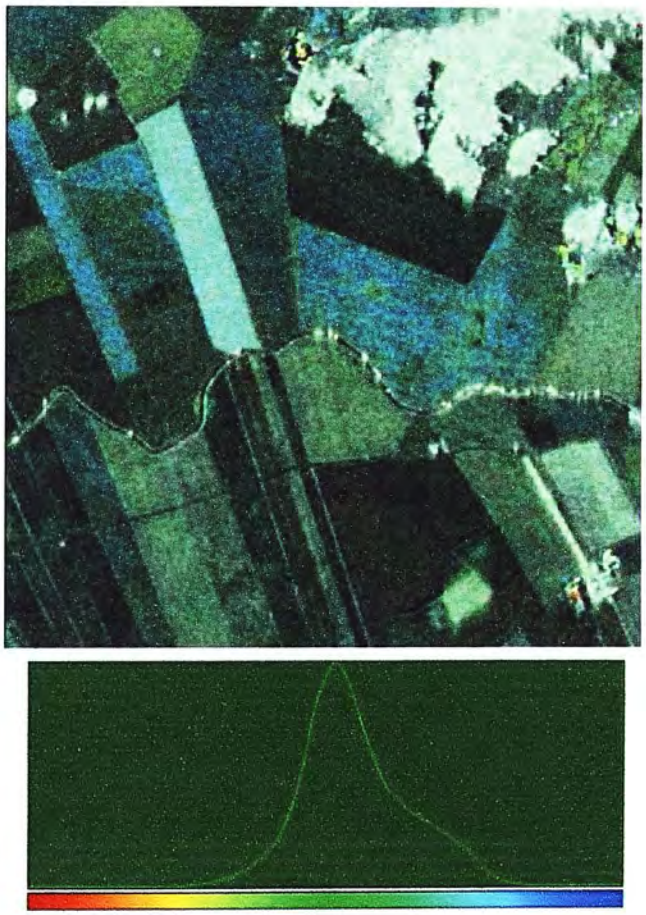

figure 3.16 –Alpha angle, entropy and total power mapped to hue, saturation and value, respectively. Note that the entropy value is inverted, so that areas of low entropy are represented by highly saturated pixel. The image used shows an agricultural area in Fjardhundra, Sweden.

To achieve this, the alpha angle is rescaled to range between 0° and 240° (red to blue), the entropy is inversely mapped to the saturation channel, and the intensity (value) channel represents the total power. Figure 3.16 shows this visualisation technique applied to the same area as in figure 3.12. This image illustrates the advantages of using basis-invariant variables for visualisation. In figure 3.12, the use of a basis-variant variable (the polarimetric phase difference) led to a more 'noisy' image. this is due to an increased randomisation of phase difference values which occurs as the coherence falls. As the values are random, it is possible that resolution elements with low coherence values will return phase difference values which suggest either dihedral or surface interactions. The alpha angle effectively represents the average phase difference over all polarisations, and is thus more effective in discerning volume scattering from areas where there is a single dominant scattering mechanism. This results in a 'cleaner' image, allowing well-defined targets to be identified more easily.

Alongside the Freeman decomposition, the Cloude decomposition has now become a standard treatment of polarimetric radar data, and can be extended to extract other values (A and β) which provide information on the shape and orientation of scatterers (Cloude and Pottier, 1996, Pottier and Lee, 1999). Despite their common usage, however, few researchers chose to visualise these parameters in a manner which accentuates the interdependence of the variables. Most commonly, the variables are represented as separate images, often using rainbow-colour scales (for example, see Cloude et al., 2003), which, in themselves, may lead to false perceptual groupings related to natural breaks in the hue cycle which are unrelated to the structure of the

data (Rogowitz and Treinish, 1998). A new method for visualising these additional parameters, which builds on the technique proposed by (Imbo et al., 1999), is presented in a later chapter.

3.9 – Polarimetric Interferometry

In recent years, developments in instrumentation and data processing techniques have allowed the fields of polarimetry and interferometry to be combined. Whilst still in its infancy, the field of polarimetric interferometry (PolInSAR) has nevertheless shown great promise, particularly with respect to the derivation of canopy and ground elevations in forested areas (Papathannassiou and Cloude, 2001).

Whilst a detailed analysis of PolInSAR is outwith the scope of the current research, it is nevertheless instructive to analyse the means by which data derived from experiments which combine polarimetry and interferometry have been visualised.

In figure 3.17, an image is shown which represents the results of an experiment conducted using a ground-based polarimetric interferometer. The experiment, carried out at the European Microwave Signature Laboratory in 1996, involved placing a 5m high Balsam Fir tree *Abies Nordmanniana* in an anechoic chamber and measuring the full scattering matrix using a two dual polarized horn antennas (Fortuny and Seiber, 1999). The resulting backscatter intensity images, which show both volumetric representation and individual slices of the fir tree, illustrates the three-dimensional structure which can be extracted using this technique.

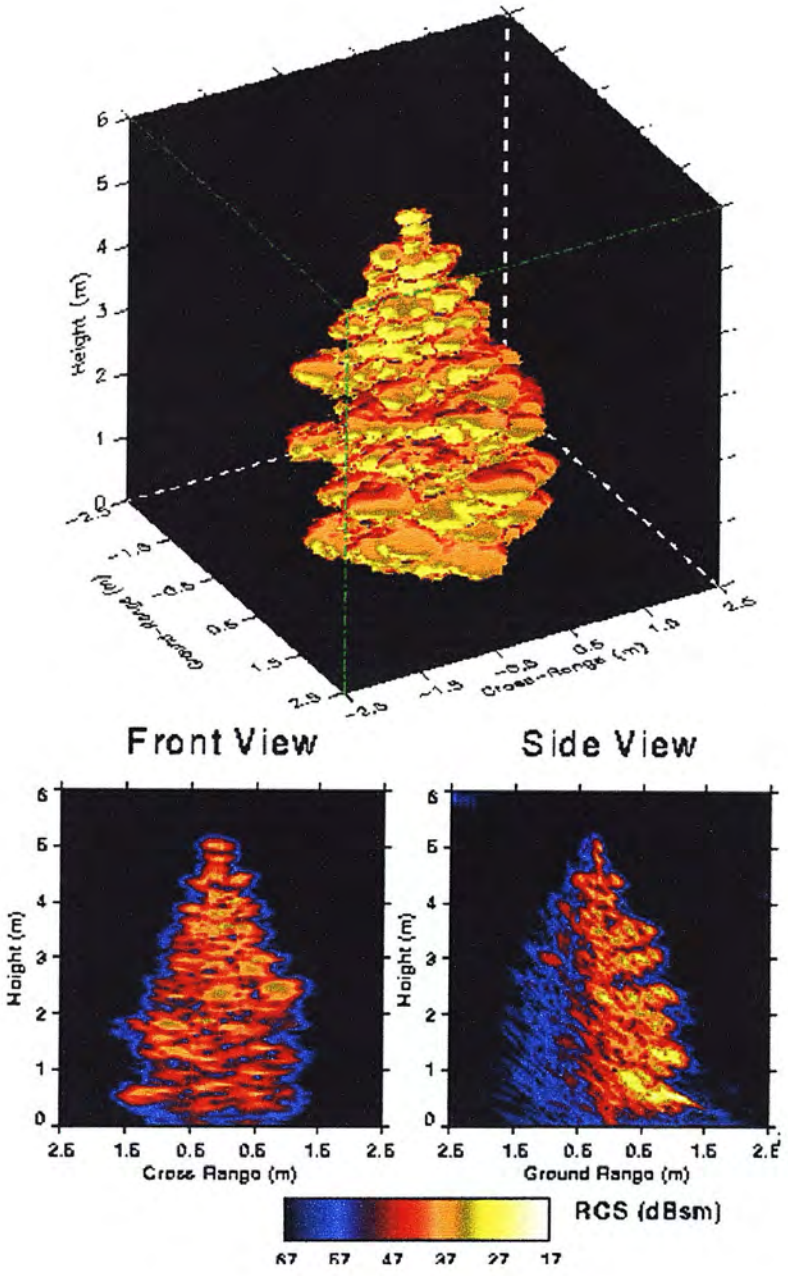

figure 3.17 – Visualising intensity for a three-dimensional polarimetric dataset. The isometric projection shows the total vv backscatter for the fir tree, whilst the lower image shows the contribution of individual slices (Fortuny and Seiber, 1999).

The development of radar polarimetry, therefore, allows an assessment of the three-dimensional structure of landscapes in a manner that cannot be achieved using traditional remote sensing techniques. This ability has been demonstrated, at the landscape level, by (Reigber and Moreira, 2000), using a technique termed radar tomography. Again, by using the principles of both polarimetry and interferometry, a volumetric representation of a landscape can be constructed. In figure 3.18, an image representing the first demonstration of this technique is shown. The image shows a vertical slice through a three-dimensional dataset, and uses the coherency matrix intensities to form an RGB colour composite (as described in section 3.5). Note that despite the extra dimensionality and density of this dataset, however, the main features are still described with respect to dihedral, volume and surface scattering.

Figure 3.18 – Visualisation of a 'slice' through a multi-baseline (i.e. interferometric) polarimetric dataset. Colour intensities are based on the coherency matrix so that R = hh-vv, G = 2hv and B= hh+vv (from Reigber and Moreira, 2000)

As mentioned earlier, one of the more promising research areas in polarimetric interferometry is the derivation of canopy and ground heights in forested areas. Such information is of particular use to environmental scientists as accurate estimations of tree height can be used to infer other values, such as vegetation type and biomass levels (Treuhaft and Siqueria, 2000). The derivation of such information, however, is not straightforward, and requires the analysis of a large number of data values. For example, figure 3.19 shows an image presented in Papathannassiou and Cloude, 2001), which is used in the initial stages of tree-height recovery. The graphic, which is similar in structure to those shown in figure 3.13, represents the change in interferometric coherence which occurs as a result of changing polarisation parameters. Each point, therefore, represents the interferometric coherence and phase for a given polarisation combination. When processed, these points can be joined to form a straight line which bisects the unit circle in two places. The separate phase values for these two locations can then be used judge the distance to the coherent scattering centres located at the base and top of a forest volume.

Note, however, that as with the polarimetric response graph, the visualisation of PolInSAR data at this level of detail does not allow for an analysis of spatial variations. Such an analysis, however, may be useful in understanding the effects of features such as forest edges and canopy gaps, evidence of which are clearly visible in the intensity images shown in figures 3.17 and 3.18. The investigation of visualisation techniques is one means by which the advantages of both the synoptic and specific scales of enquiry can be combined, allowing scientists too quickly analyse vast datasets for the occurrence of interesting patterns and relationships.

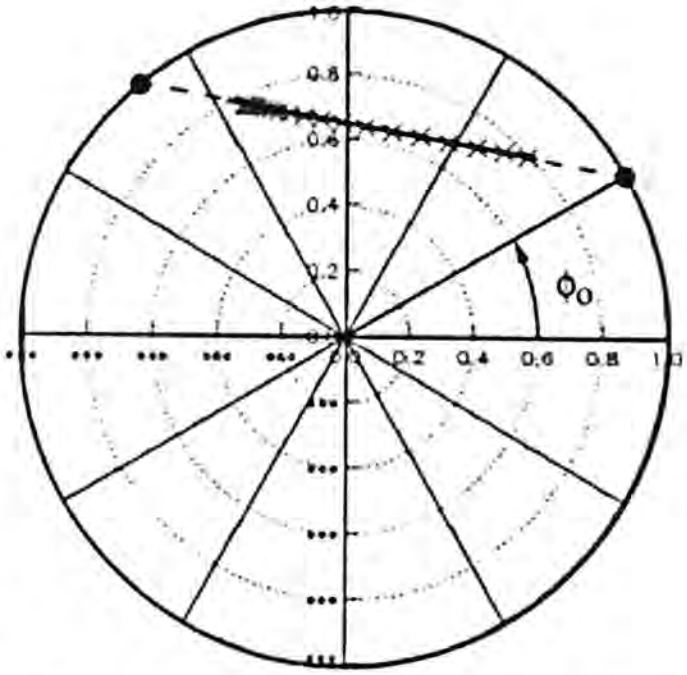

Figure 3.19 – Migration of interferometric phase with respect to polarisation over forest stand visualised using a polar plot, where the argument and magnitude for each point represents the interferometric phase and coherence, respectively. A straight line projected through the calculated points will intersect with the unit circle at two points. These points represent the phase (and thus distance) to the scattering centres representing the canopy top and forest floor (from Papathannassiou and Cloude, 2000)

3.10 – Summary

In this chapter, the theory behind radar polarimetry has been introduced, alongside descriptions of how datasets derived from radar polarimeters are most commonly visualised. Radar polarimetry is unique in terms of remote sensing techniques both in terms of the data which is collected, and the information which is contained therein. These unique qualities, however, means that the application of 'traditional' visualisation techniques outlined in chapter 4 are insufficient to fully appreciate the intricacies of the data.

In analysing the visualisation techniques commonly employed in the study of polarimetric data, it is notable that a dichotomy exists between two different scales of enquiry: namely, the specific and the synoptic, the characteristics of which are outlined below:

- Site specific, high detail graphics representing a single pixel or group of pixels, which are difficult to understand without prior knowledge of radar polarimetry.
- Synoptic images which either inadequately represent the scope of the data in question, or are otherwise presentations of pre-defined interpretation techniques (most commonly based around volume, surface and dihedral scattering).

The synoptic approach can be criticised for attempting to apply standard image processing techniques in a manner which ignores, and thus suppresses, the unique qualities of radar polarimetry. Similarly, however, the specific approach can also be criticised for ignoring the contribution of spatial analysis techniques to the observation of pattern and anomalies in remotely sensed datasets.

A gap therefore exists for the development of new synoptic exploratory visualisation techniques, which attempt to overcome the limitations of the pixel-based approach. In the following chapter, the means by which it is hoped this can be achieved are presented.

CHAPTER 4 –

METHODOLOGY

In the previous two chapters, the field of scientific visualisation was introduced, and applied to the analysis of remotely sensed data. This was subsequently extended to incorporate the analysis of a more recent innovation in remote sensing technology: that of radar polarimetry. It was shown that both the format of polarimetric radar data and the characteristics of the natural environment that it measures have a number of unique characteristics which mean that traditional visualisation techniques struggle to represent patterns in the data in a manner which allows for exploratory analysis. In this chapter, these weaknesses are more closely identified, and used as the basis for the development of two new visualisation strategies, which will form the remainder of this thesis.

4.1 Analysis of Current Techniques

In the previous chapter, a number of visualisation strategies employed in the analysis of polarimetric radar data were examined in detail. In figure 4.1, the most commonly used techniques are collated in a table, alongside an analysis of their visual characteristics.

The criteria defined on the table are chosen in order to combine the findings of the previous two chapters, and to allow the identification of weakness in current visualisation techniques. The first column, therefore, examines the number of variables represented for a single geographic location. This highlights the discrepancy between the number of values needed for an in-depth analysis of polarimetric response (i.e. 648 for the polarimetric response graph) and the three which can be represented using an RGB colour composite. The second column reiterates the fact that current visualisation strategies rely on a limited number of visual variables, using only location and colour to encode data variables.

Technique	No. of data variables per geographic location	visual variables used	synoptic?	'raw' data?	interactive?
grey-scale intensity	1	x,y,value	✓	✓	✓
covariance matrix rgb	3	x,y,red,green,blue	✓	✓	✓
coherency matrix rgb	3	x,y,red,green,blue	✓	✓	✓
phase difference hsv	3	x,y,hue, saturation,value	✓	✓	
Cloude/Pottier decomposition hsv	3	x,y,hue, saturation,value	✓		
Freeman Decomposition rgb	3	x,y,red,green,blue	✓		
Polarimetric Response Graph	648	x,y,z		✓	
Circular Phase Plots	2	x,y		✓	

figure 4.1 – An analysis of commonly used visualisation techniques in polarimetric radar data.

The final three columns can be viewed as an attempt to apply the axes of MacEachren's visualisation cube (discussed in chapter 2) to the analysis of remotely sensed data. The first column described whether a visualisation technique is synoptic. This property of remote sensing visualisation can be tied to MacEachren's concept of exploratory analysis. In remote sensing, as with cartography and geography in general, it is frequently the spatial patterns in datasets that reveal much of the

information that is contained therein. As we have seen in chapter 2, the analysis of remote sensing data has traditionally benefited from and relied on the synoptic viewpoint as a means of data exploration. This tradition, and the ease by which such images can be achieved, explains the frequent usage of RGB colour composites in the analysis of polarimetric datasets, despite their low information content with respect to modern sensors. It is notable, in this respect, that two descriptors of polarimetric data, namely the polarimetric response graph and the coherence/phase plot, have no spatial component, and thus cannot be used for the analysis of geographical patterns.

The following column, headed 'raw data', can be ascribed to the axis of MacEachren's cube which analyses whether an images is designed to reveal unknowns, or to display knowns. The processing of any dataset, be it from a remote sensing platform or any other recording device, involves a degree of subjectivity in that each stage in processing involves simplifying of discarding parts of the original datasets to some degree. Visualisations derived from such data, therefore, are bound by the assumptions inherent in each processing stage. In the case of the two decomposition techniques described, both involve an interpretation of the original dataset, and thus do not represent the 'raw' dataset in the same manner as values derived directly from the scattering matrix.

A further level of analysis can be applied to the two decomposition techniques with respect to the variables that are extracted. In the case of the Entropy/α decomposition, the variables derived are abstract mathematical values with no

inherent physical interpretation. Their visual representation, therefore, can be seen as an attempt to associate these variables with different scattering mechanisms, and thus give the mathematical values a physical interpretation based on observation. In the case of the Freeman decomposition, however, each of the derived variables is given a definite physical interpretation, and the visualisation of these values as RGB composites are more akin to the presentation of results rather than an exploration of their effectiveness.

The final column analyses the 'interactivity' of each form of representation. The RGB colour composites are described as the most interactive as a result of the number of tools which are available in image processing packages for this purpose. Note that the HSV composites are described as being less interactive as many of the tools used for RGB analysis (such as histogram adjustment, Principal Components analysis, and classification algorithms) operate either solely or more effectively on linearly scaled intensity values. The polarimetric response graph and the circular phase plots are described as having no interactive component as, once formed, there are no means of affecting their visual appearance in order to extract further information.

From this analysis, we can identify a number of problems and questions that can be used for the development of new visualisation techniques. Firstly, it is apparent that visualisation strategies in remote sensing are bound to a limited number of visual variables which are borne from the reliance on pixel-based imaging. It can therefore be hypothesised that if the number of visual variables employed is increased, then the

number of data variables can also be increased. This, in theory, should allow the relationships between a wider range of parameters to be examined simultaneously, and thus improve current visualisation practices.

4.2 - Development of New Visualisation Strategies

The remainder of this thesis concentrates on the development of new visualisation strategies for the analysis of polarimetric datasets. The development of these techniques aims to overcome the weaknesses in current visualisation strategies by applying the principles and concepts of scientific visualisation outlined in chapter two. The newly developed techniques, however, also aim to retain some of the characteristics of traditional visual analysis in remote sensing by retaining the synoptic overview which is afforded by the pixel-based intensity images.

Two new techniques, therefore, are presented that allow for the synoptic visualisation of multiple variables extracted from polarimetric datasets. These techniques represent a distillation of a large number of experimental visualisation designs which were applied to a range of different polarimetric variables. Each experiment, however, had the aim of trying to move away from conventional imaging techniques, and towards exploratory, icon-based strategies which allow for the representation of multiple data variables at a single geographic location.

The first of these techniques, described in chapter 5, attempts to apply the visualisation strategies developed at Brown University to the analysis of polarimetric datasets. In (ref), it was shown that the use of an ellipse as a data icon permits the

assignation of multiple data values to a single, geographic location. This technique is subsequently adopted and applied to variables derived from the Entropy/α decomposition developed by Cloude and Pottier (1996). Current visualisation strategies for these variables rely on either a classification of Entropy/α space (Cloude and Pottier, 1997), or use HSV colour composites (Imbo et al, 1999) to represent these variables alongside total power.

The decomposition technique developed by Cloude and Pottier, however, allows further variables to be derived from the eigenvalues of the coherency matrix. These variables (namely the anisotropy and beta angle) have been used recently in academic papers as an aid to extracting further information from polarimetric datasets (Hajnsek et al, 2003, Lumsdon and Wright, 2003). The visualisation of these variables, however, is most frequently achieved using either grey-scale intensity images, or single-variable colour scale representations. Such an approach, whilst providing an overview of the spatial patterns inherent in each variable, does not allow an analysis of the patterns which may exist *between* different variables. Such relationships, it can be argued, are of fundamental importance in the exploratory analysis of new types of data, and, as such, provide an ideal testing ground for the utility of new, icon-based approach to visualisation.

The visualisation strategy outlined in chapter five, therefore, represents an attempt to develop a *top-down* approach to data visualisation, which takes an existing framework (namely, the visualisation strategies developed at Brown University) and illustrates how they can be applied to polarimetric radar data. This is achieved by

presenting a series of images which demonstrate the application of the ellipse-based visualisation strategy to a number of real datasets over a number of different environments. It is shown that the application of this technique allows for the identification of regions where the assigned variables exhibit interesting spatial relationships. These relationships, it is argued, not only allow us to better understand the nature of the variables in question, but also allow for the identification of regions which would benefit from further investigation.

The visualisation of variables derived from a decomposition technique, however, does not represent a visualisation of 'raw' polarimetric radar data, as it is based on a mathematical interpretation of the original data. Whilst the visualisation of such variables is important in examining their potential information content, it remains that no adequate visualisation technique exists for the vast number of intensity 'channels' which can be derived from the process of polarisation synthesis.

In chapter three, the polarimetric response graph was described as a means of representing 648 individual intensity values using a single isometric surface graph. This graphical technique has been used since the initial development of radar polarimetry as an active research field (ref), and continues to be used today. Whilst the graphic is commonly used to describe backscatter from single resolution elements or areal averages, however, there are no examples of the response graph being used in the analysis of spatial patterns in polarimetric response.

In chapter 6, the properties of the polarimetric response graph are examined in detail, in order to identify reasons why the polarimetric response graph is unsuitable for synoptic visualisation. This is subsequently followed by the development of a new graphic for the representation of polarimetric response, which aims to overcome the limitations of the traditional technique.

Where the ellipse-based visualisation in chapter 5 describes a 'top-down' approach to visualisation, the redevelopment of the response graph represents a 'bottom-up' approach. This involves the development of a unique form of visualisation, based on the properties of an existing, traditional approach. The new visualisation, however, attempts to represent these properties in a manner which allows a more intuitive and immediate understanding of the variables which they represent. To achieve, an iconic representation of the polarimetric response graph is created, where the axis variables (namely orientation and ellipticity) are intuitively mapped to the visual variables of the icon.

It is subsequently demonstrated that the resulting icon is suitable for the synoptic analysis of polarimetric response patterns. This is achieved by integrating the new visualisation technique into a software package which encourages exploratory visualisation. This package, detailed in the last half of chapter 6, encourages the exploration of polarimetric datasets by allowing access to a wide range of traditional visualisation strategies. The newly developed technique is integrated into this package, allowing users to select areas of interest from simple intensity images, and view the individual polarimetric response contained therein in detail.

Chapter 7 serves as both an assessment and demonstration of the possible application of the new visualisation strategy developed in chapter 6. The first section is devoted to illustrating the cognitive benefits that the new polarimetric response icon has over the traditional polarimetric response graph. This is achieved via a web-based user survey, which asks respondents to identify patterns in various configurations of polarimetric response patterns. This survey purposefully uses a pool of non-experts (with regards to radar polarimetry) in order to demonstrate that the new technique effectively represents patterns, which can be identified regardless of background knowledge.

The latter half of chapter seven presents a case study that illustrates the use of the polarimetric response globe at different stages of a research project. As identified by MacEachren and Kraak (1994), imagery can play an important role throughout a research project, from initial exploratory visualisation, through synthesis and testing of ideas and hypotheses to the final presentation and dissemination of results. It is shown that the polarimetric response icon can also be used in this manner. An area of similar response patterns, first identified using the synoptic technique outlined in chapter six, is used as a basis for the development of a scattering model. This scattering model is itself based around the unusual visual characteristics of the observed response pattern. It is demonstrated that, in seeking to understand these visual characteristics, a deeper understanding of the nature of polarimetric scattering can be achieved. It is also shown that the formulation of this understanding, and the

characteristics of the model which was developed as a result, can be clearly explained using the response icon as a tool of dissemination.

In the final chapter, the findings of this project are described in a wider context, and the benefits of developing new visualisation strategies are weighed against the costs of devoting both time and effort to their construction. Future developments in radar polarimetric are also considered, and the potential role of visualisation analysed.

CHAPTER 5 – VISUALISING THE ENTROPY/α DECOMPOSITION

5.1 – Introduction

This chapter marks the beginning of the attempt to actively employ the principles of scientific visualisation to the study of polarimetric radar data. As means of an introduction, a relatively simple visualisation strategy is described which uses graphical icons to describe five of the variables that can be extracted from the Entropy/α decomposition, which was introduced in the previous chapter. This is subsequently used to create synoptic images that can be used to simultaneously examine the spatial inter-relationships between these five variables.

The conceptual basis for the visualisation strategy exploits the varying perceptual qualities of visual variables to map total power, entropy, alpha angle, beta angle and anisotropy. As some of these variables have explicit geometric qualities, they can be mapped to the parameters of an ellipse. Even when the variables used do not relate directly to the geometric properties of scatterers, the use of the ellipse as an icon provides a match between the technical language of polarimetry and the graphical language developed by Bertin (Bertin, 1989). As such, the proposed visualisation strategy expands on the use of the ellipse as a visual motif, which, as described in the previous chapter, is commonly used in the description of wave polarisation.

While the visualisation strategy is relatively straightforward, it is less straightforward to implement the strategy in a digital environment. To this end, a series of procedures have been developed using IDL that allows data variables to be mapped to a series of visual parameters. IDL is a data visualisation package that is commonly used in the polarimetric radar remote sensing community, and thus it is anticipated that the routines can easily be integrated into the scientists workflow.

Despite the structural simplicity of the proposed visualisation technique, it is notable that resulting images represent the first time, to this author's knowledge, that more than three polarimetric variables have been represented in a single synoptic image. This author believes that they provide an informative methodology for initial data inquiry. Although not a substitute for model-based data analysis and classification maps, it forms an effective first-stage of visualisation that is not difficult to implement.

5.2 –Extracting Further Variables from the Entropy/α Decomposition

In the previous chapter, the Entropy/α decomposition was introduced as a means of extracting two variables that characterise the nature of interactions found in polarimetric datasets. The alpha angle and entropy were described as basis-invariant analogues of the polarimetric phase difference and coherence variables, which can be estimated directly form the coherency matrix (Cloude and Pottier, 1996). In addition, it was shown that images could be created from these variables that are similar in structure to interferograms. Such images have proved useful in relating the alpha

angle and entropy to the scattering properties of different landscape components (Imbo, 1999).

Here, the visualization technique is extended in order to visualize two more variables that can be derived from the Entropy/α decomposition; namely the anisotropy (A) and the beta angle (β). These variables can be extracted from the eigenvalues and eigenvectors of the coherency matrix (Cloude and Pottier, 1996), and represent parameters which are less well-understood than α and H in terms of their application to vegetation studies. Both A and β, however, have properties which may be useful in the analysis of vegetation: β, for example, is linked to the orientation of scatterers in a plane perpendicular to the incident wavefront (Cloude and Pottier, 1996), whilst A is believed to provide information on the number of scattering elements in high to medium entropy environments (Pottier and Lee, 1999). Both variables have been applied to classification strategies over vegetated environments. In (Pottier and Lee, 1999), anisotropy was used to improve an unsupervised classification procedure based on entropy and alpha angle values, whilst in (Lumsdon and Wright, 2003), β was used in the classification of forested areas, where it was found that the parameter could be used to isolate areas of deep water.

However, classification assumes at least a bimodal distribution of the variable, otherwise it lies on a continuous distribution with no clear discrete boundary with which to define the class. Additionally, while there may be interdependences between the variables, the spatial patterns of these interdependences are lost in the

classification process and results are constrained by our prior assumptions of class boundaries.

Few attempts have been made to visualise the nature of these variables with respect to their spatial distribution, or in a manner which allows analysis of their relationship with other parameters which can be derived from the Entropy/α decomposition. In cases where some attempt is made at spatial analysis, there tends to be a reliance on standard image processing procedures. In (Lumsdon and Wright, 2003), for example, an intensity image is shown representing the distribution of β for data collected over Glen Affric. The resulting image appears very noisy, with only lake surfaces providing areas of continuous values.

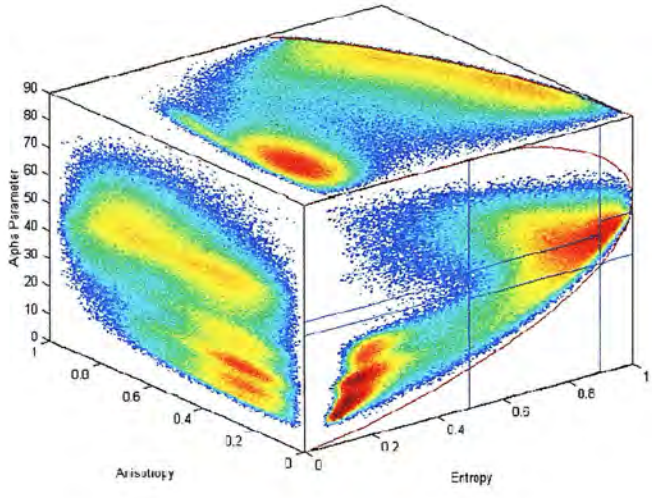

figure 5.1: Visualisation of α, H and A presented as an image cube (from Pottier and Lee, 1999).

Similarly, The visualisation of A uses either single channel intensity or rainbow colour scale images to represent the geographic distribution of values, which in general contain fewer recognisable geographic features than either H or α (for examples, see Cloude et al., 1999 or Schuler et al., 2003). In (Pottier and Lee, 1999), the visualisation of H-α space (normally represented as a 2D scatterplot) is extended to a three-dimensional image cube, using A as the third dimension (as shown in figure 5.1). Although this allows an assessment of the inter-relationships between these three variables, it does not allow for an assessment of any spatial anomalies in their distribution that may be instructive in gaining further understanding of the nature of these parameters.

5.3 – Derivation of β and A

In (Cloude and Pottier, 1997), the eigenvector decomposition of the coherency matrix was used to generate a number of parameters in addition to the now widely used alpha and entropy variables. Two of these values (the beta angle and anisotropy) are of particular interest as they contain information relating to the nature of scattering within the resolution elements. The anisotropy provides information on the number of scattering mechanisms in high to medium entropy environments, and has been used to improve classification procedures (Pottier and Lee, 1999) and to aid the inversion of surface parameters (Hajnsek et al., 2003). The beta angle, in contrast, is less well understood, and has only, to this authors knowledge, been used once as an aid to classification (Lumsdon and Wright, 2004).

The beta angle (β) varies between -π and π and describes the orientation angle of a scatterer about the radar line of sight (Cloude and Pottier, 1997). A value for β can be extracted from the eigenvectors of the coherency matrix as follows:

$$\overline{\beta} = \frac{1}{2}\tan^{-1}\left(\frac{2\Re(k_{1,2}k_{1,3}^*)}{k_{1,2}k_{1,2}^* - k_{1,3}k_{1,3}^*}\right),$$

where $k_{i,j}$ represents the j_{th} element of the i_{th} eigenvector (k).

A value for the anisotropy (A) of the target can be derived from the second and third eigenvalues (k_2 and k_3, respectively) of the coherency matrix using the following:

$$\overline{\beta} = \frac{1}{2}\tan^{-1}\left(\frac{2\Re(k_{1,2}k_{1,3}^*)}{k_{1,2}k_{1,2}^* - k_{1,3}k_{1,3}^*}\right),$$

Anisotropy is believed to provide information on the number of scattering mechanisms in high to medium entropy environments. Low anisotropy values indicate the presence of numerous different scatterers, whilst high values indicate that the observed response is the product of two separate scattering mechanisms. The value of anisotropy in low entropy environments dominated by a single scattering mechanism is believed to be negligible, as the low values for the second and third eigenvalues in this case make the parameter susceptible to system noise (Titin-Schnaider, 1999)

5.4 – Development of the New Visualisation Technique

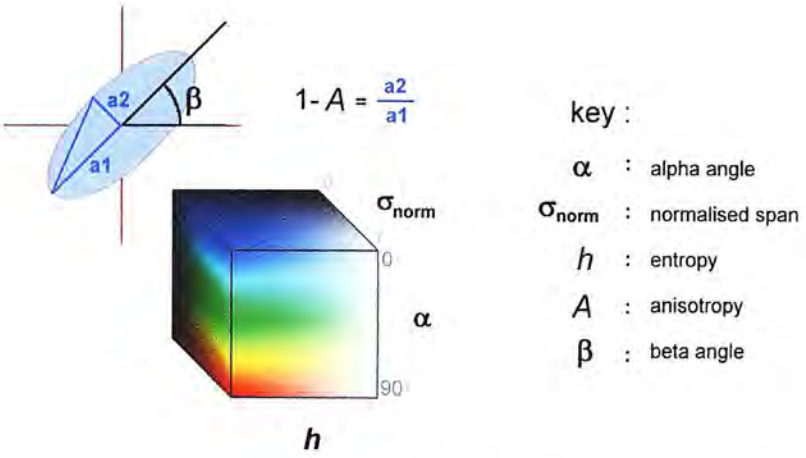

figure 5.2: parameterisation of the visual variables of an ellipse icon using data variables derived from the Entropy/α decomposition.

In this section, a new visualisation technique is presented which allows five variables to be mapped to a single location through the use of coloured ellipses, in a simplified version of the technique used by (Laidlaw et al., 1998) for visualizing diffusion tensors in a mouse's spinal column. In figure 5.2, the visual parametrisation of the ellipse is illustrated. The construction of images from these ellipses is achieved using a procedure written using IDL code, the stages of which are outlined below:

1. Prior to the creation of each symbol, a vector is created which sorts the dataset in terms of decreasing entropy, for reasons which are discussed later

2. Using this vector, values for A, α, β, H, and the normalized total power (σ_{span}) are stored in temporary vector, which is assigned to an image location where the ellipse will be created.

3. The initial size of the ellipse is found by setting the major axis to a value equal to the normalized total power (σ_{span}).

4. The anisotropy (A) is then used to define the minor axis, and is equal to 0.1 + 0.9 * ((1 - A)σ_{norm}). This means for locations where A = 0, a circular icon is produced, and where A = 1, a thin ellipse is used. The size of the minor axis is restricted to a minimum of 0.1 in order to ensure that the icon remains visible for high anisotropy values

5. The ellipse is subsequently oriented about its centre by β to represent scatterer orientation.

6. Finally, using the visualisation technique proposed by (Imbo et al., 1999), the colour of the ellipse is defined by the alpha angle (α), entropy (H) and normalised total power (σ_{norm}), which are ascribed to hue, saturation and intensity values, respectively. The alpha angle is inverted and re-scaled to range between 240° and 0°, and the saturation channel inverted, so that low entropy surface interactions appear as saturated blue ellipses, and low entropy dihedral interactions as saturated red ellipses.

The images presented in the following section are the result of many iterations, whereby the visualisation structure was adapted on order to produce an optimum

strategy which allowed the maximum information to be derived from the variables. Such iterations were based on visual analysis of output images, and included alterations to the maximum size of ellipses, and the scaling of intensity values. Preliminary visualisations, for example, placed ellipses in a sequential column-row structure, leading to visual artifacts in the final image caused by pronounced vertical bands of ellipses. In order to remove the banding, the ordering of the ellipses was changed. Instead of using the column/row structure of the data, the ellipses were placed at geographic locations based on the sorting of the entropy channel from high to low values. This produces a 'jitter' effect (Laidlaw et al., 2001), which acts to apparently randomize the placement of icons.

An additional advantage of this approach is that the high entropy values (from which little information can be derived) are plotted first, and form an underpainting onto which the higher entropy ellipses are placed. This is particularly useful as very low entropy icons are pushed to the front of the image, guiding the viewer to areas where potential information content is highest.

Even after this adjustment, however, the quality of the image was compromised due to the overcrowding of ellipses. In order to overcome this, it was decided that only one in every four data points would be represented on the image. This resulted in a cleaner image where the properties of individual ellipse could be more easily analysed. However, this approach runs the risk of 'missing' single low entropy targets, such as corner reflectors, which often form the most easily recognizable features in polarimetric datasets. For this reason, the routine was altered so that all

ellipses for the final ten percent of the dataset (when sorted in order of decreasing entropy) were represented.

5.5 – Examples and Analysis

The following examples illustrate the application of the new visualisation technique to polarimetric datasets. The first example, shown in figure 5.3, shows L-band data collected over San Francisco by the JPL airborne polarimeter. This dataset is commonly used in polarimetric research as a means of testing new techniques, as it contains a variety of well-defined landscape components, including zones of urban development, vegetation, open water and bare rock. Other features of interest include geographical landmarks such as the Golden Gate Bridge, and individual buildings in Golden Gate Park. Examples of the usage of this dataset thus stretch from the first papers to appear on radar polarimetry (Zebker et al., 1987) up to the present day (Gu et al., 2004, Lee et al. 2004).

figure 5.3 – Visualisation of L-band data over San Francisco (near range is at the top of the image)

The visualisation shown in figure 5.3, however, is unique in that it allows for the spatial analysis of five separate variables derived from the Entropy/α decomposition, and reveals a number of interesting relationships and anomalies. In general, there is a clear divide between the three major landscape components. The ocean area, which dominates the majority of the image is characterised by low backscatter values, which decrease with increasing range distance. The dominant blue colouring is indicative of low entropy surface scattering, although this is masked in areas of very

low backscatter. The urban areas, in contrast, are characterised by high backscatter values and higher alpha angle values, evident in the yellow/red colouring of the ellipses. The final general regions of the image are the vegetated areas (including Golden Gate Park), which are characterised by high entropy values, and thus contain little colour information.

It should be noted that the images presented in this section are purposefully presented without a key to explain the characteristics of the individual ellipses. This is to emphasise the perceptual qualities of the image, rather than concentrate on the information content. The viewer is thus encouraged to 'look at' rather than 'read' the image, allowing patterns in the data to be established prior to the application of any prior knowledge relating to the nature of polarimetric scattering. If required, however, figure 5.1 acts as a key for all of the images used in the remainder of this chapter.

A further advantage of the icon-based approach is that it allows for multiple-scale enquiries. While the overview of Figure 5.3 allows a quick orientation and assessment of the major scattering properties, a closer inspection allows a more detailed assessment of particular features. Figure 5.4 shows a zoomed area of figure 5.3, and allows us to contemplate the extra information encoded in the beta angle and anisotropy values. Of particular interest is the difference between the cliffs and the built-up area. It is immediately apparent from the shape of the ellipses that the cliff are characterised by variable anisotropy values, whilst the urban area appears to be dominated by higher values. Both regions, however, have well-defined hues and so

are low entropy environments, suggesting the presence of well-defined scattering regimes.

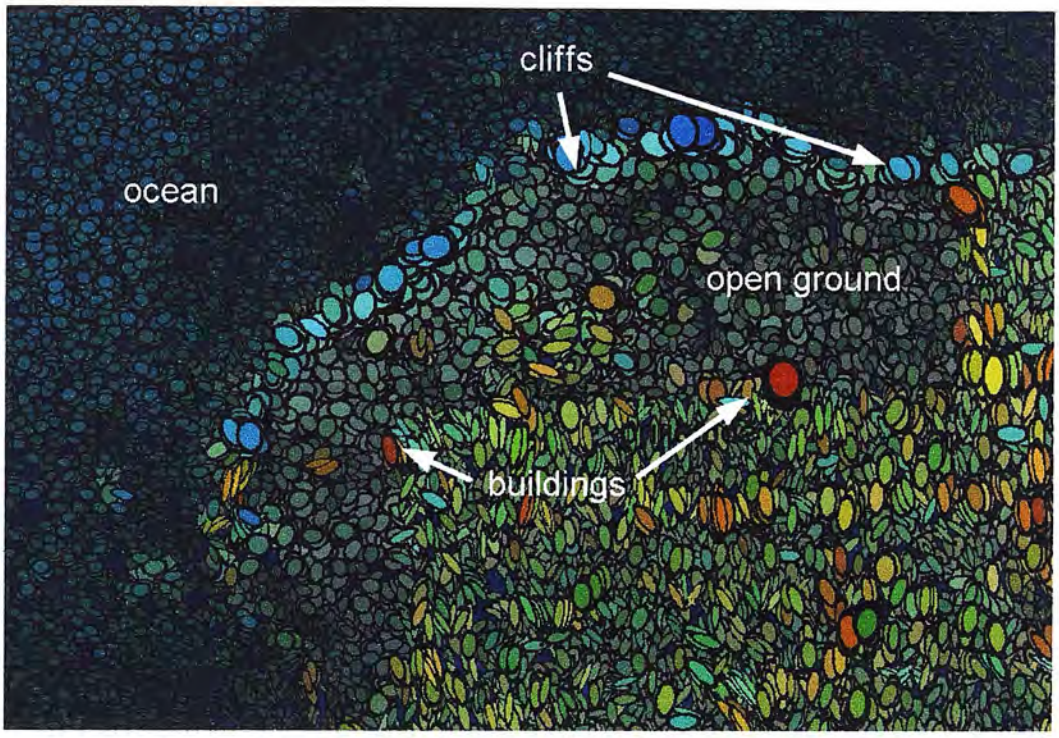

figure 5.4: Close-up of San Francisco dataset, showing the different patterns evident for different landscape components.

Over the cliffs, the low anisotropy and low alpha angle values support an interpretation of strong single scattering events caused by direct reflection . In the case of the built-up area, there is more variation in the anisotropy, and it is notable that many of the anisotropic ellipses have a yellow/green hue indicating intermediate alpha angle values. Where anisotropy is low, the alpha angle tends to be closer to 180°, leading to red, circular icons. This relationship offers support for the assertion that anisotropy is related to the number of scattering mechanisms in a resolution element. In the built-up area, the bright red circular icons are likely to be indicative of pure dihedral scattering, especially as the most obvious of example of this

phenomena (to the right of the 'buildings' arrow in figure 5.4) occurs on the range-ward side of the urban expanse. Deeper into the urban areas, backscatter is more likely to be dominated by a combination of dihedral scattering and direct backscatter, leading to higher anisotropy values, and intermediate alpha angle values.

The proposed visualisation technique allows sets of hypotheses similar to those outlined above to be quickly applied to other regions of the image. For example, the presence of low entropy, low anisotropy surface scattering is also evident on the range-ward side of the San Bernardino mountain range in the lower portion of the image.

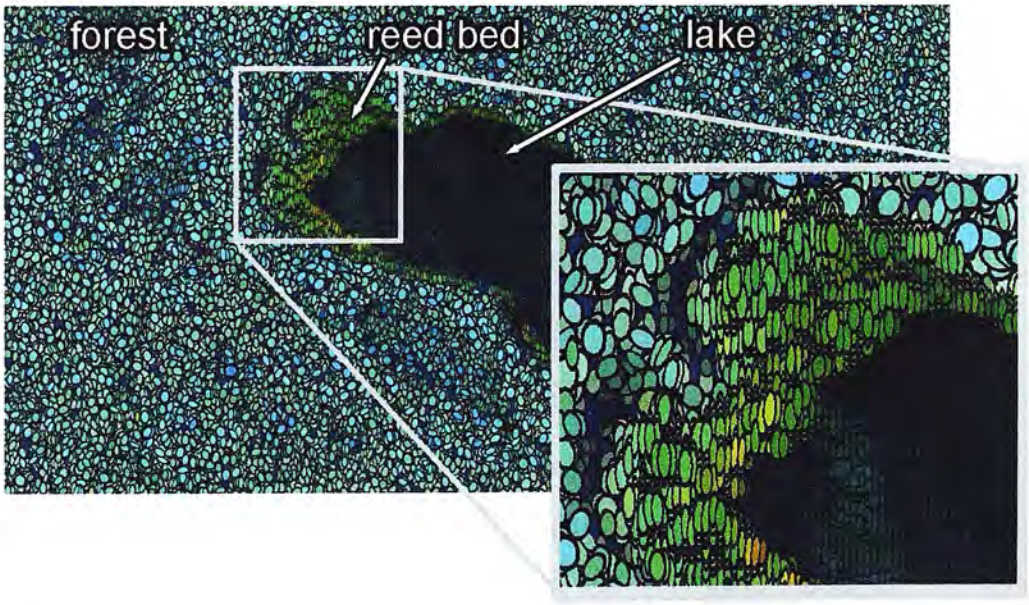

figure 5.5: Visualisation of C-band data over a forested region. Note that while no patterns are evident in the forested area, an area of reed beds on the lake shore exhibits spatial continuous values for A and β.

In figure 5.5, a second visualisation is presented which shows C-band data collected by the EMISAR airborne polarimeter (Woodhouse and Hoekman, 2000). Unlike the

previous example, the majority of this datasets is dominated by a single landcover type, namely, managed boreal-type forest. The application of the new visualisation technique immediately reveals that little information can be obtained from the anisotropy and beta angle parameters over this region, both of which assume random values. The blue/green hue of the ellipses over the forested region suggests a mixture of direct canopy scatter and volume scattering.

What is also immediately apparent, however, is the presence of a region in the image which exhibits spatially continuous values for A and β. This region corresponds with an area of reed beds towards the shore of lake Siggefora, and is shown in the inset of figure 5.5. Note that the continuous beta angle values suggests the presence of vertically oriented scatterers, whilst the high anisotropy values indicate the presence of more than one dominant scattering mechanism. It is also notable that the alpha angle parameter is also continuous over this region, assuming an intermediate value. This is particularly interesting, as intermediate alpha angles are more typically associated with volume scattering (Pottier and Lee, 1999). The low entropy angles, however, suggest the presence of a well-defined scattering regime that, on the basis of this visual representation alone, is worthy of further investigation. The region shown in figure 5.5 is revisited more extensively in chapter 8, when polarimetric response patterns over this region are examined in more detail.

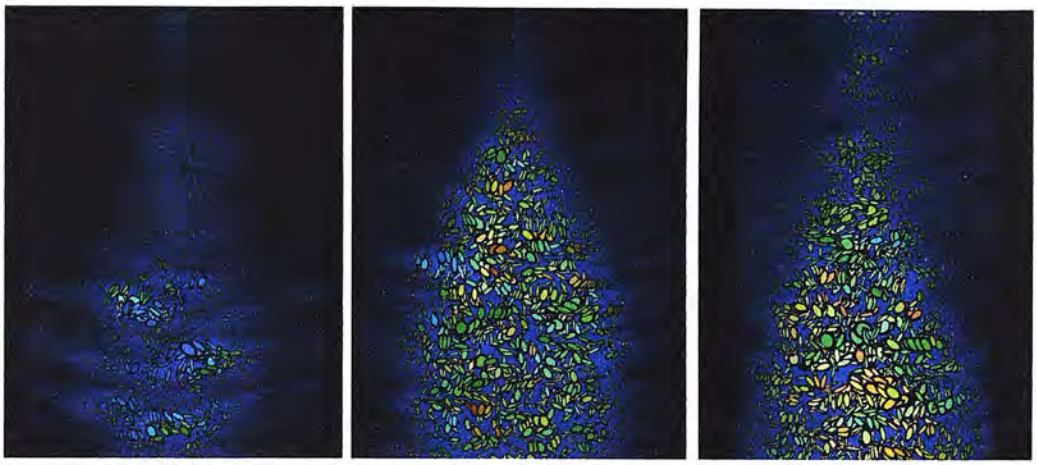

figure 5.6: Azimuthal slices through a three-dimensional dataset of a fir tree, taken from a time series animation. When viewed in series, the ellipses show the scattering properties of individual branches.

The final example in this section illustrates how the new visualisation technique can be applied to a wide variety of polarimetric datasets. In figure 5.6, the newly developed visualisation technique is applied to a three-dimensional dataset derived from an experiment carried out at the European Microwave Signature Laboratory in 1996 into the application of polarimetric interferometry. The experiment involved placing a 5m high Balsam Fir tree (*Abies Nordmanniana*) in an anechoic chamber and measuring the full scattering matrix using two dual polarized horn antennas (Fortuny and Seiber, 1999).

The images shown in figure 5.6 are constructed using the same technique used for the previous 2D synoptic images. By viewing each of the individual slices, it is possible to examine the scattering properties of vegetation elements such as the tree trunk and major branches. The exploratory nature of these images can be further enhanced by creating animations that illustrate variations in polarimetric properties

with respect to canopy depth, an example of which is included on the enclosed CD as an AVI file.

On viewing this animation, a number of features are readily apparent which can be used to describe the recorded data. The initial images, for example, contain blue, almost circular icons that represent the initial surface backscatter from the major branches in the tree. As the animation proceeds, these ellipses apparently become more anisotropic and migrate towards intermediate alpha angle values. Towards the end of the animation, the lower middle part of the image is dominated by highly anisotropic red ellipses, as a result of dihedral interactions between the chamber floor and the tree trunk. These ellipses also have similar beta angle values, suggesting the presence of vertically oriented scatterers.

5.6 - Discussion

In this chapter, a straightforward visualisation technique has been presented which allows for the visualisation of five separate parameters which describe different aspects of polarimetric scattering. The use of an iconic approach to visualise variables at specific geographic locations overcomes the overcomes the three-channel limitation of both RGB and HSV pixel-based images and provides an intuitive link between the jargon of polarimetry and the visual image. This approach thus allows two less well-understood variables (namely, the beta angle and anisotropy) to be compared with three regularly applied variables (the alpha angle, entropy and total power).

The visualisation technique has been applied to a number of different datasets, highlighting areas where the inter-relationships between the five variables may provide further information on how each variable relates to different scattering properties. The value of such images is that the viewer is drawn to areas where strong patterns are apparent, and encouraged to develop hypotheses based on their spatial location and extent. Such an approach can be contrasted with other forms of visualisation in remote sensing which rely more heavily on the identification of training areas, or areas of known cover type, and which therefore inherently involve either *a priori* assumptions or background knowledge of the area in question.

A further advantage of this visualisation strategy is that it is adaptable, and can be simply adjusted to accommodate different variables other than those used above. In addition, the structure of the visualisation can be adapted to emphasise particular aspects of the dataset. For example, in the above images, decreasing entropy was used to order the sequential layering of the ellipses. A minor adjustment to the IDL procedure would allow this ordering to be based on the total power, or indeed, any of the other variables used. This flexibility encourages an exploratory approach to visualisation, whereby hypotheses can be quickly constructed and examined.

In summary, therefore, it can be stated that the proposed visualisation technique effectively allows the synoptic comparison of polarimetric variables which improves on the standard practice of using either small multiples or non-geographic scatterplots. This approach, however, is limited by the fact that, by using a set of derived variables, any interpretation must be weighed against the validity of the

chosen set of parameters as adequate indicators of polarimetric properties. The problem of how to adequately visualise 'raw' polarimetric data, therefore, remains unanswered. In order to address this problem, the following chapters detail a new technique for the synoptic visualisation of polarimetric response patterns.

CHAPTER 6 – VISUALISING POLARIMETRIC RESPONSE PATTERNS

6.1 – Introduction

In the previous chapter a new visualisation technique for a commonly-used decomposition technique was presented. Whilst this technique effectively conveyed a larger number of variables that are normally represented in synoptic images, the problem remains that the variables used consist of interpreted data values. The synoptic visualisation of raw intensity values from polarimetric datasets, therefore, remains unresolved. In response, this chapter introduces a new visualisation technique for the analysis of polarimetric response patterns.

Polarimetric response graphs are commonly used research tools in polarimetric radar, and appear regularly in published journal articles (Evans et al., 1990, Dong and Forster, 1996). Most commonly, they are used as a means of analysing response patterns over areas of known land-cover type (Skriver et al., 1999), or to validate the output of polarimetric scattering models (Durden et al, 1989), or as a means of calibrating datasets (Zebker, 1991).

The analysis of polarimetric response patterns, however, is hindered by two major constraints. Firstly, the standard means of presenting response patterns as an isometric surface has a number of significant design problems that make the graphic

difficult to read. Secondly, the density of data values on a single graph, in conjunction with the isometric projection, means that no effective method of analysing multiple, spatially organised response patterns has been proposed, or even attempted. These constraints reduce the effectiveness of the polarimetric response graph as a tool for exploratory visualisation, and inhibit the observation of patterns in polarimetric response at the synoptic level.

This chapter, therefore, proposes a redesign of the current response graph in order to produce a graphic that conveys the variables that define polarimetric response in a more straightforward manner. This design results in an iconic representation of polarimetric response that can be understood without the need for axes. By presenting response patterns as icons, it is subsequently possible to create images that, for the first time, allow that analysis of spatial variations in polarimetric response.

In order to ensure that the new visualisation technique complements already established means of representing polarimetric data, a software application is described which combines the response pattern viewer with a number of the visualisation techniques discussed in chapter 4. This IDL-based application (www.rsinc.com) is described in section 6.5, which also gives examples of the response viewer in action.

While this chapter discusses the design theory and implementation of the new visualisation technique, no attempt is made to prove the effectiveness of the new

technique until the following chapter. In this chapter, the effectiveness of the new technique is assessed in terms of both its visual effectiveness, and its potential as a research tool.

6.2 – Applications of the Polarimetric Response Graph

In chapter 4, the polarimetric response graph was introduced as a means of examining polarimetric response patterns for idealised scattering objects (Ulaby et al., 1990). It was then described how the understanding of these idealised objects has subsequently informed the manner in which polarimetric data is discussed in research literature (Zebker et al., 1991, Freeman and Durden, 1998).

When presented in polarimetric radar literature, the polarimetric response graph is used to describe either point targets (for example, trihedral or dihedral calibration corner reflectors (Cloude et al., 2001)), or to describe the response patterns for units of landcover, such as agricultural fields (Skriver et al., 1999) or forest stands (Durden et al., 1989). Response patterns have also been used for a variety of different applications, including the characterisation of geomorphological landscape units (Dall et al., 1995), and as an aid to topographic analysis (Schuler et al., 1996), and as a means of validating the output of scattering models (Durden et al, 1989).

In some published papers, the response patterns derived either by spatial averaging or by modelling, have been termed 'polarimetric signatures' (Skriver et al., 1999, Conradsen et al, 2003). In order for a response pattern to be considered a signature,

however, it is necessary that the same response pattern can be observed not only at times and locations, but also at different scales. Thus in order for an areal response to be considered a 'signature' of a particular landscape component, it is necessary that this single response pattern adequately represents the nature of the individual responses which make up the spatial average.

This kind of analysis, however, is notably absent from polarimetric radar literature. Even in papers which rely heavily on the use of polarimetric response patterns to characterise landcover (from example in Skriver et al., 1999), there is little proof offered that the observed patterns are indeed characteristic of the landscape component in question.

A possible reason for this, it is proposed, lies in the nature of the polarimetric response graph as a data visualisation technique. In the following section, therefore, it is described how the structure of the response graphic inhibits the analysis of multiple response patterns, and provides alternative representations which suggest how its design may be improved.

6.3 – The Polarimetric Response Graph: A Design Perspective

The polarimetric response graph is most commonly presented as a pair of isometric surfaces, which define both the co- and cross-polarised response patterns for a single scattering matrix, which may be derived from an areal average. Despite its widespread use, there exists no reason why the isometric presentation is favoured, other than through force of habit. Despite this, few authors have chosen to stray from

the standard representation which was first used by Zebker in an early paper concerning the application of polarimetric radar to environmental applications (Zebker et al., 1987).

By analysing the alternative representations that have appeared, however, the visual effectiveness of the standard approach is shown to be lacking. For example, in Agrawal and Boerner, 1989, a large number of response graphs are used to describe scattering from simple canonical radar targets. The response patterns, though presented as 2-dimensional intensity images, are identical to the standard response graph.

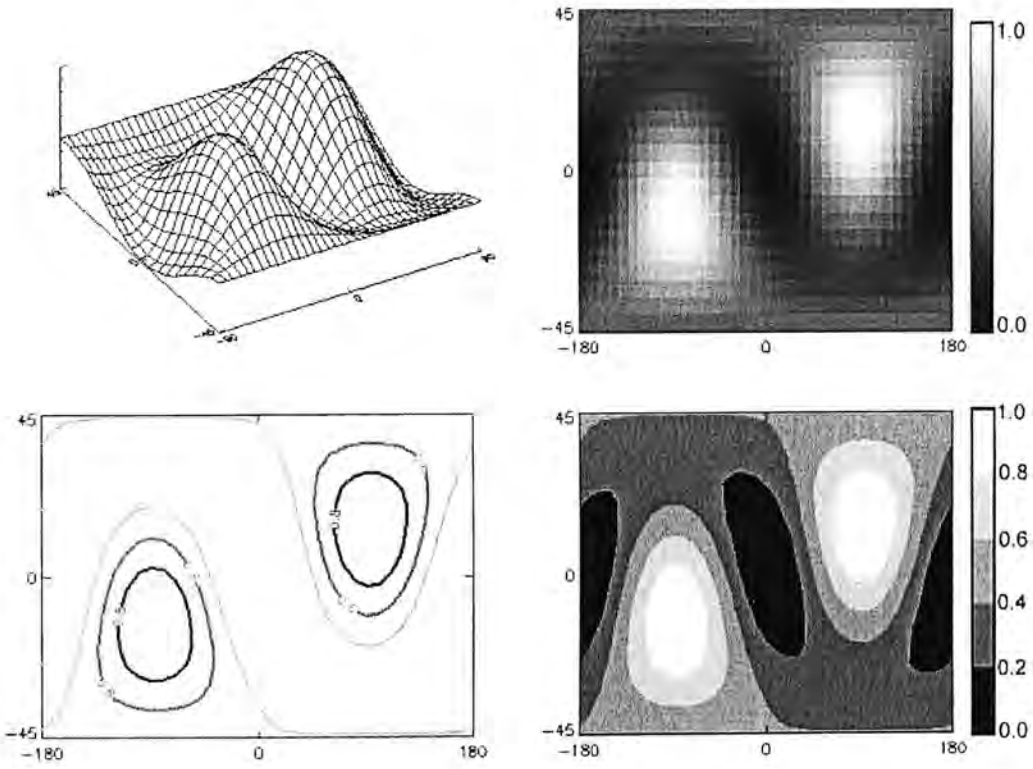

Figure 6.1: Alternative representations of the polarimetric response graph, which obviate the need for a third dimension. Note that in the 2D representations, the area of null response between the two peaks is more clearly visible.

In figure 6.1, the advantage of using a 2D graphic over the isometric approach is illustrated. Note that the response pattern contains an area of low response that is occluded in the isometric representation, as the peaks are aligned towards the line of sight of the viewer. The alternative representations, which use an intensity image, a contour overlay, and a five-step choropleth representation, both show the location of the area of low response more clearly. In addition, the 2D representation allows axis values to be read more easily, as the user must translate over only two dimensions, as oppose to the three required for the isometric representation.

A further design flaw of the traditional visualisation is the use of linear axes to represent what were shown in chapter 5 to be cyclical variables; namely the orientation (ψ) and ellipticity (χ) angles. This has the effect, in the case of the orientation angle, of imposing a 'break' in the data where it does not actually exist. This issue is compounded by the inconsistent labelling of the orientation angle axis, an example of which can be found by comparing (Ulaby and Elachi, 1990) and (Zebker et al., 1987).

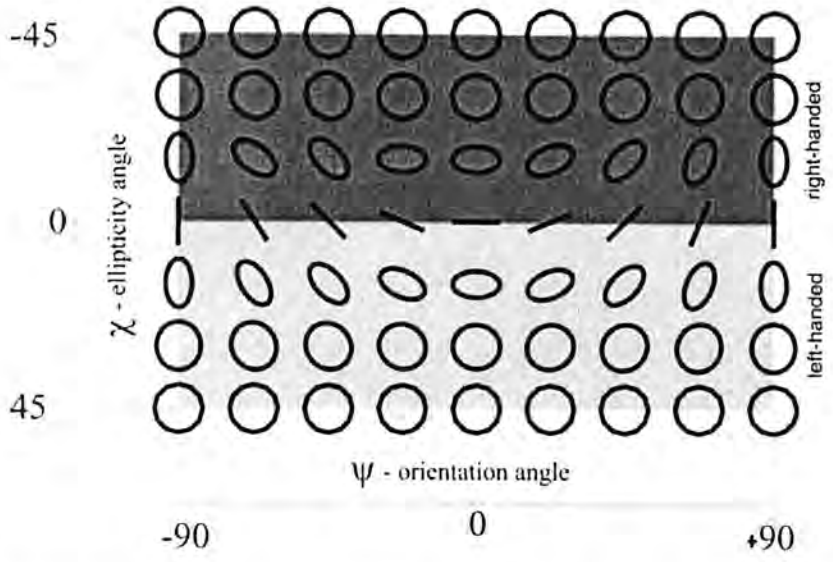

Figure 6.2: Distribution of transmitted polarisation states across the surface of a polarimetric response graph. Note the repetition of data values for the circular polarisations.

With respect to the ellipticity angle, the use of a linear axis has a more subtle effect, which can be explained with reference to figure 6.2. This diagram represents the distribution of polarisation states across the surface of the traditional response graph, which has been reduce to two dimensions, for clarity. Note that as the magnitude of the ellipticity increases towards the edges of the graph, the effect of the orientation angle of the waveform becomes less noticeable. The value of the orientation angle becomes irrelevant for the circular polarisations, which are invariant to rotation. As a result, where χ = +/- 45°, the value recorded by the response graph is identical for every value of ψ.

In terms of data visualisation, this is an example of redundancy that contributes to the lowering of the 'data-ink ratio' defined by Tufte (1986). In addition, the repetition of data values gives undue emphasis to the circular polarisations at the expense of the linear polarisations, where it is expected that the orientation of the transmitted wave is most likely to have an affect on the backscatter response.

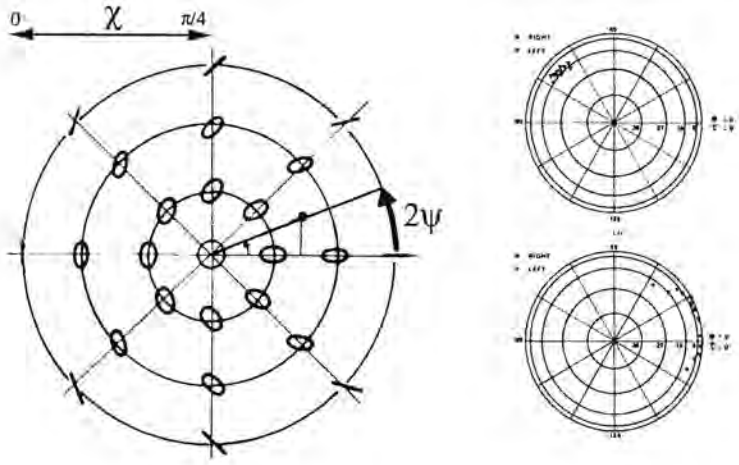

Figure 6.3: An alternative representation of polarimetric response, as used in (Giuli, 1987). Note that an angular visual variable is now used to map the orientation angle.

An alternative configuration of the two axes used to define polarisation can be found in (Giuli, 1987), which uses a circular graph to map the polarisation of peak responses for hard targets, such as vehicles and aircraft. The graph (an example of which is shown in figure 6.3) can be described as a polar azimuthal projection of the Poincaré sphere (as shown in figure 5.5). Values for ψ are thus mapped to an angular parameter, which can be read around the circumference of the circle. The value for χ is subsequently equal to the distance from the centre of the graph, so that the circular polarisations are now represented as a single point at the centre of the graph, and the linear polarisations are more 'spread out' around the circumference.

Note that the resulting graph remains counter-intuitive with respect to the orientation angle, however. The angle measured around the circumference of the graph, as with the Poincaré sphere, is equal to 2ψ. As a result, the horizontal axis of the graph is used to map both the horizontal and vertical polarisation states, whilst the vertical axis is used to map orientation values of +/-45°. Nevertheless, by mapping the variable of orientation angle to an angular visual variable, the continuity of the axis is maintained. Note however, that if a response pattern were to be mapped to the surface of this graph, then two separate graphs would be required to represent the left- and right-handed polarisations. As the graph design shown in figure 6.3 was intended to display individual radar echoes, their respective polarisations can be mapped to a single point. The difference between left- and right-handed polarisations, therefore, is represented using two different symbols.

By displaying alternative representations of polarimetric response patterns, it would appear that the current isometric presentation of polarimetric response is one that has persisted due to its habitual usage, rather than any advantages it offers as an effective data graphic. The alternative representations which have been discussed also contain design problems which mean that the graphics are difficult to interpret without first examining the axis definitions used. order to be understood. Using the terminology of Bertin, therefore, the representations of polarimetric response so far discussed can be considered as 'reading' graphics, rather than 'looking' graphics (Bertin, 1980).

In view of this, the following section describes a new means of representing polarimetric response patterns that combines the advantages of the alternative

representations described above in order to produce a graphic that enables a more immediate interpretation.

6.4 – Development of The Polarimetric Response Globe

In the previous section, two alternative representations of the polarimetric response graph were presented as alternatives to the standard isometric representation. It was shown that the use of a two-dimensional graphic allowed axis values to be read more easily, whilst the use of a circular graphic ensured that the different polarisation states were more evenly represented.

In figure 6.4, a new graphic, dubbed the 'Polarimetric Response Globe' is presented which combines the advantages of the previously discussed alternatives with some further improvements. The diagram shown in figure 6.4 shows the distribution of polarisation states across the response globe, and should be compared to figure 6.2.

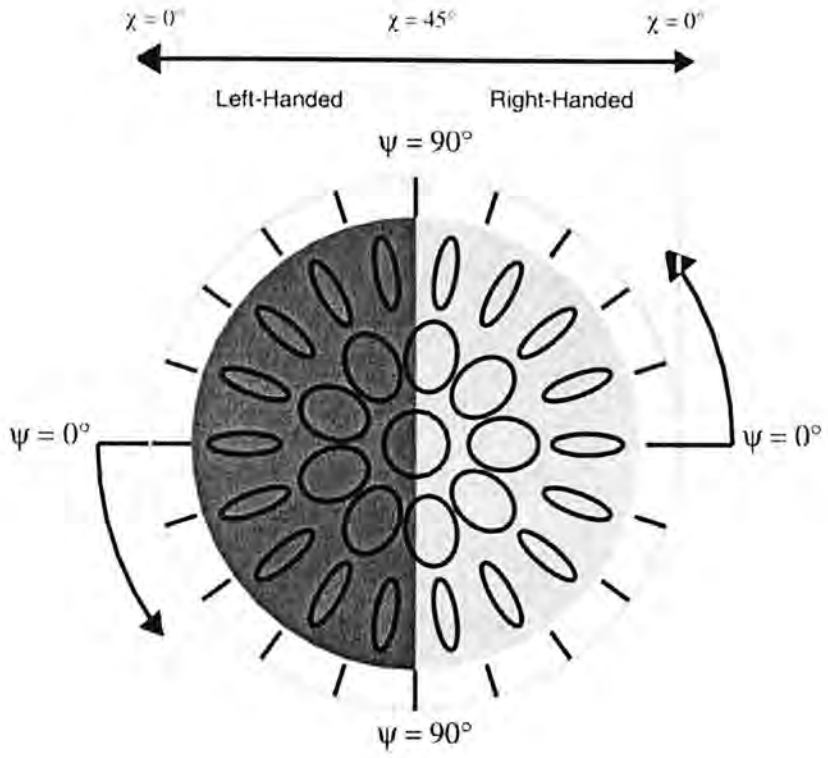

Figure 6.4: Distribution of polarisation states across the surface of the Polarimetric response globe. Note that this differs from figure 6.3 in that both the left- and right-handed polarisations are mapped to a single graph.

The structure of the new graphic follows the technique used by (Giuli, 1987), and is based on an equal area, polar azimuthal representation of the Poincaré sphere (Robinson et al., 1995). However, where the new graphic differs to both the Poincaré sphere and the aforementioned azimuthal plot is that both the left- and right-handed hemispheres are mapped to a single graphic. This is achieved by replacing the angular variable of 2ψ with ψ around the circumference of the globe, and mapping the left- and right-handed responses to the left and right halves of the globe, respectively.

The advantages of this approach should be immediately apparent on viewing figure 6.4. In addition to the left- and right-handed polarisations being unambiguously mapped to separate halves of the globe, there is also a direct correlation between ψ, and the angular value mapped to the circumference of the globe. Put more simply, the horizontal and vertical axes of the graphic now correspond to the horizontal and linear polarisations.

In figure 6.5, a number of co-polarised response patterns extracted over an areal of boreal forest in Sweden are presented using both the traditional response graph, and the newly developed response globe. To facilitate a comparison between the two techniques for non-idealised scatterers, figure 6.5 shows response globes and graphs which have been derived from data collected over a forested area near Siggefora in Sweden (Woodhouse and Hoekman, 2000). For clarity only the co-pol response patterns are shown as examples to facilitate ease of comparison. Each of the examples illustrate polarimetric characteristics which can be clearly identified using the new visualisation technique. Response (a) for example, is the result of a dihedral interaction, producing a graph with a characteristic cross shape. With the new method, however, it can also be observed that there is a preference for the horizontal linear polarisation, which is less clear in the traditional graph. Within a forest, such a response suggests not only ground-trunk interactions, but also from the horizontal ground or larger branch structures. A small preference for left-handed helicity is also apparent in the new projection.

Example (b) in figure 6.5 demonstrates a typical depolarised response. In traditional polarisation response graphs, a depolarised response is characterised by a 'pedestal'

(Zebker et al., 1987), and usually indicates a high volume scattering contribution (such as a vegetation canopy). Such an effect is evident in the new visualisation by a marked lack of contrast in the diagram. Orientation preferences in the polarized component of the measurement, however, are still clearly visible, but there is no evidence of any helicity.

It may be argued that depolarisation effects are more apparent in a surface plot than a grey-scale image, but of course it is possible to present both methods as either a grey-scale, contoured plot, or as an isometric surface, if that is preferred.

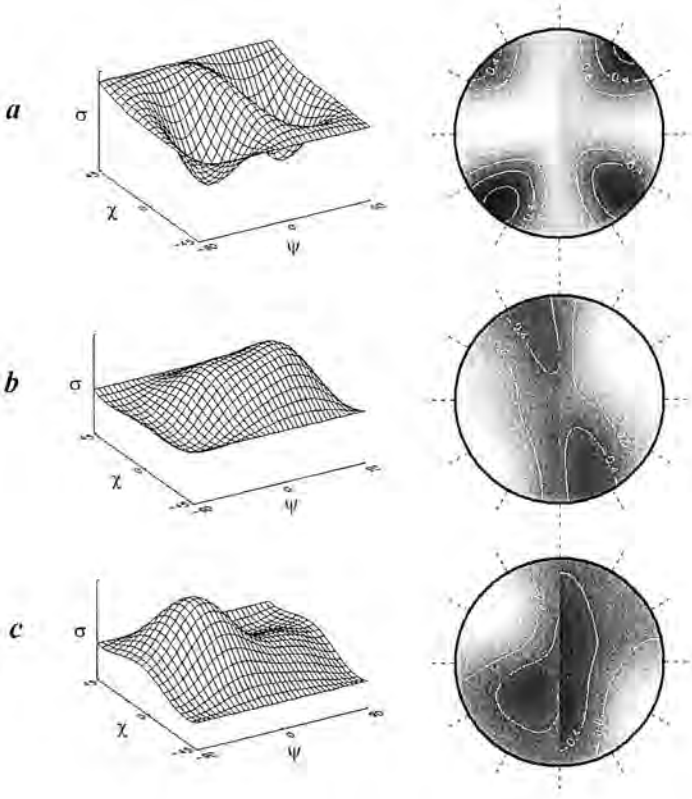

Figure 6.5: Co-polarised response patterns derived over a forested region represented using both the traditional and newly developed polarimetric response graphs.

Finally, response (c) appears to be an oriented surface with an orientation of -30°. The new visualisation is consequently characterised by a relatively dark centre (representing the circular polarisations) surrounded by a lighter circumference with maxima indicating a preferred orientation. This pattern is less clear in the traditional response graph, especially in terms of resolving the preferred angle of orientation.

6.5 – Adding Colour to Polarimetric Response

In addition to combining the left- and right-handed polarisations on a single graph, it is also possible to combine both the co- and cross-pol responses by assigning each set of responses to a separate intensity channel. Earlier experiments with different channel combinations showed that using green to represent the co-pol response and red to represent the cross-pol response were most effective at separating the individual responses, as the blue channel tended to lose definition at low intensities.

In figure 6.6, the response patterns for the idealised scatterers discussed in chapter 5 are presented using the new visualisation technique, and using the green and red channels to represent the co- and cross-polarised response patterns, respectively. On analysing the response patterns in figure 6.6, it is apparent that, in areas where the co- and cross-pol response values are equal, the observed response appears darker than in areas where the total power is distributed in just one channel.

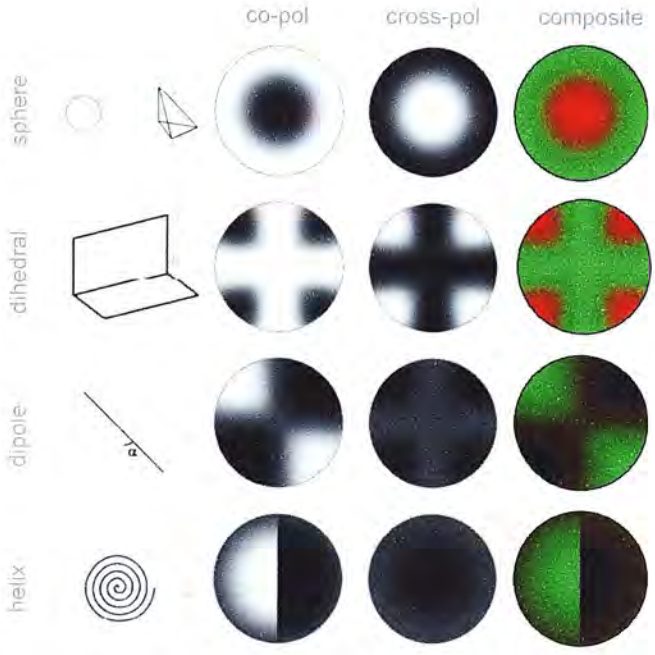

figure 6.6: Idealised response patterns visualised using the polarimetric response graph. The coloured globed show both the co- and cross-pol response patterns, which are assigned to the green and red channels, respectively.

This gives the (incorrect) visual impression that the total backscattered power along what will be hereafter termed 'saddle points' is less that for either the co- or cross-pol maxima. A saddle point can be defined as an area of the response graph where the dominant backscattered response switches from co- to cross-pol. This is particularly evident in the response patterns for surface and dihedral interactions, which appear to contain 'rings' of low response between the maxima for the co- and cross-pol responses, despite the total backscattered power being invariant over all polarisations.

In order to rectify this visual discrepancy, and to make these saddle points more dominant the colouring scheme can be redesigned. Instead of mapping the co- and cross-pol values to separate intensity channels, the total power backscatter power is

instead mapped to a greyscale intensity. The ratio between the co- and cross-pol values can subsequently be used to drive the hue variable. Where the co-pol response dominates, the hue angle is set to green (i.e. 120°). As the relative cross-pol intensity increases, the hue can be shifted towards red (i.e. 0°) using the following mathematical procedure.

$$\text{Hue} = 120^{*}(\sigma_{co}/(\sigma_{co} + \sigma_{cx} + 0.0001)) \quad (6.1)$$

Where σ_{co} and σ_{cx} represent the normalised backscatter for the co and cross-pol channels, and the value of 0.0001 is added to ensure no division by zero.

Where the co and cross-pol responses are equal, the hue angle is equal to 60° (i.e. yellow), which forms a natural breakpoint in the hue cycle. This breakpoint is demonstrated more clearly in figure 6.7, which compares the hue-based scale to the two-channel intensity scale used in figure 6.6. Note that the apparent fall in intensity described previously is clearly visible in the two-channel colour bar, but is absent from the hue cycle colour bar.

In figure 6.8, polarimetric responses graphs for the idealised scatterers are presented using the hue-based colour scheme. Note that the saddle points for both the surface and dihedral response patterns are now clearly evident, with the high total intensity values preserved. As such, these saddle points can be distinguished more effectively from the regions of low total backscatter for both the helical and dipole scatterers.

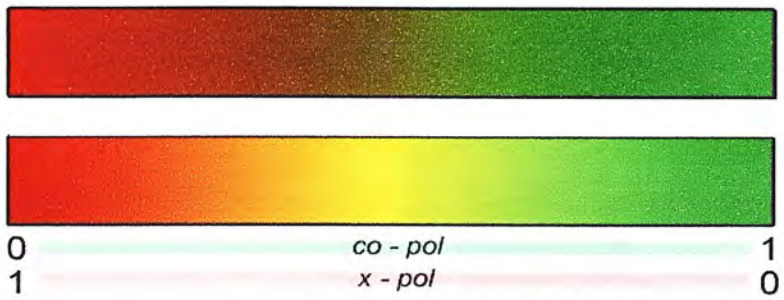

Figure 6.7: Alternative colour scales for representing polarimetric response. The upper bar uses a combination of two intensity channels and appears darker where both channels are equal. The lower bar uses a constant intensity, and varies the hue depending on the ratio of the two channels. Note that a clear yellow bar occurs where both channels are equal.

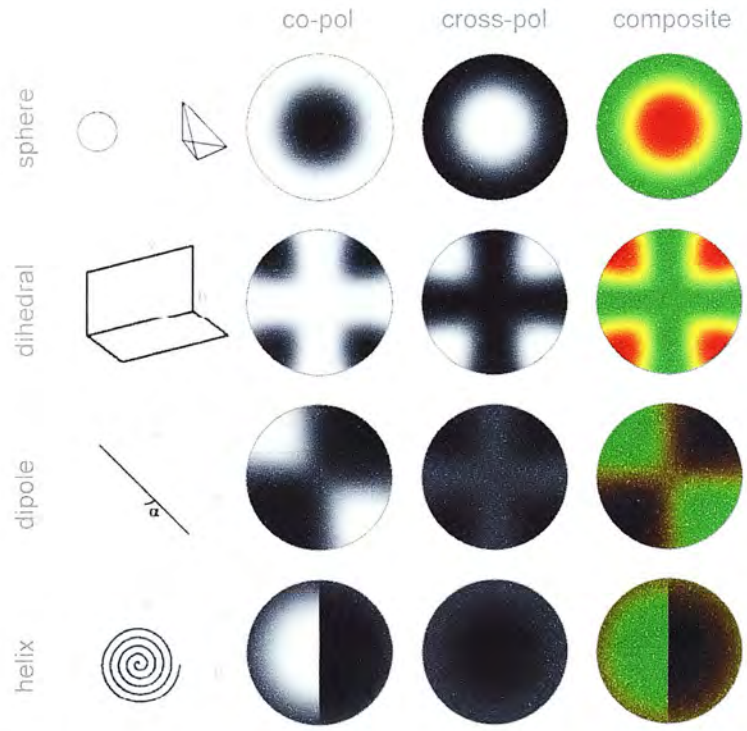

figure 6.8: Idealised response patterns visualised using the polarimetric response graph. The coloured globed use a hue-variant scale to represent the dominance of either the co-pol (green) or cross-pol (red) response. Saddle points, where the dominance switches, are marked as yellow bands.

6.5.2 – Adapting the Response Globe for Colour-Blind Viewers

The use of colour as a visual variable, whilst commonplace in remote sensing, is hindered by the fact that many individuals suffer from abnormal colour vision, which is more commonly termed colour-blindness. This affliction is present in only 0.05% of the female polulation, but is much more common among males, where 8% are affected (Pirenne, 1967, pp.169).

The colour scheme chosen for the polarimetric response globe is unfortunately incompatible with two of the main forms of colour blindness, namely protanopia and deutanopia, both of which affect the ability of the viewer to distinguish between red and green hues. The effects of these forms of colour blindness, alongside the less common form of trinatopia, are illustrated in the upper diagram in figure 6.9. Using a web-based tool (found at http://colorfilter.wickline.org), the polarimetric response curves for a sphere and a dipole are presented in a manner which simulates the different types of colour deficiency. For both the protanopia and tritanopia, it is not possible to distinguish between the co- and cross-polarised response patterns, both of which are represented using a yellowish-hue.

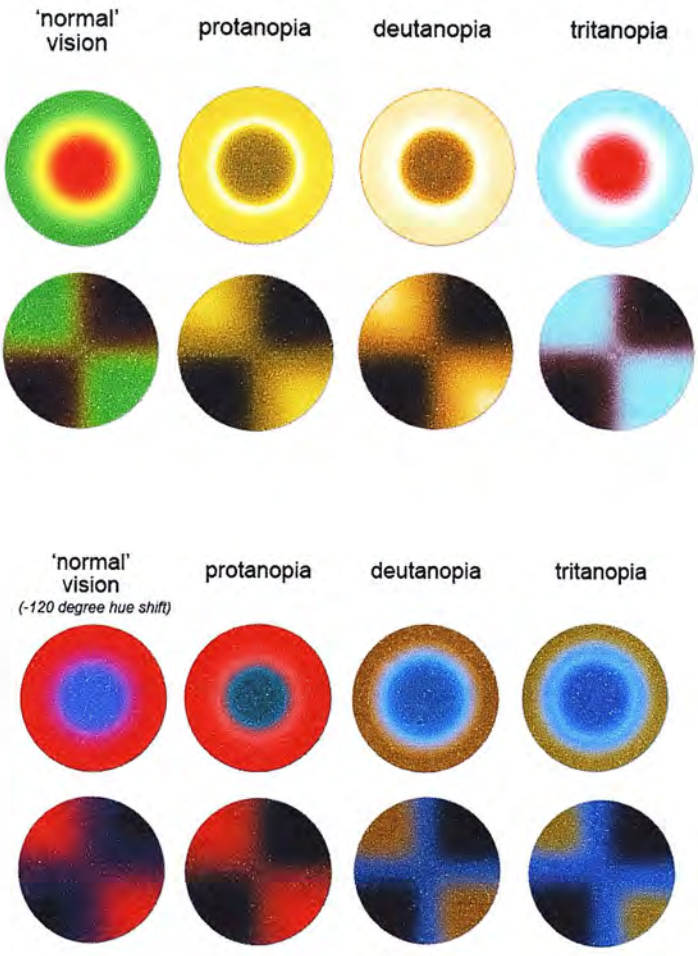

Figure 6.9 The effect of different types of colour blindness on the observed response globe (top) and how these can be partially overcome through manipulation hue scale values (bottom).

The colours chosen to represent polarimetric response patterns, therefore, pose a serious limitation for colour deficient users. This problem can be partially overcome, however, by applying a hue shift to the images produced by the visualisation routine. An example of this is shown in the lower portion of figure 6.9, whereby the hue of the original output image is shift by -120°. This allows the nature of the co- and cross-polarised response patterns to be more clearly distinguished across the range of colour sensitivities.

6.6 – The Synoptic Analysis of Polarimetric Response Patterns

The new visualisation technique for polarimetric response graphs developed in the previous two sections addresses the problems with the standard technique, outlined at the beginning of this chapter. The orientation angle (ψ) is now mapped to an angular visual variable, and the data values are more evenly represented with respect to the ellipticity angle (χ). In addition, it is possible to map both the left- and right-handed polarisation states intuitively to a single graph, as well as representing both the co- and cross-polarised response patterns using a colour scale. The visual efficiency of the new technique is explored and tested in more detail in the following chapter. At this stage, however, it is hypothesised that the new representation produces a graphic which conveys the nature of an individual polarimetric response pattern in a more straightforward manner. Where the traditional response requires the viewer to 'read' the axes of the graphic before extracting information, the response globe allows a more immediate and preattentive appreciation of the nature of the response.

In order to exploit this quality further, a programming routine was created which allowed multiple response patterns to be presented in a synoptic manner. As described in chapter 4, small scale intensity images typically form a preliminary stage in the analysis of remote sensing datasets, and are often instrumental in revealing patterns and anomalies which drive subsequent research. It was therefore hypothesised that a similar representation of individual response patterns at the small scale may reveal useful pattern and anomalies could inform researchers using radar polarimetry.

The first attempt at achieving this aim was presented as a poster at the IEEE International GeoScience and Remote Sensing Symposium (IGARSS 2002). Using a 400*400 pixel subset of polarimetric data collected by the E-SAR airborne polarimeter over Sweden, response patterns were sequentially calculated for each 5*5 pixel region. 1,600 response patterns were then overlain on a total power intensity image, allowing the spatial analysis of response patterns at the synoptic scale (Turner and Woodhouse, 2002).

This initial visualisation strategy allowed for the observation of a number of interesting areas of different response types, and provided the impetus for the research carried out in the latter half of the following chapter. This approach was soon discarded however, as the physical size of the images produced exceeded the size of desktop display units. In order to produce an image that both preserved the resolution of the individual response patterns, yet still allows for a synoptic overview requires access to a printer capable of producing A1 output. The cost of regularly producing images of this size, therefore, was deemed a factor that would discourage the adoption of the visualisation technique among the wider research community.

6.7 The Polarimetric Response Globe Viewer

Subsequent research into the use of the polarimetric response globe focuses on how the synoptic visualisation technique can be adapted to be suited to a desktop computing environment. To this end, a software application is presented that allows

spatial patterns in individual response patterns over small areas to be analysed. The design of this application is detailed in the following subsections.

6.7.1 - Overview

The Polarimetric Response Globe Viewer (PRGV) is a software application written using IDL, a dedicated program-led application that allows the development of interactive visualisations based around graphical user interfaces known as 'widgets'. The PRGV initially presents the user with a grey-scale intensity image based on a total power variable derived from a polarimetric dataset. The dataset must be formatted as six separate files, each of which represents a unique element of the covariance matrix (as discussed in chapter five).

Using a series of drop-down menu bars, the user chooses the means by which the polarimetric response patterns will be visualised. The presented options are as follows:

1) Individual response
2) Area average response
3) Synoptic responses

If the individual response selection is chosen, the user can analyse the polarimetric response graph for a single pixel simply by clicking on the intensity image. On selecting the area average response option, the user is required to draw a polygon

over an area of interest. The pixels covered by this polygon are subsequently averaged, and the resulting response pattern displayed. For both of these options, an additional drop-down menu allows the user to choose between the traditional polarimetric response graph, and the newly developed response globe. Examples of both the single and average response options are shown in figure 6.10.

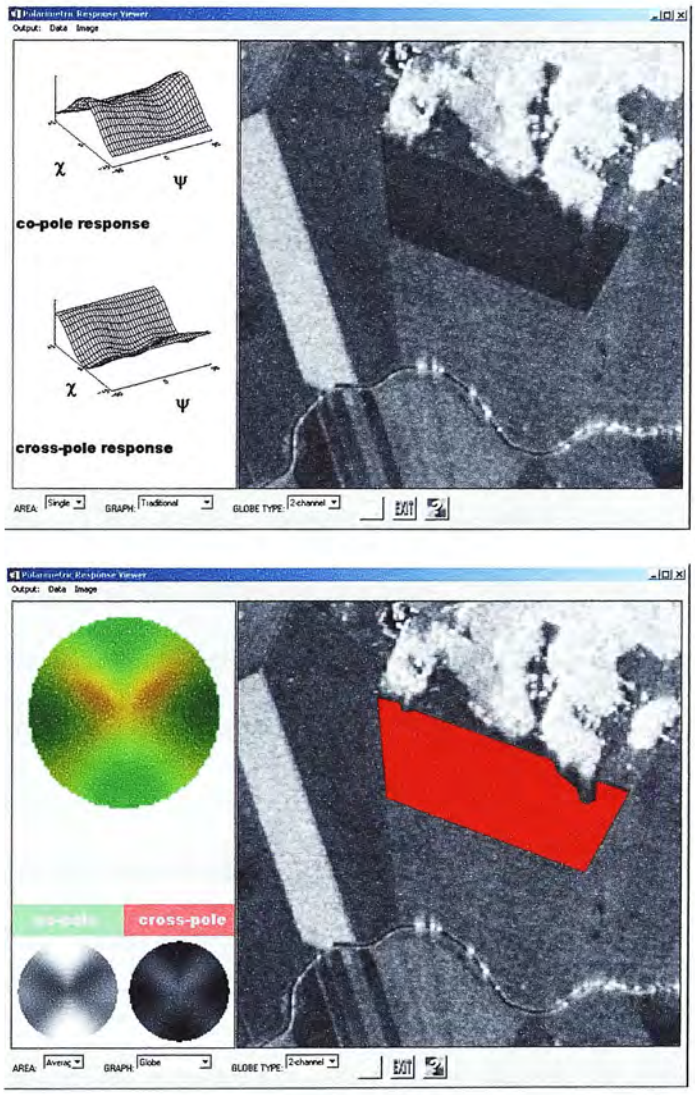

Figure 6.10: Using the polarimetric response viewer to assess individual response patterns. The upper image shows the response for an individual pixel, visualised using the traditional response graph. The lower image shows an average response for an area defined by the red polygon, and is represented using the polarimetric response globe.

These two options together are designed to allow researchers to examine polarimetric response patterns in a manner similar to the approaches used in most academic papers that examine polarimetric response patterns. The third option provides an adaptation of the synoptic approach detailed in the previous section, and thus allows researchers to examine the spatial qualities of variations in polarimetric response that, to this author's knowledge, have not been considered in research literature. Whilst this technique also uses the response globe, it also provides a number of separate options, and are thus described in the following, separate subsection.

6.7.2 – The Synoptic Response Viewer

Upon choosing the 'synoptic responses' selection, the user is required to select an area of the displayed intensity image, as was previously described for the areal average selection. Upon closing the polygon, however, a routine is initiated which sequentially calculates the individual response pattern for each enclosed pixel. A response globe is subsequently created, and overlain on a greyscale background value that represents the total power at the given pixel.

The use of a hexagonal gridding system was based on two factors. Firstly, the offset alignment of individual vertical lines of response allows the user to more easily between the range and azimuth directions. In SAR instruments, a single range line represents a continuous time-variant response. By aligning the input dataset so that the range direction falls along the vertical axis, this continuity is preserved in the visualisation. The second factor that led to the choice of the hexagonal plotting

system, as discussed in chapter 2, is that it allows a single response to be compared with six equidistant neighbours. The use of circular icons in this manner results in an apparently denser 'packing ratio' (Staunton, 1989) and also lessens the moiré effect caused by the rectilinear arrangement of icons at the large scale .

The resulting image, when calculated is presented in an 800*800 pixel viewing window. The size of this window places a constraint of the number of response patterns that can be effectively visualised as a minimum resolution of 20*20 pixels is required in order to produce a readable response pattern. In order to account for this, the routine measures the horizontal and vertical extent of the selected area, and resamples the data so that neither axis exceeds 40 pixels. It is recommended, where possible, to use even smaller areas as this will reduce the time needed to calculate the individual response patterns. An annotated example of the visual output of this procedure is shown in figure 6.11.

Upon completion, further drop-down menus allows the output image to be manipulated in a number of different ways. The options provided are as follows:

1) Standard visualisation
2) View background intensity image
3) View co-pol response only
4) View cross-pol response only
5) View intensity adjusted image

Each option can be assigned to either a mouse-press or mouse-release event, allowing the user to 'flick' between different representations. Option 2 'turns off' the response globes, allowing the background image to be examined. Options 3 and 4 deletes either the cross- or co-pol response from the viewing window, respectively. The final option adjusts each individual response pattern, so that the maximum intensity value used is equal to the normalised total power intensity. Thus pixels with a high total power become more visually dominant, whilst response in areas of low backscatter disappear. Examples of each of the image display options are presented in figures 6.11-6.14.

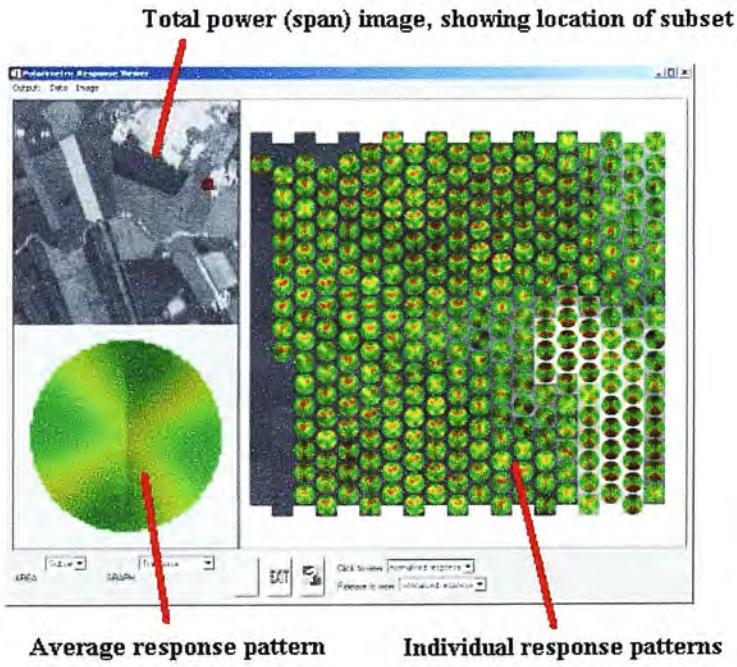

Figure 6.11: Output of the Synoptic Polarimetric Response Globe Viewer: Standard Visualisation.

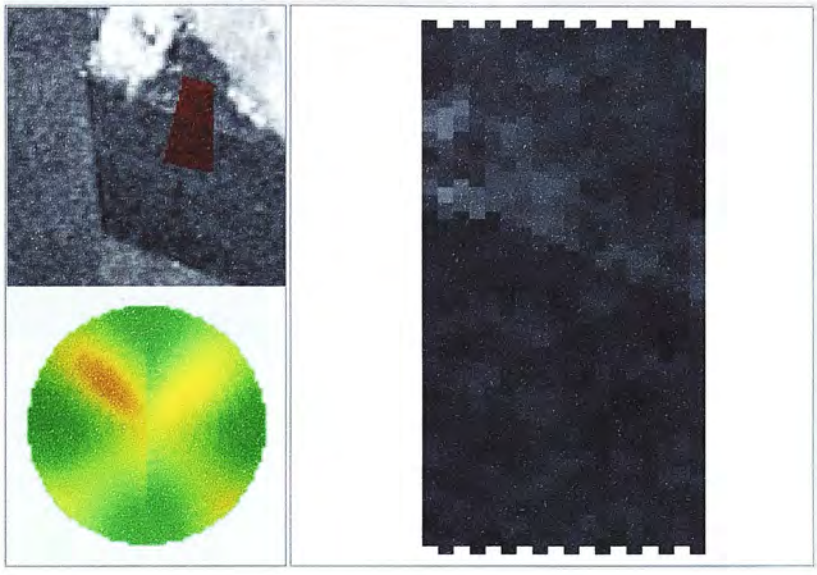

Figure 6.12: Output of the Synoptic Polarimetric Response Globe Viewer: Background intensity image.

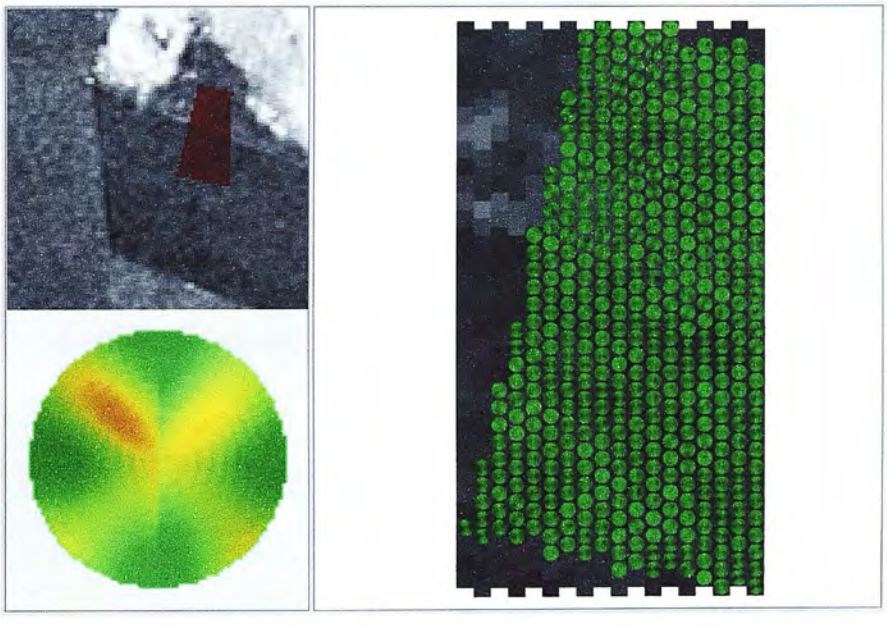

Figure 6.13: Output of the Synoptic Polarimetric Response Globe Viewer: Co-pol response only.

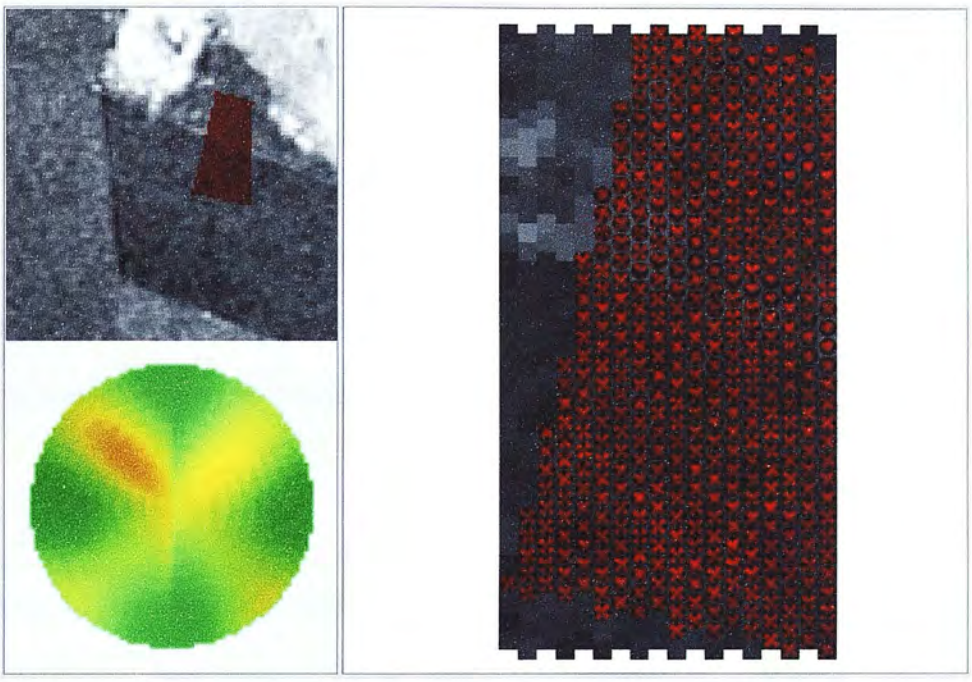

Figure 6.14: Output of the Synoptic Polarimetric Response Globe Viewer: Cross-pol response only.

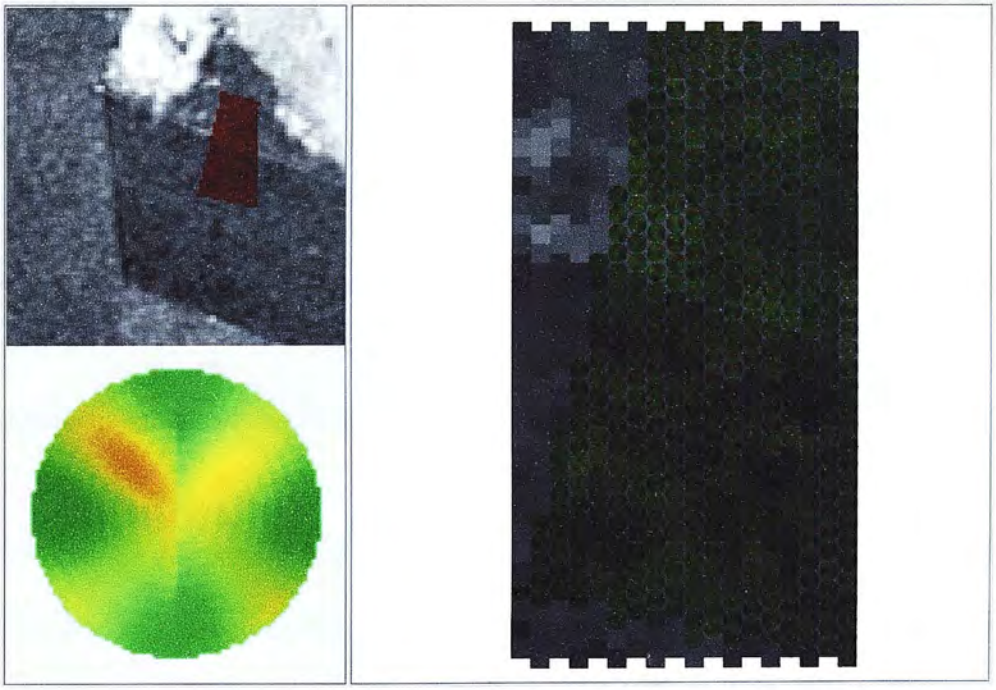

Figure 6.15: Output of the Synoptic Polarimetric Response Globe Viewer: Intensity Adjusted Image.

6.8 – Examples

In order to further explore the benefits of the newly developed visualisation technique, a number of examples are provided in figures 6.15-6.17. Each of these examples use data from airborne polarimeters and illustrate how the polarimetric response globe may be integrated into current research approaches.

In remote sensing studies it is common to use areas of homogenous landcover as the basis of training sets, which are used for classification algorithms. In radar polarimetry, homogenous areas have been used as a means of obtaining a 'polarimetric signature' for a particular landcover type (for example, in Skriver et al., 1999).

In figure 6.16, response patterns from a C-band datasets collected over a forest stand in Siggefora are presented. The large icon to the bottom left of the image shows the average response pattern for the region, which appear similar to that of a surface-type response. This type of response is to be expected at C-band, if the forest canopy is dense enough to act as a homogenous surface.

To describe this pattern as a 'polarimetric signature', however, would be misleading. This can be illustrated with reference to the synoptic overview of response patterns within the subset provided by figure 6.16. Even a cursory examination of this image reveals that response patterns are highly variable within the region in question. While some surface-type response patterns are apparent, there are also a considerable

number of dipole-like response graphs, as well as a number of graphs which do not resemble any of the idealised scatterers discussed so far.

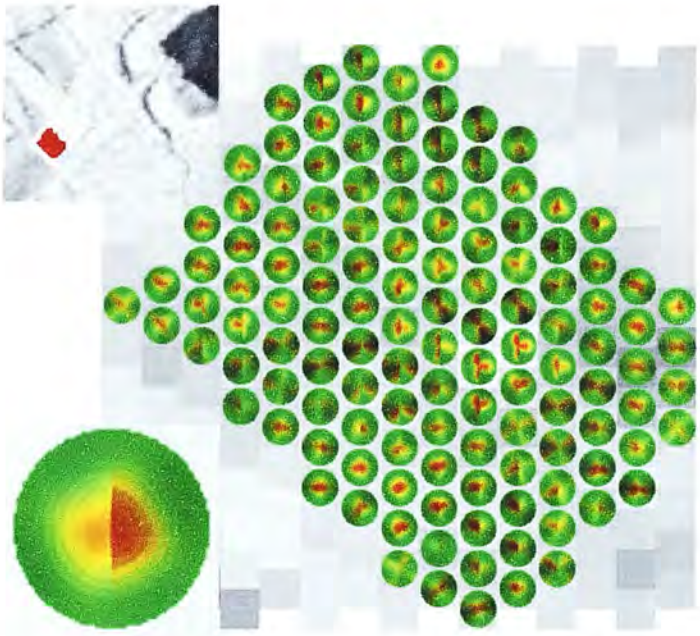

figure 6.16 :Response patterns derived from C-band data over a forested region near Siggefora, Sweden. Note the high variability between individual response patterns, which is inadequately represented by the average response (bottom left).

The variability that is clearly evident in figure 6.16 thus suggests that the use of the term 'polarimetric signature' for spatial averages is ill-advised, at least in forested areas. The application of the polarimetric data viewer to the analysis of response patterns, however, provides scientists with a fast and effective means of assessing the degree to which spatial averages represent individual resolution elements.

In some cases he application of the response globe viewer may result in the identification of regions which do have a characteristic scattering regime. In figure

6.17, for example, cross-pol response patterns derived from L-band data over an agricultural field are presented. In this case, the observed response patterns have a greater degree of spatial homogeneity, with a clear divide existing between two 'types' of response in the upper and lower halves of the selected region.

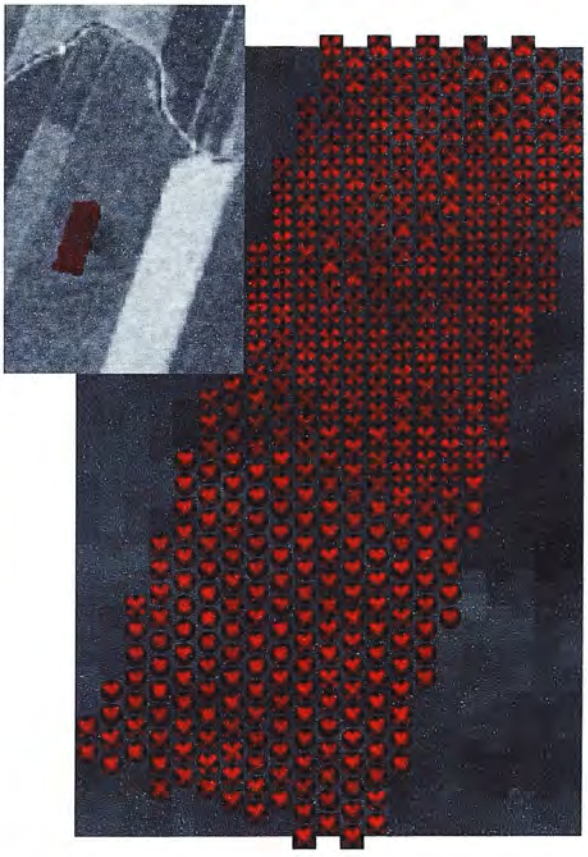

Figure 6.17: L-band cross-pol response patterns over an agricultural field near Siggefora. By isolating the cross-pol response, two distinctive patterns are clearly visible.

The observation of spatially homogenous response patterns is particularly useful, as it encourages the researcher to further question the nature of polarimetric interactions in a given area. In figure 6.17, for example, the upper half of the imaged region is dominated by dihedral-type response patterns. The lower half of the region, in

contrast, is dominated by response patterns, which, by virtue of the asymmetry between the upper and low halves of the globe, have no immediate analogue in the idealised scatterers presented in chapter 5. The fact that this pattern remains relatively stable over a defined geographic region, however, would suggest that the observed response pattern is nevertheless the result of a particular type of polarimetric interaction, which merits further exploration.

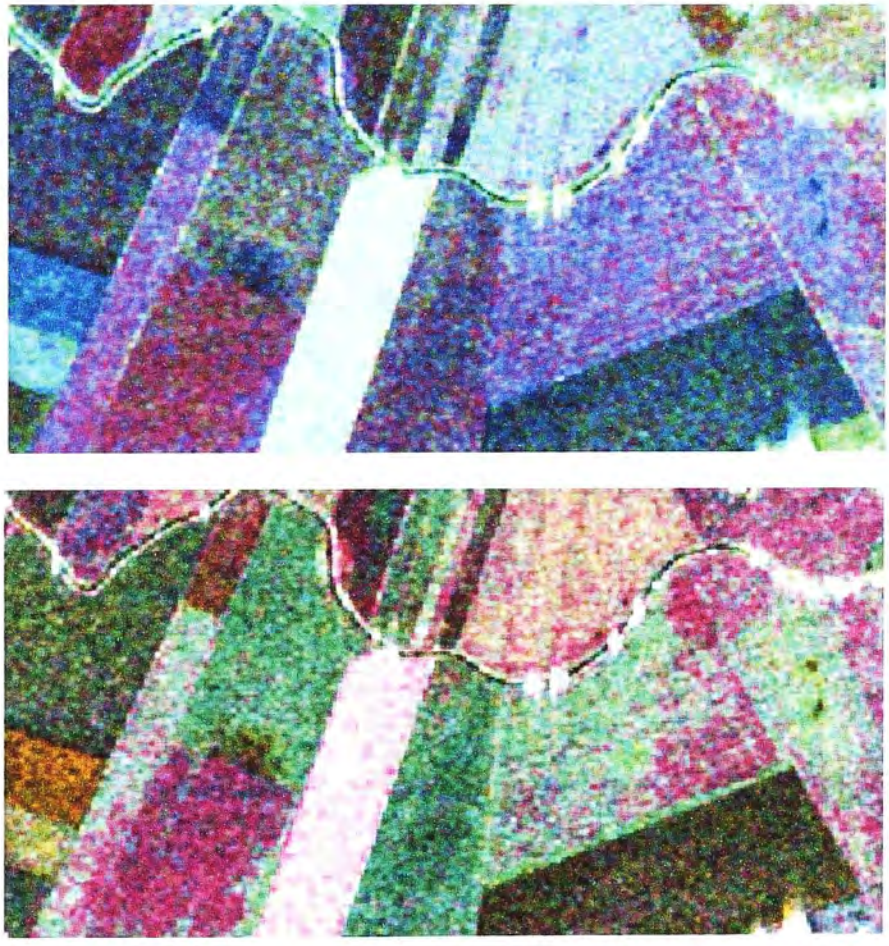

figure 6.18: Two RGB composites of an agricultural area in Sweden at L-band. The top image shows a standard RGB colour composite (hhhh, hvhv, vvvv), whilst the lower image shows an RGB composite based on the response patterns observed in figure 6.17.

Whilst the response viewer may be used as a research tool in its own right, it is also possible that observations made using this tool can be used to influence the application of other visualisation techniques. In figure 6.18, for example, two RGB colour composites are presented for the region surrounding that used in figure 6.17. The upper of the two images shows a simple RGB composite formed from the diagonal elements of the covariance matrix (as discussed in chapter 5). The lower image, in contrast, presents an RGB composite formed from polarisation combinations suggested by the response patterns in figure 6.17

The resulting colour composite clearly separates the two distinct scattering regimes discovered in figure 6.17 in a manner that is not achieved with the standard RGB composite. In addition, it is also apparent that similar boundaries exist in other nearby fields. The use of the polarimetric response globe, therefore, has allowed the researcher to take the information from individual response patterns, and apply it to visualisation strategies at the small scale. The synoptic response viewer has, in this case, provided a useful 'bridging' tool between different spatial scales of enquiry.

6.9 – The Polarimetric Data Viewer

As a means of encouraging the use of the polarimetric response globe viewer described in the previous section, a software application has been designed which allows the response globe viewer to be used in conjunction with a number of other standard image processing functions. This software runs using IDL (versions 5.0 or higher) (www.rsinc.com) and can be found on the CD enclosed with this thesis. The

package is also available by contacting either the author (dtr@geo.ed.ac.uk) or Iain Woodhouse (ihw@geo.ed.ac.uk). This software is provided as an exploratory tool, and should be considered as a beta testing version only. The author accepts no responsibility for any problems which may be encountered in using the software, although any questions regarding the operation of the package can be sent to the above e-mail address.

Also included on the CD is a test dataset taken over Siggefora, Sweden (Woodhouse and Hoekman, 2000), which can be used to analyse the various components of the package. Full instructions on how to load this dataset, alongside details of how to format other datasets, are included in the appendix.

Figure 6.19 shows the initial data selection screen, with the test dataset loaded. The use is required to select a subset of this data, which is then carried through to the visualisation modules. These modules are displayed in figure 6.20, and each produce either RGB or HSV colour composites using the various visualisation techniques discussed in chapter 5. For the RGB colour composite modules, the user can set the upper and lower bounds for each channel interactively, using on-screen histograms (as shown in figure 6.21). For the HSV colour composites, the same function is provided for the saturation and intensity channels only (as shown in figure 6.22).

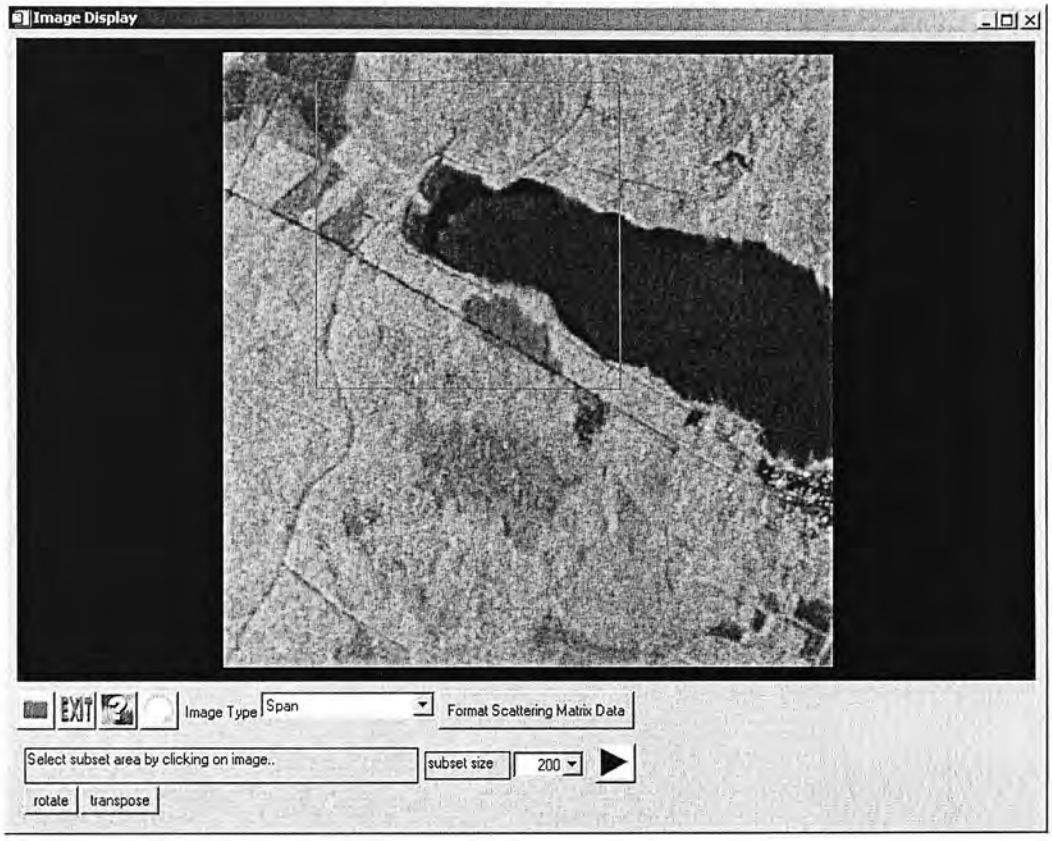

figure 6.19: The initial data selection screen for the Polarimetric Data Viewer. A total power intensity image is used to choose an area for further visual analysis.

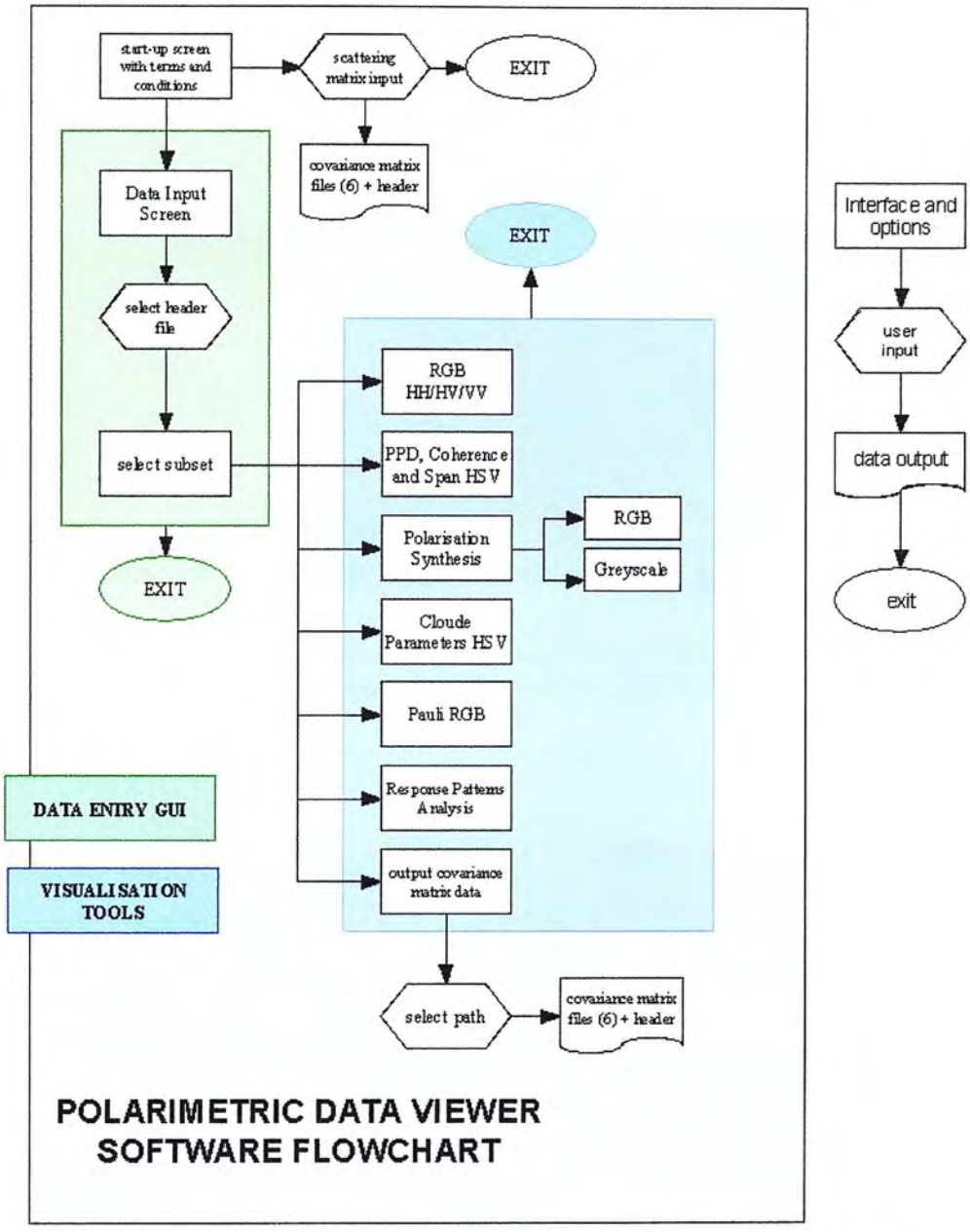

figure 6.20*: Flowchart showing the main components of the polarimetric data viewer. Each visualisation tool presents the viewer with a separate, interactive widget.*

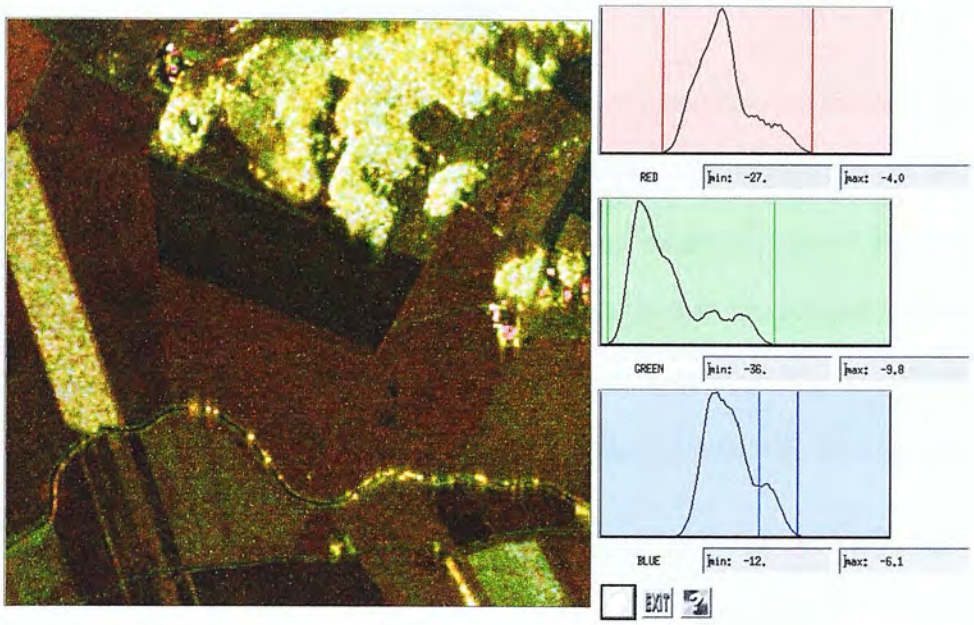

Figure 6.21: RGB colour composite module from the polarimetric data viewer. The user can set the upper an lower bounds for each image channel interactively using the histograms to the right of the image.

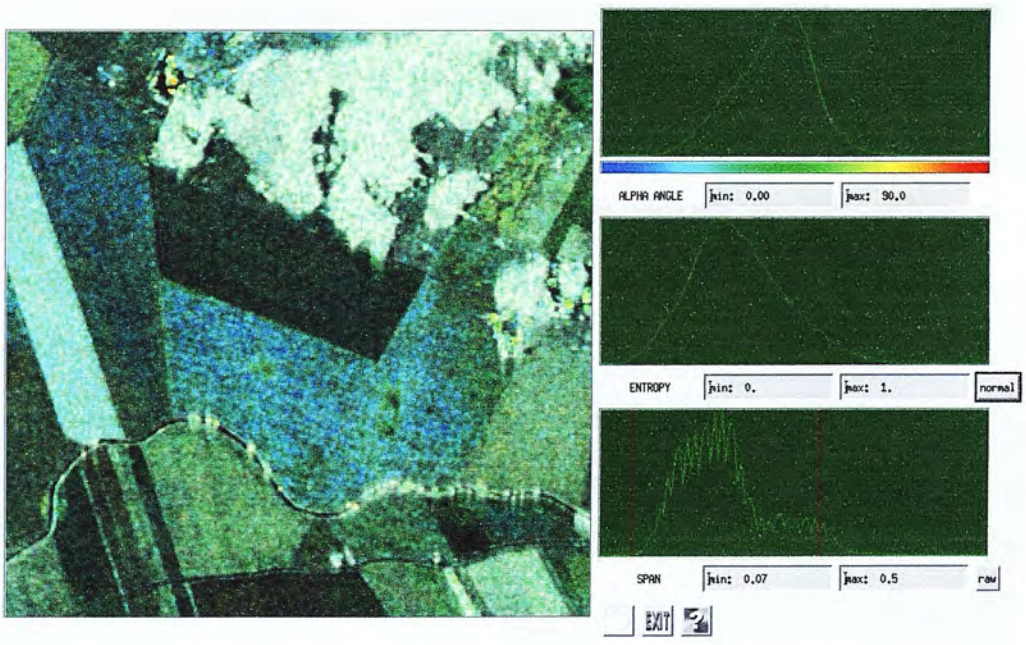

Figure 6.22: HSV colour composite model from the polarimetric data viewer. The user can set the upper and lower bounds for the saturation and intensity channels, whilst the hue channel remains fixed. The saturation channel can also be inverted, to produce images similar to that shown in figure 5.11.

The purpose of collating the various visualisation techniques in the manner permitted by the Polarimetric Data Viewer is to encourage the application of multiple visualisation strategies to datasets at the preliminary stages of research. By using this package, a researcher is able to quickly generate several images that can then be analysed together. Any patterns or anomalies can be subsequently by investigated further using the polarimetric globe viewer, which in turn can be used to direct further research.

As such, the Polarimetric Data Viewer can be viewed as an example of an exploratory visualisation tool, as described in chapter 3. Using the criteria specified by Maceachren and Kraak (1997), it is possible to demonstrate the validity of this claim. Firstly, the package is designed for private, exploratory research that can be used in the early stages of research projects. Secondly, the software is interactive, offering the user multiple options to quickly alter aspects of the visualisation strategy. Thirdly, and most importantly, the package can be used to 'reveal unknowns'. This is facilitated primarily by combining standard visualisation techniques for polarimetric radar (as were outlined in chapter five) with the new polarimetric response globe viewer. In the following chapter, the means by which the viewer can be used as a research tool is described in more detail, and also analyses the effectiveness of the polarimetric response globe as a visual icon.

CHAPTER 7 – THE POLARIMETRIC RESPONSE GLOBE: ASSESSMENT AND CASE STUDY

7.1 – Introduction

In the previous chapter, a new technique for the visualisation of polarimetric response patterns was introduced. It was shown that, by reprojecting the traditional polarimetric response graph, backscatter intensities could be represented using an icon which was suitable for synoptic visualisation.

In this chapter, the effectiveness of the new visualisation technique is tested. This is achieved in two ways. Firstly, the effectiveness of the design of the polarimetric response globe is analysed via a web-based user survey. This survey asks respondents to describe the patterns visible in images composed of different response graph representations. The second test involves the application of the polarimetric response viewer to the analysis of patterns in an actual dataset, and demonstrates how the developed technique can be used to guide research. This is achieved through the construction of a backscatter model which attempts to describe the nature of polarimetric interactions over an area of homogenous response patterns. The use of the response globe as a tool for exploration, analysis and synthesis is central to the development of this model, and as such, reflects my own growing understanding of polarimetric radar data. The diagrams used to illustrate the concepts embodied in the

model, therefore, are intended to act as tools of communication, and to illustrate how the development of the model has been derived from the 'visual thinking' facilitated by the response globe.

These two tests described in this chapter are proposed in order to analyse not only the visual effectiveness of the new technique, but also its potential application as a research tool. In both cases, however, it is hoped that the results of these tests support the validity of both the polarimetric response globe as a research tool, and the application of scientific visualisation techniques in general.

7.2 – Assessing the Visual Effectiveness of the Response Globe

In remote sensing, a common means of testing the resolution of an instrument is to examine a calibration target. For polarimetric radar data, the most commonly used target is the trihedral corner reflector (Cloude et al., 2001, Zebker et al., 1991), which results in high backscatter values and a well-defined polarimetric response curve. Such targets are primarily used as a means of calibrating the measured data. For optical remote sensing applications, calibration targets more commonly take the form of painted areas near testsites. These areas are painted with a variety of patterns, which can subsequently be located in the measured data, and analysed (Campbell, 1996, pp.271). Such targets are useful for providing a nominal spatial resolution for an instrument, but may also be used to calibrate spectral resolution.

The following section uses an abstraction of the traditional calibration target as a means of comparing different modes of representing polarimetric response. In order

for a visualisation technique to be deemed 'effective', it must display variables in a manner which allows the underlying physical phenomena to be interpreted accurately, quickly and without bias (Laidlaw et al., 2001). One means of testing the visual effectiveness of the polarimetric response globe, therefore, is to construct 'test patterns' of scattering matrices, and to assess whether these patterns are evident after the application of the aforementioned visualisation technique.

In chapter 4, a number of polarimetric response graphs were presented for idealized geometric scatterers. These patterns were used again in chapter 6 to illustrate the structure of the newly developed polarimetric response globe. Using these simple geometric objects, it is possible to construct 'visual calibration targets' which can be used to assess the visual efficiency of different modes of representing polarimetric response patterns.

Examples of such patterns are shown in figure 7.1 and figure 7.2. In each case, a 5*5 array composed of several of the idealised scatterers (namely, a trihedral, a dihedral and various dipoles) is used to create twos pattern. In the first pattern, the arrangement of scatterers exhibits a clear radial pattern, whilst in the second the pattern radiates from the base of the image in a 'crown' formation.. Figures 7.3 and 7.4 presents the polarimetric response patterns for each of these targets visualised using both the traditional and newly developed techniques described in the previous chapters.

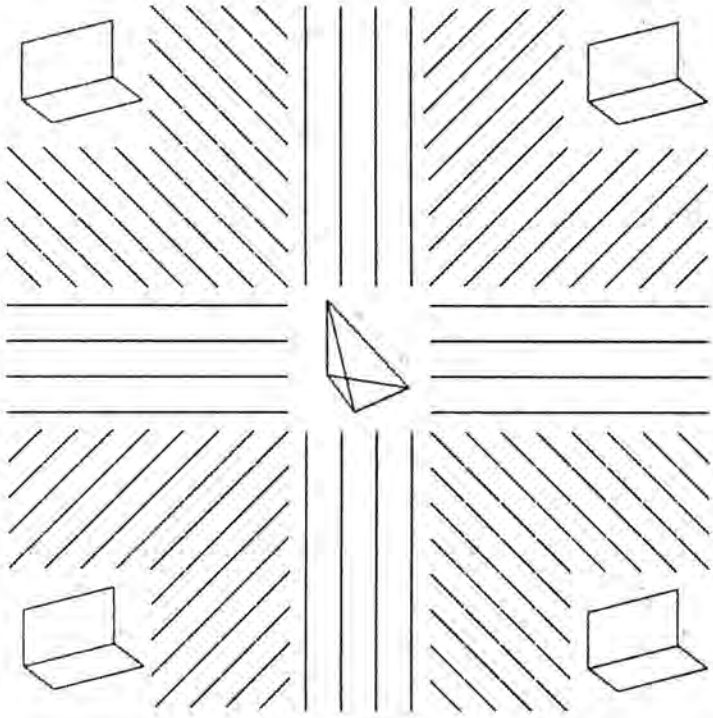

figure 7.1 – A theoretical polarimetric calibration target with a star-shaped radial pattern, constructed using dipoles, dihedrals and a trihedral.

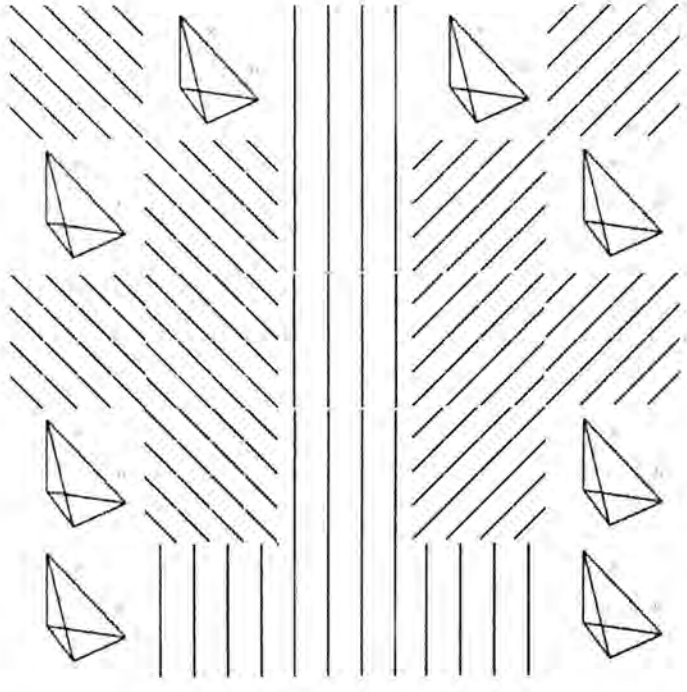

figure 7.2 – A theoretical polarimetric calibration target with a crown-shaped radial pattern, constructed using dipoles and trihedrals.

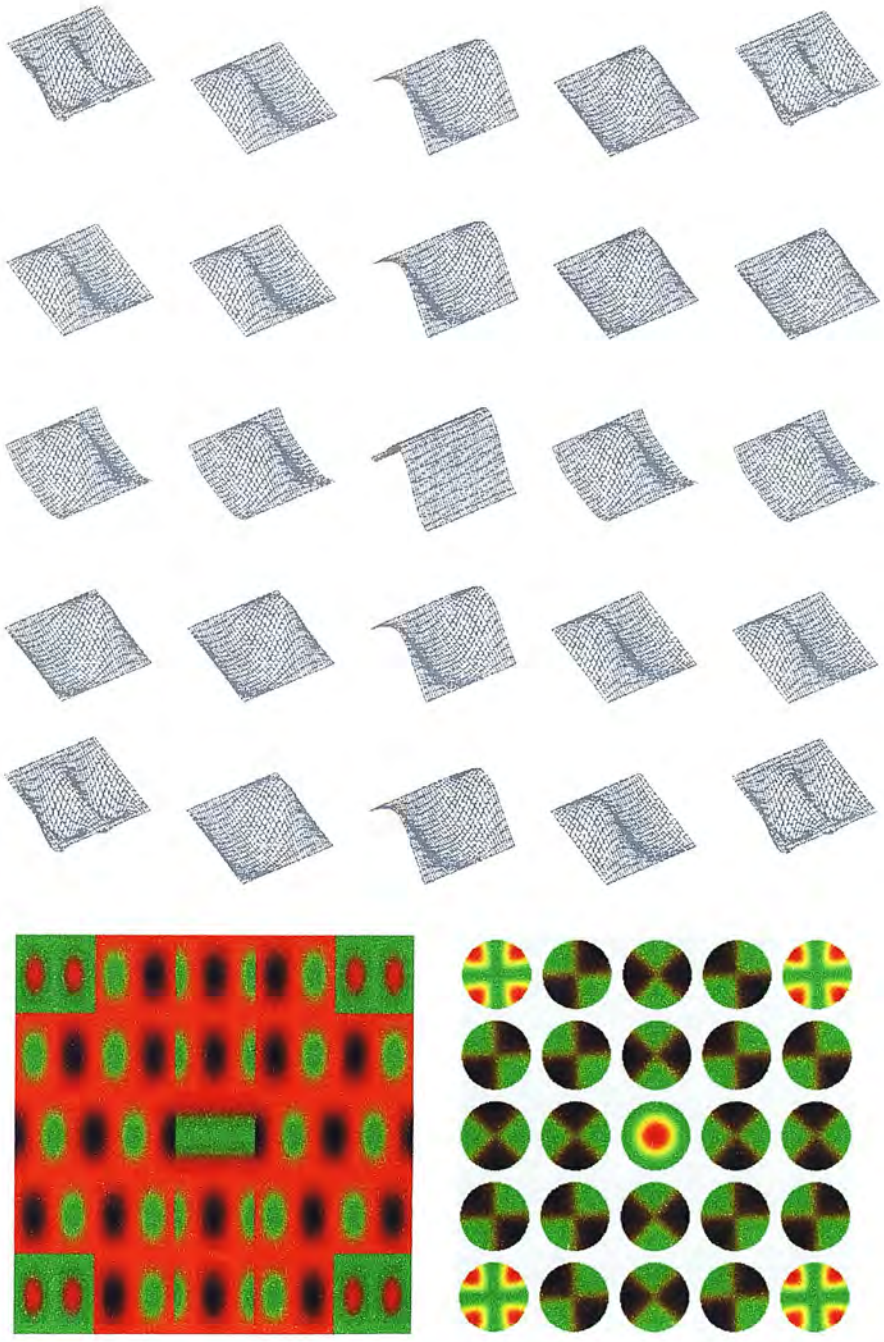

figure 7.3: The calibration target shown in figure 7.1 visualised using different representations of polarimetric response: (top) traditional isometric graph (co-pol only), (bottom left) 2D projection of traditional and, (bottom right) the polarimetric response globe.

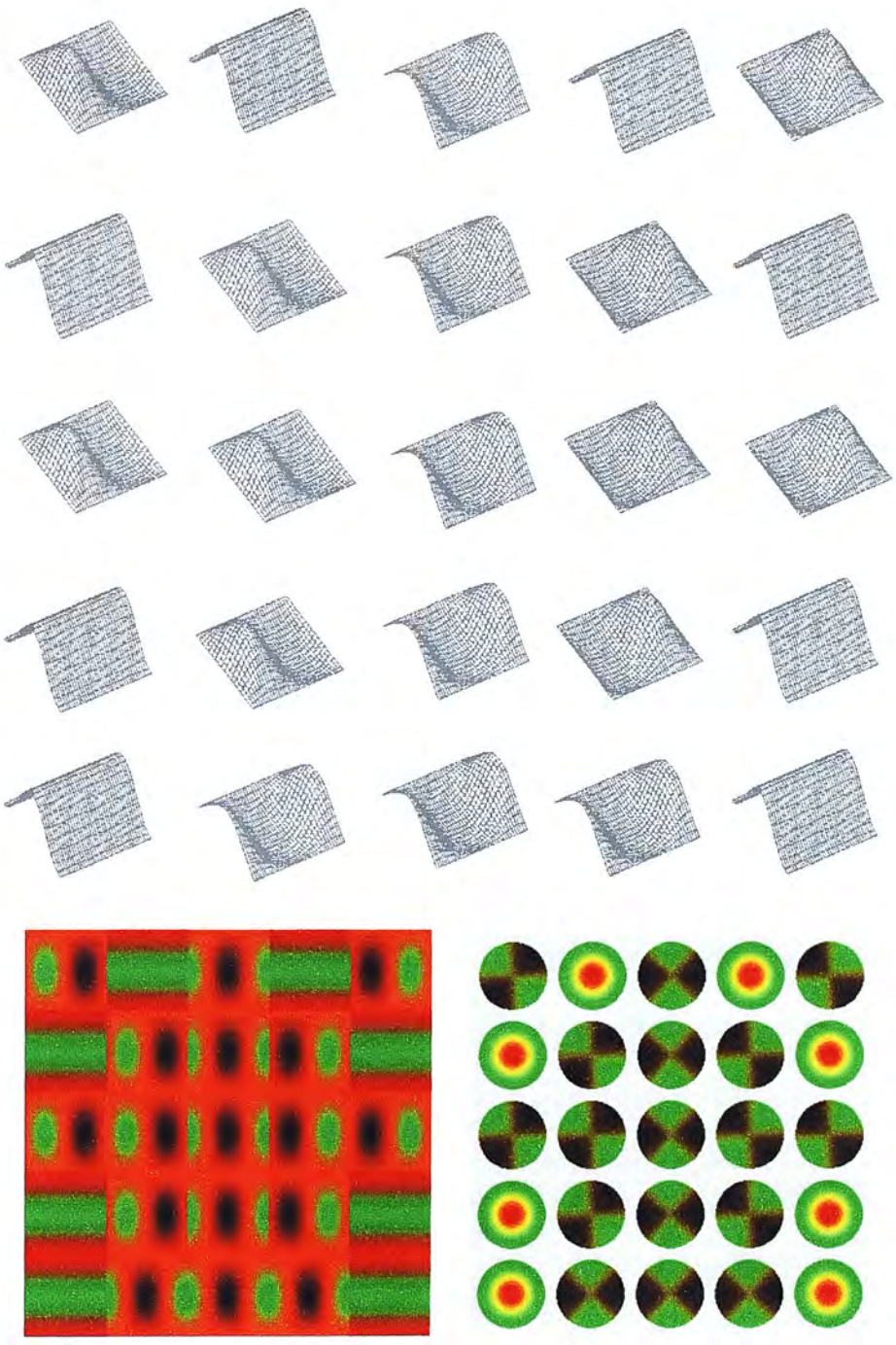

figure 7.4: The calibration target shown in figure 7.2 visualised using different representations of polarimetric response: (top) traditional isometric graph (co-pol only), (bottom left) 2D projection of traditional and, (bottom right) the polarimetric response globe.

These patterns are subsequently used to form the basis of a web-based user-survey (a copy of which can be found in the appendix), which asks participants to examine a series of images. For each image, the participant is required to select either a triangle, square of crown pattern, and to attach a level of confidence to each answer depending on which pattern is most visible.

The questionnaire was circulated amongst MSc and PhD student in the Geography department of the University of Edinburgh. 40 respondents completed the questionnaire, all of whom were asked to indicate their familiarity with radar polarimetry. Of the 40 respondents, 50% had never heard of radar polarimetry, and a further 40% knew it only by name. Of the remaining ten percent, three respondents indicated that they had only basic knowledge, while only one possessed any research experience.

The target audience of the questionnaire, therefore, were non-specialised users who can be said to be representative of the 'applied' side of remote sensing (as oppose to the more theortical, mathematical side). The reason for this choice was to assess how well the proposed visualisation technique stood up against the traditional methods of representation without the burden of preconceived attitudes towards how polarimetric radar data has been previously analysed.

For this very reason, prior to completing the questionnaire no information was presented relating to the usage of the icons, or the nature or application of polarimetry in environmental research. By structuring the test in this manner, and by using a survey group with a limited knowledge of radar polarimetry, it is ensured that the results of the test will indicate the effectiveness of the newly developed technique for the representation of patterns, independent of any background knowledge.

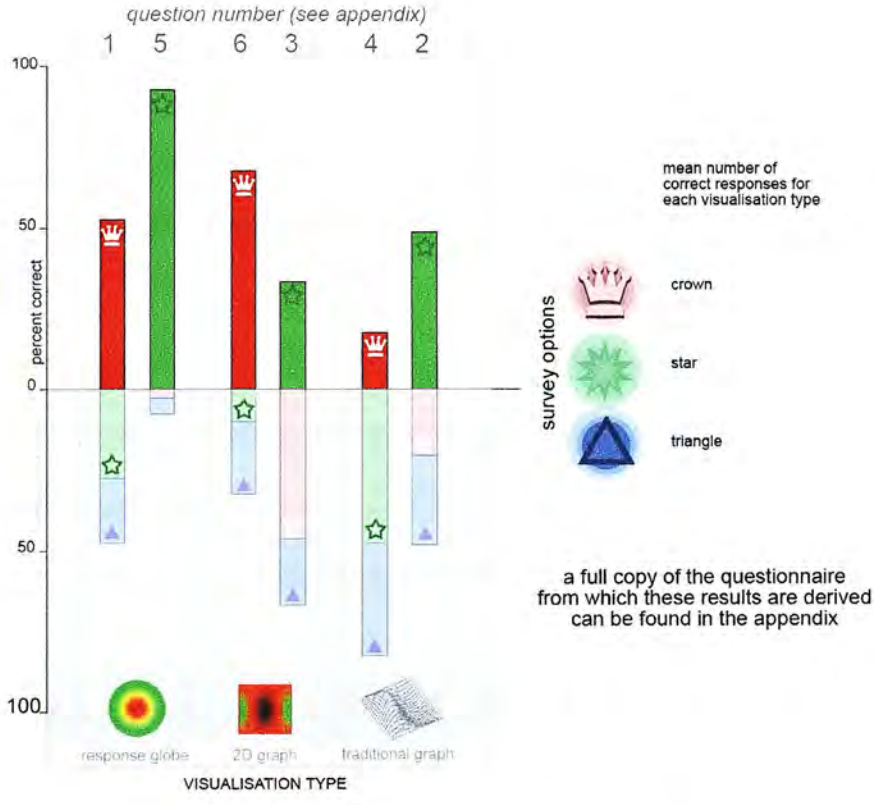

figure 7.5 – Comparison of correct versus wrong answers for the polarimetric response pattern questionnaire, taken from a sample of 40 respondents.

In figure 7.5, the results of the questionnaire are presented. For each of the six questions, the responses are presented as a stacked bar chart, with the number of

correct responses in the upper half of the figure, which can be compared to the number of incorrect responses, which are in the lower, shaded portion of the figure. The colour of the bar chart indicates the shape chosen by the respondent, with the crown, star and triangle represented by red, green and blue, respectively.

It is immediately apparent that all of the techniques used in the survey have a degree of ambiguity, as over 25% of respondents chose the wrong pattern for all but one of the questions posed. It is only for the polarimetric response globe, however, that the majority of respondents chose the correct pattern for both answers. The high result for the radial 'star' pattern also indicates that the parameter of orientation is represented more successfully using the new technique.

This can be demonstrated more effectively by examining the results for the 2D representation of the star pattern, where just under 50% of respondents mistook the pattern for the crown shape. The reason for this, as can be seen in figure 7.3 lies with the discontinuity of the orientation angle in the 2D representation. As the eye is sensitive to continuity (Kohler, 1930), the peaks and nulls in the co-pol (green) response pattern appear to form a radial pattern which emanates from the base of the graph, and thus more closely represents a crown shape.

With the globe representation, however, this ambiguity is resolved through the mapping of the orientation angle to an angular visual variable. The use of a circular icon ensures that individual responses are read as discrete entities, and that any patterns in the data are represented as the relationships between individual icons.

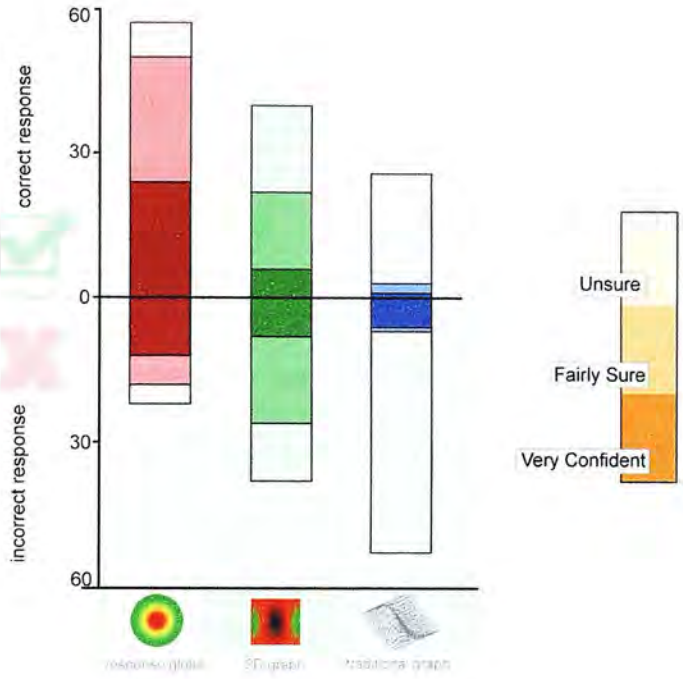

figure 7.6 – Confidence levels (represented using saturation) for each of the different response visualisation techniques, shown for both correct and incorrect responses.

It is also interesting to note that the traditional isometric projection fares the worst of the three representations, despite being the most commonly used in polarimetric radar literature. This relationship is even more apparent in figure 7.6, which shown the confidence that each user attached to his/her choices. For the isometric presentation, 87% of respondents were unsure of their answers, compared to only 14% for the response globe.

Note also that for the response globe, a larger number of respondents who answered 'very confident' or 'fairly sure' chose the correct response pattern. For the 2D representation, in contrast, more of this group chose the wrong response (caused primarily by misinterpretation of the 'star' pattern discussed previously). What is

most important, however, is that the majority of respondents felt most comfortable using the response icons over the other representations (70% indicated that they preferred the globe), and that the use of these icons led to more accurate analyses of the 'target' patterns.

From this, it is possible to state that the polarimetric response globe, as a visualisation design at least, has a number of advantages that indicate that it is easier to read than the traditional design. In the following section, the benefits of the practical application of this approach will be explored in more detail.

7.3 – Case Study: The Response Globe as a Tool for Exploratory Analysis

In the previous section, it was demonstrated that the polarimetric response globe is a more effective means of analysing multiple polarimetric response patterns than either the traditional isometric response graph, or its two-dimensional counterpart. This assessment is based on a comparison of three different methods for representing polarimetric response patterns solely in terms of the efficiency of their design, and makes no claim to the utility of the response globe as a research tool. In the following sections, the synoptic response viewer described in chapter 6 is applied to the observation and analysis of an actual dataset in order to demonstrate the effectiveness of the new visualisation technique in terms of exploratory visualisation.

figure 7.7 – Photograph of reed beds next to Lake Siggefora (photograph courtesy of Pete Van Oevelen).

To achieve this, a dataset first introduced in chapter 6 is revisited. In chapter 6, a new visualisation technique using ellipse icons for the analysis of variables from the Entropy/α decomposition was applied to C-band data collected over a forested region in Sweden. In the resulting visualisation, a strong correlation between all five variables was observed over a region of reed beds (shown in figure 7.7).

In chapter 5, five variables from the Entropy/α decomposition were mapped to the visual variables of an ellipse. Using this technique it was found that the five variables (namely, total power, entropy, polarimetric coherence and the alpha and beta angles) exhibited a high degree of correlation over a well-defined spatial extent. In this section, the same area is analysed using a number of alternative visualisation strategies, including the synoptic globe visualisation technique. These observations are subsequently used as the basis for a model that attempts to explain the nature of polarimetric interactions in this region

7.3.1 – Observation of Polarimetric Response Patterns in the Siggefora Dataset

The research detailed in the following section is intended to serve as proof of the role visualisation can play in the serendipitous discovery of patterns and relationships in complex multi-valued datasets. This is achieved by examining distinctive polarimetric response patterns observed over an area of reed beds, and using these patterns to build a conceptual model of scattering mechanisms in this region.

The initial synoptic analysis of polarimetric response patterns on which this work is based utilised airborne SAR data from the EMISAR aircraft, taken as part of the NOPEX campaign (Woodhouse and Hoekman, 2000) for an area of boreal-type forest near Lake Siggefora, collected at both L- and C- band. The initial aim of analysing this data was to assess the possibility of using response patterns as a means of classification. Although the term 'polarimetric signature' is generally discouraged, it is nevertheless common to see response graphs presented as being in some way representative of different crop types or tree species (Conradsen et al., 2003, Durden et al., 1989).

In order to test the effectiveness of this approach, images were produced which compared the average response patterns to the individual patterns. In the Siggefora image, a number of tree stands were analysed. In all cases, and at both frequencies, it was discovered that the response patterns within each subset were very variable, and that the spatial average was in no way representative of the individual patterns. This

suggests that the use of averaged response patterns is a largely prescriptive technique that should not be used as a viable means of classification.

During the analysis of the forest patterns, however, it became apparent that large areas of the image did produce response patterns that were similar over extensive areas, and in particular over an area corresponding to a lake-shore reed bed. A spatial average taken over this area thus does produce a representative response pattern. A similar response pattern is visible at both C- and L-band, although the total backscattered power at C-band is much higher than at L-band. An image showing the location of the reed bed area, and a synoptic overview of the response patterns, is shown in figure 7.8.

The discovery of such a large area of consistent response is made more interesting by the nature of the response pattern. The modelling of polarimetric response often assumes that a backscattered signal is made up of *additive* response patterns from a number of `layers' within the landscape. Forward models will often assume that each layer is made up of simple, geometric objects (Ferrazolli and Guerriero, 1994). As a result, inverse models will often try to decompose the observed response as a combination of these idealised response patterns. An example of this is the Freeman decomposition, introduced in chapter 4, which describes observed response patterns as the additive combination of surface, dihedral and volume scattering (Freeman and Durden, 1998).

The response pattern observed in the Siggefora dataset, however, cannot be achieved through the additive combination of idealised response patterns due to a very pronounced asymmetry in the cross pole response between the upper and lower halves of the globe. The fact that this response pattern has a definite spatial location and extent means that the observed pattern is unlikely to be the result of a calibration error, or an example of random, volume scattering.

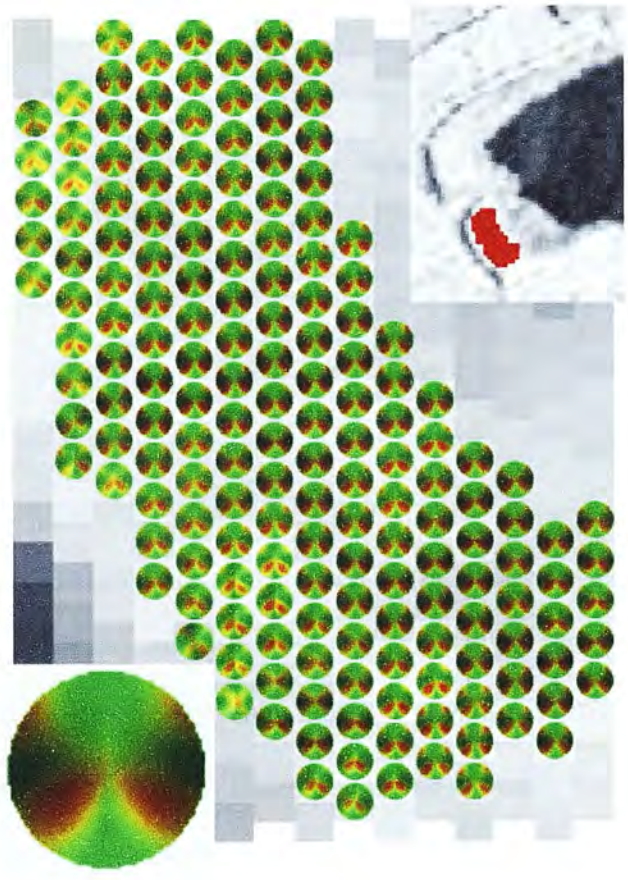

figure 7.8 – Response patterns over reed beds in lake Siggefora at C-band.

From visual analysis alone, therefore, it is clearly evident that the presence of such vertical vegetation produces a response pattern that is not adequately described by current modeling and decomposition techniques. In order to illustrate this more

thoroughly, a number of the traditional visualisation techniques described in chapter 3 are applied to the Siggefora reed bed test site.

7.3.2 – Application of Traditional Visualisation Techniques

In order to emphasise the benefits of the newly developed visualisation technique, it is instructive to apply the standard means of representing polarimetric data to the study site. By analysing the interpretations that can be derived from these representations, it can be demonstrated that the synoptic approach provides a more detailed level of insight into the nature of polarimetric scattering over this area.

In figure 7.9, the polarimetric response is represented using the traditional isometric graphs, showing the co- and cross-pol case. The peak response in the cross-pol pattern for the elliptical polarisations is still apparent using this method, and is manifest in an asymmetry either side of the central line that defines the linear polarisations. In (Zebker et al., 1991), such asymmetries are cited as evidence of calibration errors in the original radar measurements, which are subsequently corrected during data processing. It is therefore conceivable that the occurrence of such patterns, when examined in isolation, may be mistaken for evidence of similar calibration errors. Using the synoptic approach to polarimetric response pattern visualisation, however, it is apparent that this asymmetry has a definite spatial extent, and exists close to other patterns over the water surface (both in the range and azimuth directions) which are symmetrical . The synoptic visualisation therefore suggests that the observed response is a characteristic pattern associated with the

particular configuration of scatterers which exists within this region, rather than a global calibration error. The additional information contained in the synoptic visualization, combined with the unusual appearance of these response patterns therefore suggests that this region deserves closer inspection.

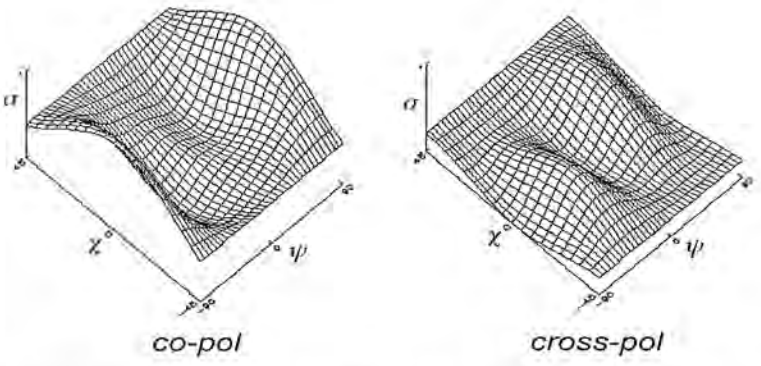

Figure 7.9 – Response pattern derived from an areal average over the reed bed in the Siggefora dataset (C-band) visualised using the traditional response graph.

In figures 7.10 and 7.11, the area containing the reed beds in the Siggefora subscene is represented using the standard visualisation techniques described in chapter 4 for the C- and L-band datasets, respectively. The first figure in each diagram shows an RGB composite of the diagonal elements of the covariance matrix, thus representing the total backscattered power for the hh, hv and vv channels. In the C-band image, it is immediately apparent that there is an area of high backscatter with a distinctive response profile. This area will subsequently be referred to as the 'reed bed area'. The purple shading of this area represents a dominance of vv backscatter, with some contribution from the hh channel, and a low hv response. Such a response profile is typical of a dihedral interaction, with the amplification in the vv channel possibly

evidence of additional dipole scattering Note also that the backscatter in this area is high in relation to the nearby lake surface. In the L-band image, conversely, the backscattered power over much of the reed bed area is lower than the nearby lake surface. It is notable, however, that the backscattered response increases nearer to the shoreline, and is dominated by vv response values.

A similar pattern is evident in the second image in each diagram, which shows the coherency matrix, or Pauli intensities. In this case, however, the hh-vv channel dominates the backscattered response over the reed bed area, indicating a dominance of dihedral-type mechanisms which contrast, at both wavelengths, with the surface and volume returns from the nearby lake and forested areas, respectively. Again, the L-band image exhibits an area of contiguous low backscattered response within the studied area. It is interesting to note, however, that the response values shoreward of this area are dominated by hh-vv intensities, which contrast with the lakeward side, which exhibits higher hh+vv returns.

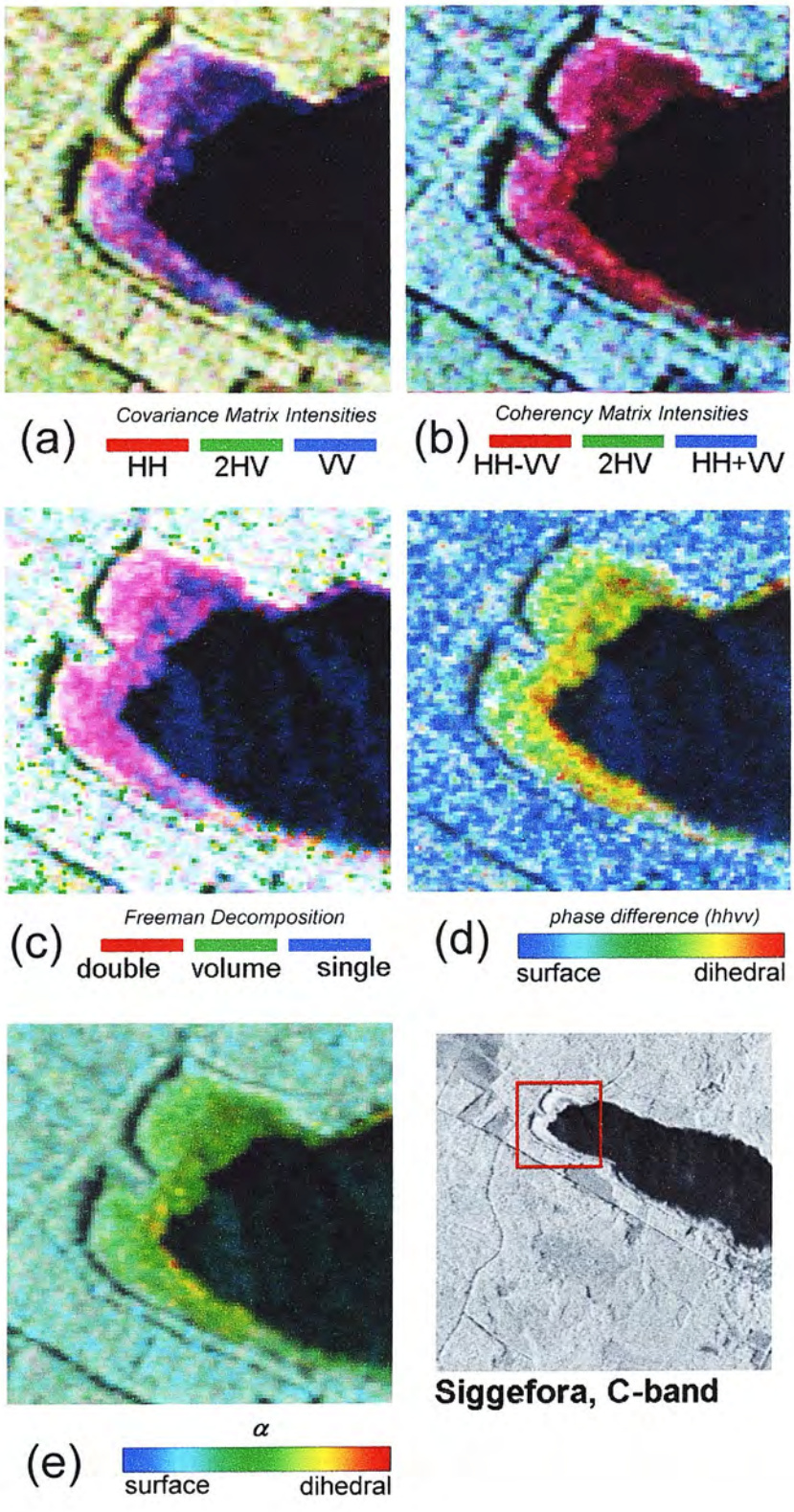

figure 7.10 – Application of traditional synoptic visualisation techniques to the Siggefora study area (C-band data).

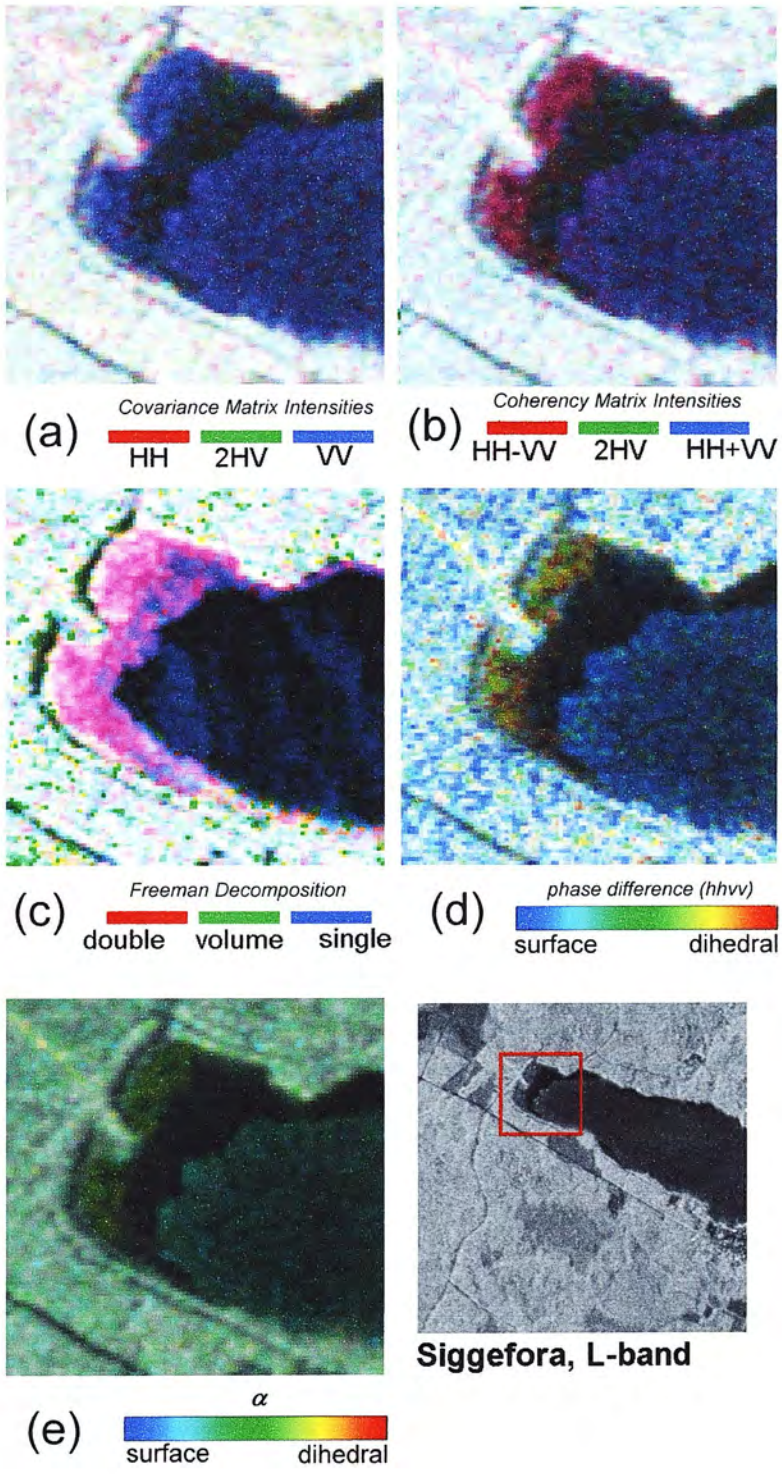

figure 7.11 – Application of traditional synoptic visualisation techniques to the Siggefora study area (L-band data).

The images on the middle row of figures 7.10 and 7.11 are both HSV composites. The first of these images shows the polarimetric phase difference as a hue value, with the coherence and total power ascribed to the saturation and value channels, respectively. At C-band, there is a dominance of intermediate phase difference values over the reed bed area, which in others areas of the image are typically associated with low coherence values. The high coherence values evident in this region, however, suggests the presence of a dominant scattering mechanism (Ulaby et al., 1987). It is also notable that the phase difference angle increases around the lakeside border towards dihedral-like values. In the L-band image, the area of low response separates two areas with different scattering properties: whilst the lake-side responses tend towards surface (blue) values, the landward side is dominated by intermediate and dihedral phase difference values.

The second HSV composite in figures 7.10 and 7.11 shows values derived from the Cloude and Pottier eigenvalue decomposition (Cloude and Pottier, 1997), and represents the alpha angle parameter using the hue channel. Despite the basis-invariance of parameters derived from the Entropy/α decomposition, the patterns which occur over the reed bed areas are similar to those discussed for the hhvv phase difference visualisation. In the C-band image in particular, the reed beds are shown as low entropy (i.e. highly saturated) pixels, with a spatially homogenous intermediate alpha angle value. Low entropy, intermediate alpha angle values are associated with dipole scattering (Cloude and Pottier, 1997). Such alpha angle values

also characterise the L-band response over the reeds, but are less evident due to the lower backscatter values.

Figures 7.10c and 7.11c show the Freeman decomposition for the same area, visualised using an RGB colour composite based on the backscattered power of the dihedral, volume and surface returns, respectively. At both C- and L-band, the reed bed area contrasts greatly with both the surrounding lake surface and forested areas. The purple hue represents dominant surface scattering with a sizeable dihedral contribution, which is evident at both C- and L-band.

In summary, each of the visualisation techniques used isolate the reed-bed area as an area of spatial homogeneity at C-band, which is markedly different to the surrounding area. The spatial extent of the same area can also be seen in the L-band image, but is characterized by low backscatter intensity values. The information relating to nature of scattering that can be obtained from each image, however, is contradictory and inconclusive. All three of the intensity-based visualisation techniques, including the Freeman decomposition, suggest a dominance of dihedral interactions combined with some surface interaction. The HSV composites, however, have intermediate angular parameters that suggest dominance of neither interaction type. In addition, where the polarimetric phase difference does deviate from the intermediate values, it tends in the direction of dihedral interactions (i.e. yellow and red pixels). The low entropy and spatial homogeneity of intermediate alpha angle values at C-band also suggests the presence of dipole interactions, the presence of which cannot be deduced from the Freeman decomposition.

It is therefore clear that the chosen study area is an example of a visual anomaly: a notable pattern which does not conform to an understanding of radar polarimetry based around the triptych of surface, volume and dihedral interactions. The RGB composites, and in particular the Freeman decomposition, do not allow for an assessment of the nature of wave interactions in this region as they are bound by the conventional description of the idealised scattering mechanisms. The HSV images, in contrast, are more useful in an exploratory context, as they encourage the viewer to question why spatially homogenous and coherent scatterers would have such well-defined phase difference and alpha angle values. None of the images presented in this section, however, allow for any further analysis other than the observation that this well-defined region has interesting scattering properties.

In the following section, the nature of the observed response patterns shown in figure 7.8 is examined in more detail. It is shown how the characteristic appearance of the response graph (when visualized using the polarimetric response globe) can be used to develop a model which attempts to replicate the observed pattern. The means by which these replicas are achieved can thus be viewed as the development of an analysis technique based wholly on visual interpretation.

7.3.3 – Further Investigation of the Observed Response Pattern

In the previous sections, polarimetric radar collected over an area of reed beds was found to have unusual characteristics that were evident when observed using a number of different visualisation techniques. In this section, it is shown that the polarimetric response globe can be used as an exploratory tool in the development and testing of a model that aims to simulate the scattering mechanism found in this region.

The information derived from the images presented in the previous section can be used to demonstrate the need for developing this model. In each of the intensity-based images that were presented, it appears the observed response over the reed bed area is a combination of dihedral and surface interactions. This is made more explicit by the results of the Freeman composition, which is based around the assumption of a three-component scattering model (Freeman and Durden, 1998). The means by which this model is constructed assumes that a single covariance matrix can be decomposed into three matrices representing the surface, volume and dihedral scattering components. The total backscattered response is then equal to the sum of these three matrices.

As the covariance matrix is used as a basis for decomposition, no absolute phase information is retained and the matrices are added incoherently. Incoherent addition assumes that there is no spatial separation between the scatterers, and that each scatterer has a separate response that does not interact with any others (Freeman and

Durden, 1998). Using this assumption, it is possible to model the effects of different proportions of surface and dihedral scattering mechanisms through the addition of differently weighted covariance matrices. In figure 7.12, a series of response patterns are presented which represent the transition between a resolution element dominated by a surface mechanism (left) to one dominated by a dihedral. It is immediately apparent that the response pattern observed in the Siggefora dataset cannot be achieved through incoherent additive combination, as the combination of covariance matrices representing surface and dihedral scattering result in response patterns in which the upper and lower halves of the response icon are symmetric.

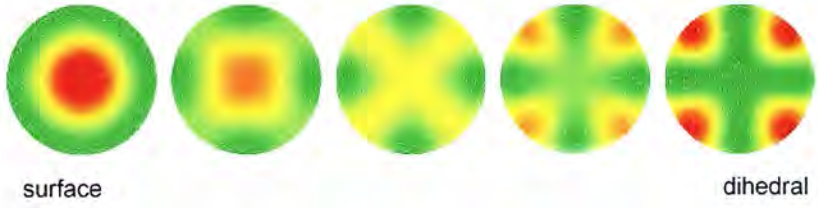

figure 7.12 – Transition between surface and dihedral scattering mechanisms, using the incoherent addition of weighted covariance matrices.

The discovery of a response pattern with a large well-defined spatial extent which cannot be derived from combinations of the commonly used 'idealised' scatterers is particularly interesting, as it may provide insight into the nature of polarimetric interactions. As additive modeling cannot produce the observed pattern, it is suggested that the observed response represents either or both of the following:

- The response is a `new' idealised scatterer, which can be added to the existing set, or
- The response is the result of coherent effects between scattering objects.

The development of coherent scattering models requires that polarimetric interactions are described as a chain of events, whereby the spatial organization of scatterers leads to changes in the polarisation of the incident wave as it propagates through space. One means by which this can be achieved is through the use of matrices describing transmission effects (Lu and Chipman, 1996). The occurrence of transmission effects has, to this authors knowledge, been underrepresented in polarimetric radar literature. In two early papers (Ulaby et al, 1987) and (Boerner et al., 1987), the observation of large areas of intermediate phase difference values over agricultural regions was hypothetically linked to the occurrence of transmission effects. Since this time, however, articles have tended to concentrate on describing polarimetric response patterns as incoherent combinations of the idealised mechanisms (for recent examples, see Fortuny-Guasch et al., 2003 and Lee et al., 2004).

In order to better understand the nature of the observed response pattern, it is useful to characterise the main features, and suggest how they can be used to build a picture of the interactions. The co-pole response in the observed patterns is perhaps the easiest to explain, as it shows a strong preference for the vertical polarisations. This suggests an interaction with a vertical dipole, as would be expected over any area where the primary vegetation structure consists of vertical stalks. The cross-pole response, in contrast, shows some evidence of dihedral interactions, in that peaks exist for the linear polarisations at 45° and 135° for both the left- and right-handed responses. This suggests that the vertical stalks may also act as dihedral reflectors.

Peaks also exist for the elliptical polarisations, but appear only in the bottom half of the globe. The exact ellipticity of the peak also varies between observed areas.

It is this top/bottom asymmetry that provides a hypothesis for explaining the nature of the interaction. Whilst it has been observed that an asymmetry between the left and right halves of the globe represents helical scattering (Ulaby and Elachi, 1990), the asymmetry observed in this dataset has not, to this author's knowledge, previously been considered as part of a characteristic response type. In the following sections, an interaction model is presented which allows for the simulation of the observed response.

7.3.4 – Developing Modeling Strategies Using the Polarimetric Response Globe

The following section attempts to develop a strategy for modeling the observed polarimetric response, which uses the idealised response patterns first introduced in chapter 5. As can be seen in figure 7.7, the study area comprises of an area of near-vertical reed beds, overlying a flat, smooth water surface. From this, it can be assumed that the major contributors of backscatter are dihedral interactions between the water surface and the reeds, and direct backscatter from the reeds themselves. It is therefore proposed that the models will be developed using idealised dipole and dihedral scattering matrices.

The observed response pattern in this area, however, does not conform to the response patterns which can be achieved through the incoherent addition of dipole and dihedral mechanisms, due to the asymmetry in the cross-pol response between the upper and lower halves of the globe, as demonstrated in figure 7.12. As this asymmetry is not a feature of any of the idealised response patterns, and thus would not be apparent in any addition of their matrices.

In order to produce such a response, therefore, it is first necessary to understand the nature of the observed asymmetry. In chapter 3 it was shown that the asymmetries between the left and right-hand sides of the globe were indicative of variations in response due to the handedness of the incident wave, exemplified by the response pattern of idealised helical scatterers. Asymmetries between the upper and lower

halves of the globe, however, have not, to this author's knowledge, been described in research literature.

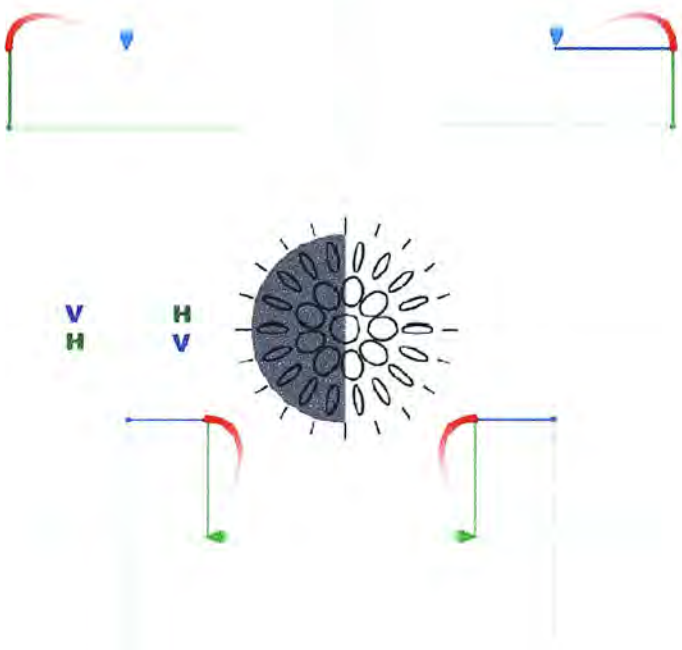

figure 7.13 – Variations in 'leading phase' are represented by the upper and lower halves of the polarimetric response globe.

Figure 7.13 shows an attempt to characterize this asymmetry using the concept of a 'leading phase'. This allows a polarisation to be defined by which wave component (either H or V) reaches it maximum magnitude value first in a wave cycle. Note that as with handedness, the leading phase is ambiguous for linear polarisations as the phase difference between the components is equal to integer multiples of π, and thus both reach their maxima at the same time. Likewise, as with the orientation angle (ψ), a leading phase cannot be described for the circular polarisations, as the difference in phase is equal to odd integer multiples of $\pi/2$. In this case, when one

polarisation reaches it maximum value, the other reaches its minimum, and neither component can be said to be traveling 'ahead' of the other.

The observed polarimetric response pattern over the reed beds in Siggefora, therefore, can be described as having variations in the cross-pol response pattern that are dependant on the leading phase of the polarisation. In order to model this response it is necessary to develop an approach that manipulates phase difference values in a manner which produces the observed asymmetry.

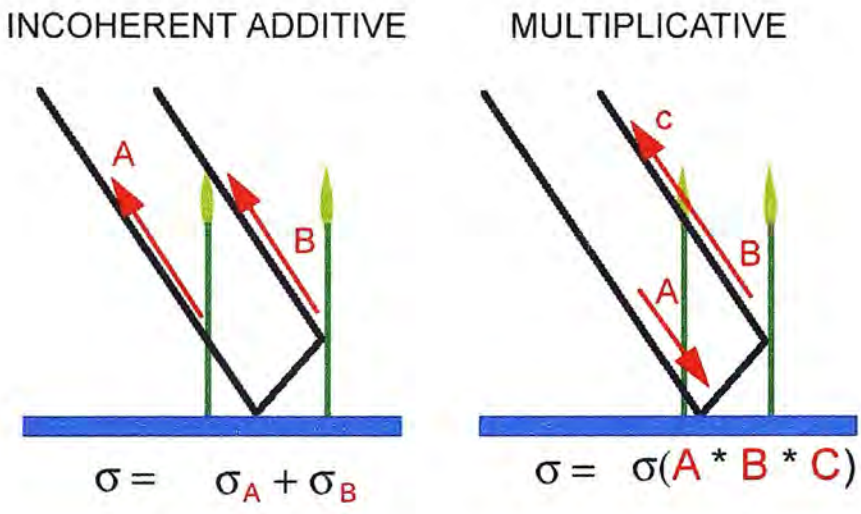

figure 7.14 – approaches to modelling polarimetric interaction.

The multiplicative decomposition model is an attempt to develop such an approach. As can be seen from figure 7.14, the multiplicative model differs from the incoherent additive approach in that it attempts to model polarimetric interactions as a chain of events, rather than as the addition of separate, independent scatterers.

The matrices used for multiplicative decomposition differ from those used in this and previous chapters in that they do not attempt to model a physical object. Rather, they are an attempt to analyse the changes in polarisation that occur as a wave travels through an object.

In (Lu and Chipman, 1996), these transmission effects are described using three Mueller matrices, representing a diattenuator, retarder and depolariser. Whilst these matrices are widely used in optical light polarimetry, there has been little usage of these descriptors in a radar context. The use of microwaves as a remote sensing tool is facilitated by the fact that the size of many objects in the natural environment approximate the discrete wavelengths transmitted by radar instruments. If we consider polarimetric radar interactions as a 'scaled-up' version of geometrical optics, it becomes possible to describe the transmittance of discrete objects which range between $0.1 - 1$m in a radar context using the aforementioned matrices.

Of particular interest in the current context is the retarder matrix. In simplistic terms, a retarder (as the name suggests) has the effect of 'slowing down' the phase of an incident wave. By defining an 'axis' of retardance, it is possible to vary the relative amounts of retardance suffered by the horizontal and vertical wave components.

In (Lu and Chipman, 1996), a retarder is defined, for the forward scattering case, as follows.

$$
\begin{aligned}
\bar{M}_R &= \begin{bmatrix} 1 & \vec{0}^T \\ \vec{0} & \bar{m}_r \end{bmatrix} \\
(\bar{m}_r)_{ij} &= \delta_{ij}\cos R + a_i a_j(1-\cos R) \\
&\quad + \sum_{k=1}^{3} \epsilon_{ijk} a_k \sin R \\
i,j &= 1,2,3,
\end{aligned}
\tag{7.1}
$$

*in which $\vec{0}$ denotes a three element zero vector, R is an angular value describing the retardance 'strength', whilst $(1; a_1; a_2; a_3)^T$ is the normalized Stokes vector for the fast axis. δ_{ij} is the Kronecker delta, Σ_{ijk} is the Levi-Civita Permutation Symbol, and m_r is a 3*3 sub-matrix which define the properties of the retarder.*

A vertically-aligned retarder can therefore be defined by setting the Stokes vector of the fast axis to:

$$(1, \cos(\tfrac{\pi}{2}), \sin(\tfrac{\pi}{2}), 0). \tag{7.2}$$

In figure 7.15, a visual matrix is presented which demonstrates the effects of different 'strengths' of vertical retarders on a number of polarisations. As would be expected, where either the horizontal or vertical amplitudes are zero (i.e. vertical and horizontally polarised linear waves), a phase difference between the two components cannot be ascertained. As a result, the propagating wave remains unchanged by the retarder. Note, however, that a linear wave that is not aligned along the cardinal axes will become more elliptical as a result of the retarder interaction. Likewise, the circular polarisations will become less elliptical (i.e. more linear).

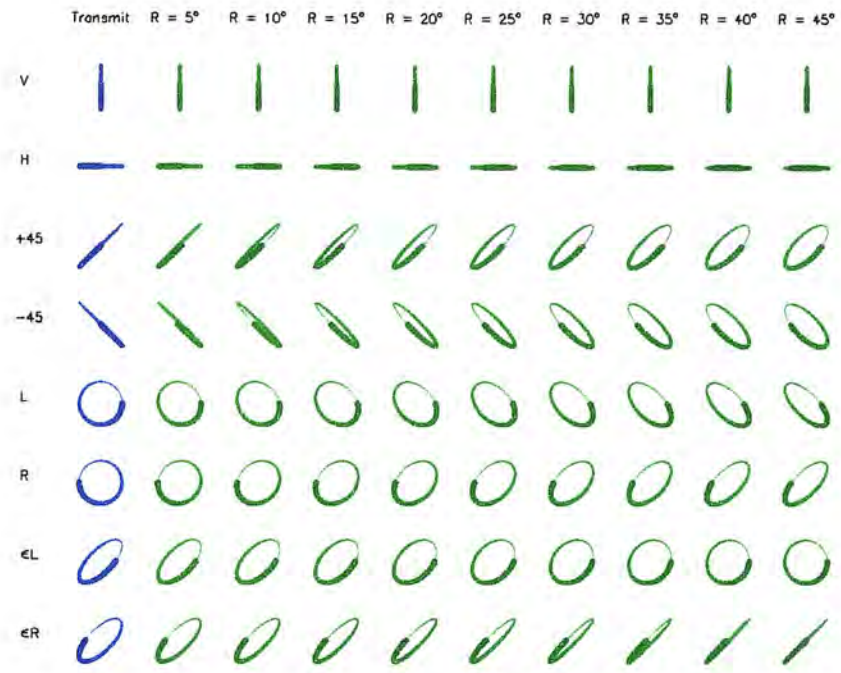

figure 7.15 – The effect of increasing 'strengths' retarder on different wave polarisation states.

Most interestingly, however, is the behaviour of the elliptical polarisations. The last two rows in figure 7.15 present two elliptical polarisations that are identical save for differing directions of rotation. Note that for the left-handed case the wave becomes more circular, whilst for the right-handed case the wave becomes more linear. This variation as a function of handedness can be attributed to the leading phase component for each polarisation state. It is simple to demonstrate that if V leads H, then a vertically aligned retarder will reduce the phase difference, and the polarisation of the transmitted wave will move towards (and eventually through,) the linear polarisations. Similarly, if H leads V then the phase difference will increase, and the polarisation state of the propagating wave will move towards the circular polarisations.

From figure 7.15, it is apparent that by using a retarder matrix in a multiplicative decomposition model, then the asymmetry observed in the cross-pol response can be achieved. Figure 7.16 therefore describes a conceptual scattering model, which combines two retarder matrices with a dihedral interaction to describe the transmission of polarized waves through a reed bed.

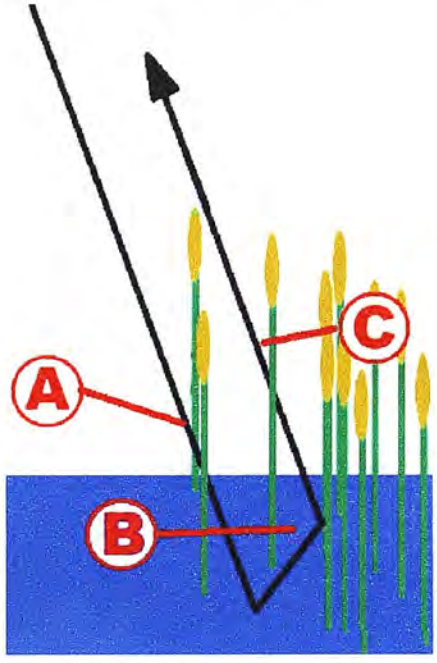

A : Dipole acting as a retarder.
B : Dihedral interaction.
C : Dipole acting as a retarder.

figure 7.16 – Conceptual representation of retardance over reed beds.

This can be represented mathematically as:

$$\bar{\mathbf{M}}_{\mathbf{dr}} = \bar{\mathbf{M}}_{-\mathbf{R}}\bar{\mathbf{M}}_{\mathbf{d}}\bar{\mathbf{M}}_{\mathbf{R}}, \tag{7.3}$$

where $\mathbf{M_R}$ and $\mathbf{M_d}$ represent Mueller matrices for the retarder and dihedral, respectively. Note that the retardance assumes a negative value for the first matrix in order to simulate two-way propagation as shown in figure 7.16.

The resulting matrix ($\mathbf{M_{dr}}$) can subsequently be used to examine polarimetric response patterns for different strengths of retarder. In figure 7.17, these response patterns are shown, and exhibit a clear migration of the peak co-pol response that produces an asymmetry between the upper and lower halves of the globe.

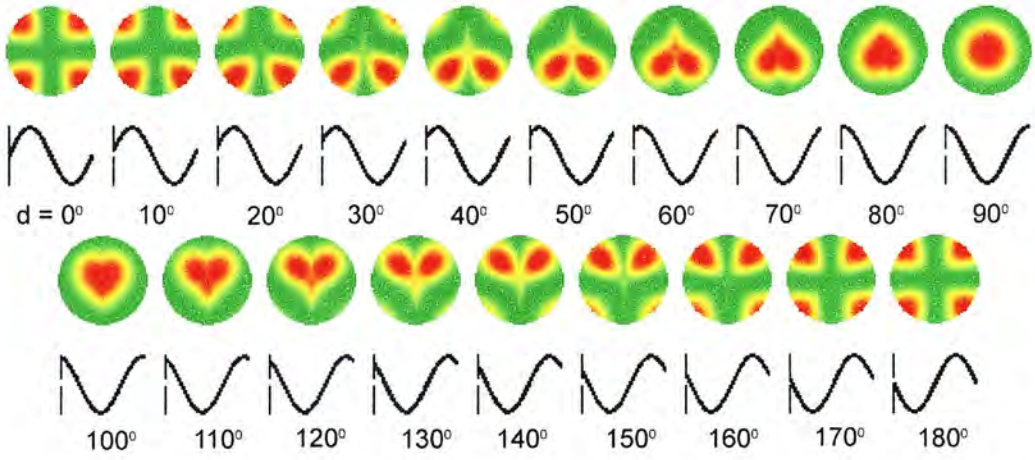

figure 7.17 – The multiplicative application of a retarder, of increasing strength, to a dihedral response graph. Note the migration of the peak cross-pol response.

Note that by setting the value of the retarder to 20° (0.35 radians), a cross-pol response pattern can be obtained that mimics the observed pattern shown in figure 7.8. The co-pol response pattern, however, does not resemble that of the observed response.

This can be improved, however, by incorporating the initial backscatter from the vertical dipole shown at (A) in figure 7.16. This can be achieved through the incoherent addition of a dipole matrix to the retarder/dihedral combination outlined above, so that:

$$\bar{\mathbf{M}}_{\mathbf{total}} = \bar{\mathbf{M}}_{\mathbf{di}} + \bar{\mathbf{M}}_{\mathbf{dr}}$$

Where $\mathbf{M_{di}}$ represents a Mueller matrix composed of a dipole scatterer.

By setting the value of the retarder to 20°, the resulting response pattern very closely simulates the response patterns found over the Siggefora reed bed area, as shown in figure 7.18.

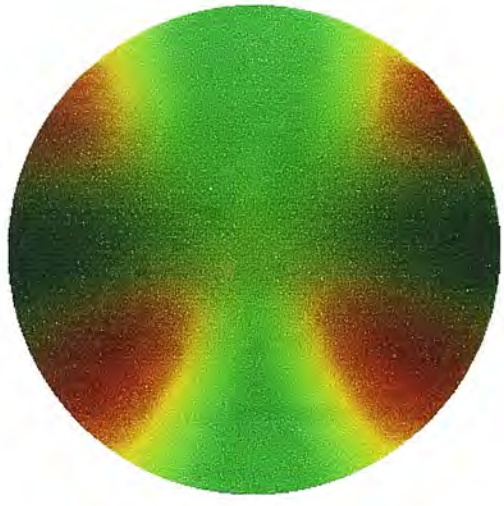

Figure 7.18 – The pattern observed over the reed bed region in figure 7.8 can be replicated using a combination of a vertical dipole, a 2-way retarder and a dihedral.

The similarity between the modeled response pattern in figure 7.18 and the observed response in figure 7.8 can be used as a means of advocating the development and use of visualisation techniques for the analysis of large, multi-valued datasets. It is beyond the scope of the current study to investigate in detail the validity of this model, as it would require further validation using ground data, or lab-based measurements. However, in the context of the current research project, what is important is that the model described in this section effectively simulates a characteristic observed response, using the physical properties of the region in which it was found. It should be noted, however, that the multiplicative technique is not the only means by which the observed response can be achieved. For example, it is possible to achieve a similar backscatter response pattern using a coherent scattering model based on regularly spaced scattering objects.

During the development of the multiplicative model, the visualisation technique that has been detailed over the previous two chapters performed a formative role in developing an understanding of the nature of polarimetric interactions. Initially, the polarimetric response globe was used as an icon that allowed for the creation of synoptic images, which led to the identification of an area containing similar yet unusual response patterns. The nature of these response patterns was subsequently investigated further using single globe representations, with several characteristics of their visual representation (most notably the asymmetry) posing questions, which in turn led to further research and the development of the proposed model.

The globe subsequently formed a useful means of testing and adjusting the model that was constructed in an effort to more closely simulate the observed response. Finally, the newly developed visualisation technique has functioned as a tool of communication, and has provided a graphical means of describing the nature of these polarimetric response patterns to others.

In summary, therefore, it can be confidently stated that the polarimetric response globe, and associated software, is an effective visualisation tool, as it encourages the exploration of polarimetric datasets in a manner which is not achievable using 'off-the-shelf' image processing options. It is hoped, therefore, that the findings of this chapter encourage researchers to apply the newly developed visualisation techniques to other datasets in the early stages of exploratory analysis. It would also be interesting to further explore the validity of the use of transmission effects as a means of understanding polarimetric interactions, and to examine lab-based datasets involving short vegetation to see if similar patterns occur.

With respect to the wider aims of this thesis, it is possible to assess the new visualization strategy in relation to MacEachren's visualisation cube (MacEachren, 1994). At various stages throughout this chapter, there have been numerous examples showing that the response globe can be used both as a tool of private investigation, and for public communication. The model developed in this section, moreover, demonstrates how the application of visualisation techniques can be used for the analysis of patterns, the synthesis of ideas and the presentation of results.

CHAPTER 8 – CONCLUSION

In this thesis, two new visualisation techniques for the analysis of polarimetric radar data have been developed and tested. In this final chapter, the structure and findings of this research project are summarised. This is followed by a discussion of the limitations and weaknesses of the newly developed techniques. This, in turn, is then used to suggest possible avenues for the application of scientific visualisation to more recent developments in the field of radar polarimetry. Finally, the main points of the thesis are reiterated in a series of closing comments.

8.1 - Summary

This thesis aimed to investigate the application of the principles of scientific visualisation to the analysis of polarimetric radar data. In order to achieve this, current visualisation strategies in remote sensing were reviewed. It was shown that current visualisation strategies are dominated by the use of pixel-based grey-scale intensity images and RGB colour composites. The appeal and utility of these images can be traced back to the historical origins of remote sensing in aerial photography. By applying similar techniques to the analysis of multi-spectral datasets, it can be said that the visualisation of remotely sensed data is dominated by an optical analogy which affects not only the way in which images are formed from datasets, but also

the manner in which remote sensing data from different sources in conceptually understood.

The visualisation of Synthetic Aperture Radar data, however, poses a problem in that it has a number of characteristics that weakens the applicability of the conceptual analogy used for data from passive sources. In particular, the importance of phase values, and the effects this has on the recorded data, cannot be represented using the visual variable of intensity. Understanding the characteristics of these values, however, can provide unique and scientifically valuable sources of information, and thus it is important that new visualisation techniques are developed which allow these values to be visually analysed. The development of SAR interferometry, and the use of the Interferogram as a tool of scientific visualisation, was then presented as an example of the effectiveness and value of novel visualisation strategies in the development and adoption of new technologies.

The following chapter subsequently analysed the visualisation strategies currently used in the analysis of polarimetric radar data. It was shown how the application of traditional visualisation techniques (including intensity images, RGB colour composites and HSV colour composites) produced images that lacked detail due to the three-variable limitation imposed by pixel-based visual strategies. Other visualisation techniques were also examined which had been developed specifically for the analysis of polarimetric datasets, such as polarimetric response graphs and phase/coherence plots. It was found that whilst such techniques allowed a detailed analysis of polarimetric properties at a specific level, they lacked the synoptic

overview provided by the traditional remote sensing approach. As a result, the visual analysis becomes divorced from the analysis of spatial patterns.

A gap can therefore be identified in current visualisation strategies for the analysis of polarimetric datasets. This gap equates to a lack of communication between the synoptic and specific scale of enquiry. It was suggested that this gap in understanding may have an adverse effect on research in radar polarimetry. On the one hand, scientists using traditional, synoptic intensity images are likely to be working with a limited set of variables and intensity channels, and thus not maximising the potential information content of the data. On the other had, scientists using site-specific highly detailed graphics may be unaware of spatial patterns within datasets which may help to explain the occurrence of certain response patterns or phase variations.

Having identified the deficiencies in current visualisation techniques for polarimetric data, two new strategies were developed which aimed to increase the number of variables that could be assigned to a single geographic location in a synoptic intensity image. The first of these techniques was based on a visualisation strategy proposed by (Kirby et al., 1999) which used the visual variables of an ellipse to map data variables relating to fluid flow. This approach was redesigned and applied to variables derived from the entropy/α decomposition developed by Cloude and Pottier (1996). This subsequently allowed the spatial patterns and inter-relationships between five different variables to be analysed. The proposed technique was particularly effective as some of the variables, such as the beta angle and anisotropy,

had direct visual analogues (namely the orientation and ellipticity of the elliptical icon) which could be used to form a conceptual link between the designated data variables and its visual representation. The effectiveness of this technique was demonstrated by applying the visualisation to a number of real datasets, which revealed areas where the relationships between the visual variables in specific geographic locations could be used to analyse the characteristics of the data variables with respect to natural and anthropogenic environments.

The effectiveness of this technique, however, is limited by the fact that it is used to represent a decomposition (and thus, a simplification) of the original data source. In order to address the problem of visualising 'raw' polarimetric data, it was necessary to develop a technique for the synoptic visualisation of polarimetric response patterns. This aim formed the basis of the second visualisation strategy, and involved the redevelopment of the polarimetric response graph into a graphical form which was easier to read, and thus could be used as an icon for synoptic analysis.

The redesign of the polarimetric response graph was achieved by reprojecting the original graph so that the axis variables (namely orientation and ellipticity) were mapped to polar, rather than Cartesian coordinates. This resulted in a circular graph where the orientation angle is mapped to a continuous angular axis, allowing orientation values to be more easily read. A further advantage of the new technique is that the different polarisation states, with respect to the ellipticity angle, are more evenly distributed across the graphic, with fewer repeated values than is the case with the traditional approach.

The redeveloped polarimetric response globe was subsequently used as the basis for a software application (included on the enclosed CD-ROM) that allows the synoptic analysis of polarimetric response patterns. This application also allows users to apply traditional visualisation techniques, and is designed to encourage an exploratory approach to the visualisation of polarimetric datasets.

Having developed this software application, it is important to demonstrate its effectiveness not only in terms of its graphical qualities, but also as a tool for scientific enquiry. The first of these aims was achieved using a web-based survey which asked a group of non-experts to identify patterns in different representations of polarimetric response. Although the overall response was limited, the test clearly demonstrated that the newly developed technique was more effective than the traditional graphic for representing spatial patterns formed by simple geometric objects.

In order to demonstrate the potential utility of the response globe in a research context, the final sections of this thesis utilised the synoptic response viewer to develop a model to explain an area of unusual response patterns observed over an area of reed beds in a polarimetric dataset. In doing this, it was demonstrated how the response globe was useful at a number of different stages of scientific enquiry. In the first instance, the synoptic response viewer was instrumental in identifying response patterns with similar characteristics that occurred over a well-defined geographic region. The 'shape' of these response patterns, which included a notable asymmetry

in the cross-pol response pattern, was then used to query the nature of polarimetric interactions in this region. By identifying the 'cause' of the observed asymmetry as a function of the leading phase of the incident polarisation, it was then possible to develop a model that used a multiplicative decomposition technique to reproduce the observed asymmetry. At this stage, the response globe formed a means of assessing and fine-tuning the model in order to produce the observed response. Finally, the last three chapters of this thesis can be regarded as an example of the response globe can be used as a tool of scientific communication. At various stages throughout this thesis, the response globe has been used not only to represent phenomenological response patterns, but also to aid in the understanding of the concepts which underlie the nature of polarimetric interactions.

In this respect, it can be said that the polarimetric response globe, when used in conjunction with polarimetric data viewer, is an example of an exploratory research tool, as defined by (MacEachren, 1994). By using the same graphical technique at a variety of different stages and scales of scientific enquiry, the response globe has been effectively employed as a tool for private data exploration, for the synthesis of ideas and testing of hypotheses, for the development of a descriptive model, and finally as a means of research dissemination. The constancy of the response icon as a visualisation tool, in this case, allows the course of this research project to be charted using what, it is hoped, can be considered as a straightforward and coherent visual language.

8.2 – Limitations of the Current Research

Despite the advantages of the newly developed visualisation techniques outlined above, it is possible that the visualisation techniques proposed in this thesis will not be used outside of the context of this current research project. In this section, some of the main limitations of the new visualisation techniques are discussed. These limitations, it is argued, are indicative of the limitations faced by the developers of any visualisation strategy in a field in which a particular type of visual approach has become established, and has influenced the manner in which scientists both conceptualise and interact with their data.

In the case of remote sensing in general, it is the pervasive optical analogy that inhibits the development of alternative modes of visualisation. Since the launch of the first Landsat satellite in the late 20^{th} century, the analysis of remotely sensed data has been dominated by the use of image processing software. These packages have, over time, incorporated a large number of analytical functions that allow users to quantify, classify and assimilate their datasets, as well as providing tools for more straightforward visual analysis.

By comparison, the visualisation techniques proposed in this thesis are relatively static. Once created, the images derived from the new techniques cannot be used for further digital analysis. In the case of the Entropy/α visualisation, for example, it is not possible to use observed patterns in the beta angle or anisotropy as a means of directly interacting with the dataset. The pixel-based image, therefore remains not only a powerful visualisation technique, but also a powerful means of interacting

with grid-based datasets, and one which is unlikely to be supplanted in the near future.

The problem of 'ingrained' attitudes to visualisation can also be found in the more specific study of radar polarimetry. In this thesis, it has been demonstrated that the traditional, isometric polarimetric response graph is a needlessly complicated and counter-intuitive means of representing the variables that define polarimetric response values. Despite this, and despite over 20 years of research into the use of radar polarimetry, few examples exist of authors using alternative representations.

The adoption of the proposed visualisation technique would face difficulties in overcoming the standardised approach that dominates current literature, as scientists using the new technique would need to 'translate' the new visual representation in order to compare it to past results, or to the results of those who continue to use the traditional technique. Therefore, whilst it has been demonstrated that the synoptic analysis of response patterns is of value in the analysis of polarimetric datasets, the graphics and techniques described would need to be adopted by more authors in order that the benefits be more clearly demonstrated.

The potential role of scientific visualisation in the study of new datasets, however, should not be underestimated. In this thesis, it has been demonstrated that an inquisitive and inventive approach to data visualisation can yield images that encourage and allow scientists to reflect on the patterns that exist within datasets, but which may not be immediately apparent. For this reason, the development of new

visualisation techniques should be promoted more widely, and researchers encouraged to engage more fully and creatively with the visual representation of datasets. In the following section, a number of suggestions for the continued development of scientific visualisation in the field of SAR research are discussed.

8.3 – Directions for Future Research

The visualisation techniques developed in this thesis have demonstrated that an experimental approach to the visual analysis of polarimetric datasets can yield valuable insights into the spatial patterns which exist both within and between different data variables. It is hoped, therefore, that the approach taken during the course of this research can be applied to other areas of research, and aid the development of polarimetric radar as a research tool.

One such area where innovative visualisation techniques may be beneficial is the study of data derived from polarimetric interferometry (PolINSAR). As shown in chapter 3, PolINSAR allows the derivation of information relating to the three-dimensional structure of landscape components. Current visualisation strategies, however, examine PolINSAR data either at a site-specific level (as in Papathanassiou and Cloude, 2001) or through the use of intensity-based synoptic images (as in Reigber and Moreira, 2000). There subsequently exists a gap, as was identified for polarimetric datasets, between two scales of enquiry which could be at least partially bridged by the application of novel visualisation strategies. The visualisation strategies developed in this thesis could therefore be adapted and applied to PolINSAR datasets. The ellipse-based visualisation detailed in chapter 5, for

example, could be applied to three-dimensional datasets using either animated sequences, or through the use of volumetric visualisation strategies.

The development of bistatic polarimetry also poses a number of interesting challenges. Unlike the traditional monostatic case, bistatic SAR systems use transmitters and receivers which are spatially separated. The advantages of such an approach include additional target information, and the possibility of collecting data using multiple offset receivers (Kähny et al, 1992). These advantages, however, incur costs when it comes to processing and analysing the data. The development of a visualisation technique which incorporates and represents these additional complexities, therefore, may aid in the further development of this field.

It is hoped that the techniques created during the course of this research will find further application in the study of radar polarimetry, especially in areas where radar polarimetry is used as a means of classification. More importantly, however, it is hoped that the concepts which directed their development will encourage other researchers to develop novel, tailored approaches to visualisation. An experimental approach to visualisation, it has been shown, supports the development of visual thinking, and can reveal patterns which would otherwise remain hidden. In the context of new or poorly understood forms of data, such an approach can be expected to yield great benefits in the early stages of exploratory data analysis.

8.4 – Conclusion

The work contained in this thesis is intended to explore and promote the application of scientific visualisation in the analysis of polarimetric radar data. The main findings of this research are thus summarised in the following statements:

- Visualisation has performed a fundamental role in the analysis of remotely-sensed data, largely through the use of intensity images.
- Recent technological advances, particularly in the field of Synthetic Aperture Radar, have produced data types which cannot be efficiently visualised using traditional techniques.
- By applying the principles of scientific visualisation, images can be created which retain some of the important characteristics of traditional synoptic images, but which increase the amount of information represented at a single geographic location.
- The effectiveness applying these techniques has been demonstrated through the development of two new approaches to the visualisation of polarimetric radar data.

The process of extracting information from images, as noted at the very beginning of this thesis, is an innate capability of the human visual system. The importance of this capability, due to its habitual usage, is often overlooked. In the search for patterns and anomalies in ever-increasing and constantly changing volumes of data, it makes sense to utilise one of the few arenas in which humans consistently and effortlessly still outperform even the most powerful computers. The true value of scientific

visualisation, as demonstrated in this thesis and summarised in the closing quote below, is, quite simply, that it helps and encourages us to think about what we see.

``Humans, since time immemorial, have found themselves to be in the midst of mystery, in a state of being asked, of being placed in a position of response.

The poetic response to the human condition is one of wonder.

Wonder leads to awe.

Reflection upon awe and wonder leads to wisdom." (Green, 1999)

REFERENCES

A.P. Agrawal and W.M. Boerner. Redevelopment of Kennaughs Target Characteristic Polarization State Theory Using the Polarization Transformation Ratio Formalism for the Coherent Case. *Trans. Geosci. Rem. Sens.*, 27(1):2-14, 1989.

J. Bertin. Graphic and Graphic Information Processing. Walter de Gruyter and Co, Berlin, 1981.

R. Blom, R. E. Crippen, and C. Elachi, Detection of subsurface features in Seasat radar images of Means Valley, Mojave Desert, California, *Geology, 12*, 346-349, 1984.

W.M. Boerner, B.Y. Foo, and H.J. Eom. Interpretation of the Polarimetric Copolarization Phase Term in Radar Images Obtained with the JPL Airborne L-band SAR System. *Trans. Geosci. Rem. Sens.*, 25(1):77-82, 1987.

W.M. Boerner, H. Mott, E. Luneberg, C. Livingstone, B. Brisco, R.J. Brown and J.S. Paterson. Principles and Applications of Imaging Radar. New York: John Wiley and Sons inc. 1998

C. Brewer, Guidelines for Selecting Colors for Diverging Schemes on Maps. *Cartographic Journal* 33(2):79-86, 1996

V. Bruce and P. Green. Visual Perception: Physiology, Psychology and Ecology. Lawrence Erlbaum Associates Ltd. 1987

E.J. Borowski and J.M. Borwein. Collins Dictionary of Mathematics. HarperCollins Publishers, Glasgow, second edition, 1989.

S.R. Cloude and E. Pottier. An Entropy Based Classification Scheme for Land Applications of Polarimetric SAR. *Trans. Geosci. Rem. Sens.*, 35(1):68-78, 1997.

S.R. Cloude and E. Pottier. A Review of Target Decomposition Theorems in Radar Polarimetry. *Trans. Geosci. Rem. Sens.*, 34(2):498-518, 1996.

S.R. Cloude, K.P. Papathanassiou, I. Woodhouse, J. Hope, J.C. Suarez-Minguez, P. Osborne, and G. Wright. The Glen Affric Radar Project: Investigating Applications of Polarimetric SAR Interferometry. *In Proceedings of the CEOS SAR Workshop, page 5, Tokyo, 2001. CEOS, ESA Special Publications.*

S.R. Cloude, I. Hajnsek and K.P. Papathanassiou. An Eigenvector Method for the Extraction of Surface Parameters in Polarimetric SAR. *CEOS SAR Workshop Proceedings, Toulouse.* October, 1999.

K. Conradsen, A. Aasbjerg, J. Schou, and H. Skriver. A Test Statistic in the Complex Wishart Distribution and Its Application to Change Detection in Polarimetric SAR Data. *Trans. Geosci. Rem. Sens.*, 41(1):4-19, 2003.

J. Dall, S.N. Madsen, C.K. Brooks, and T. Nielsen. Geologic Mapping in Greenland with Polarimetric SAR. *In Quantitative Remote Sensing for Science and Applications, volume 3, pages 2206-2208. International GeoScience and Remote Sensing Symposium, 1995.*

Y. Dong and B. Forster. Understanding of Partial Polarisation in Polarimetric SAR data. *Int. Jour. Rem. Sens.*, 17(12):2467-2475, 1996.

D. Dorling and D.Fairbairn. Mapping : Ways of Representing the World, chapter 9. Insights into Human Geography. Addison Wesley Longman ltd.,1997

B. Doyle : Way to go, Einstein! *Time for Kids Magazine Supplement, American Museum of Natural History and the Skirball Cultural Centre.* 2002

J. Dungan, D. Kao, and A. Pang. The Uncertainty Visualization Problem in Remote Sensing Analysis. *International GeoScience and Remote Sensing Symposium,* International, 2002

S.L. Durden, J.J. van Zyl, and H.A. Zebker. Modeling and Observation of the Radar Polarization Signature of Forested Areas. *Trans. Geosci. Rem. Sens.*, 27(3):290-301, 1989.

D.L. Evans, J.J. Van Zyl, and C.F. Burnette. Incorporation of Polarimetric Radar Images Into Multisensor Data Sets. *Trans. Geosci. Rem. Sens.*,28(5):932-939, 1990.

P. Ferrazolli and L. Guerriero. Interpretation and Model Analysis of Maestro-1 Flevoland Data. *Trans. Geosci. Rem. Sens.*, 15(14):2901-2915, 1994.

P. Fisher. The Pixel: a snare and a delusion *Int. Jour. Rem. Sens.*, 18(3):679-685, 1997.

J. Fortuny and A.J. Sieber, Three-Dimensional Synthetic Aperture Radar Imaging of a Fir Tree: First Results, *Trans. Geosci. Rem. Sens*, 37(2), pp1006-1014, 1999

J. Fortuny-Guasch, A. Martinez-Vazquez, D. Riccio, J.M. Lopez-Sanchez, and J.D. Ballester. Experimental Validation of an Electromagnetic Model for Rice Crops Using a Wide-Band Polarimetric Radar. *International GeoScience and Remote Sensing Symposium*, International, 2003.

A. Freeman and S.L. Durden. A Three-Component Scattering Model for Polarimetric SAR Data. *Trans. Geosci. Rem. Sens.*, 36(3):963-973, 1998.

M.R. Gearhart. From the Big Bang to the Big Crunch: Interview with John A. Wheeler. *Cosmic Search* 1(4), 1979

D. Giuli. Polarization Diversity in Radars. *Proceedings of the IEEE*, 74(2):245-269, 1986.

R.M. Goldstein, H. Englehardt, B. Kamb, and R.M. Frolich. Satellite Radar Interferometry for Monitoring Ice Sheet Motion: Application to an Antarctic Ice Stream. *Science*, 262:1525-1530, 1993.

B. Green. Rediscovering the meaning of the world: using space shuttle images to inspire poetry. *Trans. Geosci. Rem. Sens.*, 37(4):1834-1840, 1999.

J. Gu, J. Yang, H. Zhang, Y. Peng, C. Wang, and H. Zhang. Speckle Filtering in Polarimetric SAR Data based on Subspace Decomposition. *Trans. Geosci. Rem. Sens* 42(8) pp1635-1641, 2004

A. Guissard. Mueller and Kennaugh Matrices in Radar Polarimetry. *Trans.Geosci. Rem. Sens.*, 32(3):590-597, 1994.

I. Hajnsek, E. Pottier and S.R. Cloude. Inversion of Surface Parameters From Polarimetric SAR. *Trans. Geosci. Rem. Sens.*, 41(4):727-744, 2003

D.H. Hoekman and M.J. Quinones. Land Cover Type and Biomass Classification Using AirSAR Data for Evaluation of Monitoring Scenarios in the Columbian Amazon. *Trans. Geosci. Rem. Sens.*, 38(2):685-696, 2000.

D.H. Hoekman and M.J. Quinones. Biophysical Forest Type Characterisation in the Colombian Amazon by Airborne Polarimetric SAR. *Trans .Geosci. Rem. Sens.*, 40(6):1288-1300, 2002.

P. Imbo, J.C. Souyris, A. Lopes, and P. Marthon. Synoptic representation of the polarimetric information. In *CEOS SAR Workshop*, pages 341-346, Toulouse, France, 1999. ESA Special Publications.

J.R. Jensen, Introductory Digital Image Processing (2nd edit.). Prentice Hall, Upper Saddle River, NJ, 1994

C.R. Johnson and A.R. Sanderson. A Next Step: Visualizing Errors and Uncertainty. *IEEE Computer Graphics and Applications*, September/October:6-10, 2003.

D. Kähny, K. Schmitt and W. Wiesbeck. Calibration of Bistatic Polarimetric Radar Systems. *Trans. Geosci. Rem. Sens.* 30(5):847-852, 1992.

R. M. Kirby and H. Marmanis and D. H. Laidlaw. Visualizing Multivalued Data from 2D Incompressible Flows Using Concepts from Painting. IEEE Visualization '99, San Francisco, pp.333-340, 1999

W. Kohler. Gestalt Psychology. G. Bell and Sons ltd,, London, 1930.

P. Kosok. Life, Land and Water in Ancient Peru, Long Island University Press, New York, 1965.

D.H. Laidlaw, D. Kremers, E.T. Ahrens, and M.J. Avalos. Applying Painting Concepts to the Visual Representation of Multi-Valued Scientific Data. In *SIGGRAPH 98*, New Orleans, Louisiana, 1998.

D.H. Laidlaw, R.M. Kirby, J. S. Davidson, T. S. Miller, M. d. Silva, W.H. Warren and M. Tarr. Quantitative Comparative Evaluation of 2D Vector Field Visualization Methods, *IEEE Visualization 2001*, San Diego, 2001

J. Lee, M.R. Grunes, and G De Grandi. Polarimetric SAR Speckle Filtering and its Implication for Classification. *Trans. Geosci. Rem. Sens.* 37(5):2363-2373, 1999.

J.S. Lee, M.R. Grunes, E. Pottier, and L. Ferro-Famil. Unsupervised Terrain Classification Preserving Polarimetric Scattering Characteristics. *Trans. Geosci. Rem. Sens* 42(4), pp722-731, 2004

T.M. Lillesand and R.W. Kiefer. Remote Sensing and Image Interpretation. John Wiley and Sons Inc., New York, 1994.

S. Lu and R.A. Chipman, Interpretation of Mueller matrices based on polar decomposition. *Journal of the Optical Society of America (A),* 13(5), pp1106-1113, 1994

P. Lumsdon and G. Wright, A Polarimetric SAR Classification for comparison test against aerial photography images in Glen Affric radar project. *PolInSAR 2003*, Frascati, Italy. ESA Publications, 2003.

MacEachren, A.M. & M.J. Kraak (1997) Exploratory cartographic visualization: advancing the agenda. *Computers & Geosciences* 23(4), pp. 335-344.

A.M. MacEachren. Visualization in Modern Cartography: Setting the Agenda, chapter 1, pages 1-12. Visualization in Modern Cartography. Elsevier Science ltd., Great Yarmouth, first edition, 1994.

S.N. Madsen and H.A. Zebker. Principles and Applications of Imaging Radar, chapter 6: Imaging Radar Interferometry, pages 359-380. New York: John Wiley and Sons inc., 1998.

D. Massonet, M. Rossi, C. Carmona, F. Adragna, G. Peltzer, K. Feigi, andT. Rabaute. The Displacement Field of the Landers Earthquake Mapped by Radar Interferometry. *Nature*, 364:138-142, 1993.

D.L. Medin, B.H. Ross, and A.B. Markman. Cognitive Psychology: Third Edition. Harcourt College Publishers, Fort Worth, 2001.

L. Middleton and V. Sivaswamy, Edge Detection in a Hexagonal-Image Processing Framework, *Image and Vision Computing*, 19(14), pp1071-1081, 2001

M. Monmonier. How to Lie with Maps. The University of Chicago Press, Chicago, 1991.

K. Papathanassiou and S.R. Cloude. Single-Baseline Polarimetric SAR Interferometry. *Trans. Geosci. Rem. Sens.*, 39(11):2352-2364, 2001.

M. H. Pirenne. Vision and the Eye. Science Paperbacks and Chapman and Hall Ltd., 1967.

E. Pottier and J.S. Lee, Application of the H/A/a Polarimetric Response Decomposition Theorem for Unsupervised Classification of Fully Polarimetric SAR data based on the Wishart Distribution. *CEOS SAR Workshop*, Toulouse, France. ESA Special Publication, 1999.

M. Qong. A New Scattering Mechanism Enhancement Scheme for Polarimetric SAR Images. *Trans. Geosci. Rem. Sens.*, 40(12), 2002.

A. Reigber and A. Moreira. First Demonstration of Airborne SAR Tomography Using Multibaseline L-Band Data. *Trans. Geosci. Rem. Sens.*,38(5):2142-2152, 2000.

A.H. Robinson, J.L. Morrison, P.C. Muehrke, A.J. Kimerling, and S.C. Guptill. Elements of Cartography. John Wiley and Sons Inc., New York, sixth edition, 1995.

B.E. Rogowitz and L.A. Treinish. Data visualization: the end of the rainbow. *IEEE Spectrum*, pages 52-59, December 1998.

D.L. Schuler and J.S. Lee and K.W. Hoppel. Measurement of Topography using Polarimetric SAR images *Trans. Geosci. Rem. Sens.*,34(5):1266-1277, 1996.

D.L. Schuler, J.S. Lee, D. Kasilingam, and E. Pottier. Measurement of Ocean Wave Spectra using Polarimetric SAR Data. International GeoScience and Remote Sensing Symposium (Proceedings), International, 2003.

R.A. Schowengerdt. Remote Sensing: Models and Methods for Image Processing (2^{nd} edit). Academic Press, 1997.

J. Schwartz and M. McGuinness. Einstein for Beginners. Writers and Readers Publishing Cooperative Society, University Press, Oxford, 1979.

H. Skriver and L.T. Pedersen. Polarimetric Signatures of Sea Ice in the Greenland Sea. In Quantitative Remote Sensing for Science and Applications, volume 3, pages 1792-1795. International GeoScience and Remote Sensing Symposium, 1995.

H. Skriver, M.T. Svendsen, and A.G. Thomsen. Multitemporal C- and L- Band Polarimetric Signatures of Crops. *Trans. Geosci. Rem. Sens.*,37(5):2413-2429, 1999.

T.A. Slocum, H.H. Howard, F.C. Kessler and R.B. McMaster. Recent and Ongoing Development in Cartography. *ACSM Bulletin Jan/Feb,* pp.8-18, 2004.

S. Smith, G. Grinstein, and R. Pickett. Global geometric, sound and color controls for iconographic displays of scientific data. Proceedings SPIE: Extracting Meaning from Complex Data: Processing, Display, Interaction II, pages 192-206. 1991.

R. C. Staunton and N. Storey. A Comparison Between Square and Hexagonal Sampling Methods for Pipeline Image Processing. In *Proc. SPIE*, volume 1194, pages 142-151, 1989.

C. Titin-Schnaider. Radar polarimetry for vegetation observation. In *CEOS 99 SAR Workshop*, Toulouse, France, 1999.

R.N. Treuhaft & P.R. Siqueira, Vertical structure of vegetated land surfaces from interferometric and polarimetric radar. *Radio Science, 35*, 141–177, 2002

E.R. Tufte. The Visual Display of Quantitative Information. Graphics Press, Cheshire, Connecticut, 1983.

E.R. Tufte. Envisioning Information. Graphics Press, Connecticut, 1990.

D. Turner, I.H. Woodhouse and D.H. Laidlaw. A synoptic visualisation of fully polarimetric SAR data - an annotated example. In *Geoscience and Remote Sensing Symposium*, IGARSS '02, IEEE International, 2717-2719, 2002

D. Ussery. www.ebs.dtu.dk/staff/dave/roanoke/genetics9802026.html - Biology 210 (Genetics) - lecture notes, 1998

F.T. Ulaby and S. Elachi. Radar Polarimetry for Geoscience Applications. Artech House, Norwood, MA, 1990.

F.T. Ulaby, D. Held, M.C. Dobson, K.C. McDonald, and T.B.A. Senior. Relating Polarization Phase Difference of SAR Signals to Scene Properties. *Trans. Geosci. Rem. Sens.*, 25(1):83-92, 1987.

A. van Dam, A. S. Forsberg, D. H. Laidlaw, J.J. LaViola, and R. M. Simpson. Immersive VR for Scientific Visualization: A Progress Report. *IEEE Computer Graphics and Applications*, 20(6):26-52, November/December 2000.

A. van Dam, D.H. Laidlaw, and R.M. Simpson. Experiments in immersive virtual reality for scientific visualization. *Computers and Graphics*, 26(4):535-555, August 2002.

F.J.M van der Wel, L.C. van der Gaag and B.G.H. Gorte. Visual Exploration of Uncertainty in Remote Sensing Classification. *Computers and GeoSciences* 24(4):335-343. 1998

J.J. van Zyl, H.A. Zebker, and C. Elachi. Imaging radar polarization signatures: Theory and Observation. *Radio Science*, 22(4):529-543, 1987.

J.J van Zyl. Unsupervised Classification of Scattering Behaviour Using Radar Polarimetry Data. *Trans. Geosci. Rem. Sens.*, 27(1):36-45, 1989.

Z. Wang and F. Ormeling. The Representation of Quantitative and Ordinal Information. *Cartographic Journal* 33(2):87-91.

U. Wegmuller and C. Werner. Retrieval of Vegetation Parameters with SAR Interferometry. *Trans. Geosci. Rem. Sens.*, 35(1):18-24, 1997.

P. Whitehouse. Telescope snaps distant 'planet'. BBC News article (http://news.bbc.co.uk/2/hi/science/nature/3644410.stm), 10th September, 2004.

C.M. Wittenbrink, A.T. Pang and S.K. Lodha. Glyphs for visualizing uncertainty in vector fields. *IEEE Transaction on Visualization and Computer Graphics*, 2(3) pp266 – 279, 1996

I.H. Woodhouse. Stop, look and listen : auditory perception analogies for radar remote sensing. *Int. Jour. Rem. Sens.*, 21(15):2701-2913, 2000.

I.H. Woodhouse and D.H. Hoekman. Radar modeling of coniferous forest using a tree growth model. *Int. Jour. Rem. Sens.*, 21(8):1725-1737, 2000.

H.A. Zebker, J.J. van Zyl, and D.N. Held. Imaging Radar Polarimetry from Wave Synthesis. *J. of Geophys. Res.*, 92(B1):683-701, 1987.

H.A. Zebker, J.J. van Zyl, S.L. Durden, and L. Norikane. Calibrated Imaging Radar Polarimetry: Technique, Examples and Applications. *Trans. Geosci. Rem. Sens.*, 29(6):942-961, 1991.

H.A. Zebker, "Studying the Earth with Interferometric Radar," *Computing in Science and Engineering*, Volume 2, No. 3, pp. 52-60, May-June, 2000

APPENDICES

Appendix A: Contents of the CD-ROM:

Appendix B: The Polarimetric Data Viewer - User Guide

Appendix C: Code Examples

Appendix D: Survey Questionnaire

Appendix A: Contents of the Enclosed CD ROM

1) The Polarimetric Data Viewer

The Polarimetric Data Viewer, introduced in chapter 6, is included as an executable zip file on the CD-ROM under the folder 'Polarimetric Data Viewer'. IDL version 5.6 or above is required to use this application. Full instructions for installation and operation are provided in the following section

2) Siggefora L-band polarimetric dataset.

A subset of a L-band polarimetric dataset taken as part of the NOPEX campaign is provided on this CD. This is under the 'Data' folder, and consists of seven files. The first file (sigg_sub_l.hdr) is a header file which enables the dataset to be input into the Polarimetric Data Viewer. The remaining six files each contain data for the six unique elements of the covariance matrix. The purpose of these files two-fold. Firstly, the data acts as a means of investigating the data viewer. Secondly, the organisation of the datasets, and the content of the header file is intended to act as a template for those interested in using the viewer with other datasets.

3) Animation of a 3D Dataset

In chapter five, a new visualisation technique was proposed for the Entropy/α developed by Cloude and Pottier (1997). An animation based on the proposed visualisation technique can be found under the 'Animation' folder. The data used for this animation was derived from an experiment carried out at the European Microwave Signature Laboratory in 1996 into the application of polarimetric interferometry. The experiment involved placing a 5m high Balsam Fir tree (*Abies Nordmanniana*) in an anechoic chamber and measuring the full scattering matrix using two dual polarized horn antennas (Fortuny and Seiber, 1999).

The animation uses ellipses to represent five variable derived from the Entropy/α decomposition, namely entropy (H), alpha angle (α), total power, beta angle (β) and anisotropy (A), full details of which can be found in chapter 5. Images derived from this animation were used in figure 5.6.

The animation is provided in two different formats (.avi and .wmv), both of which should be compatible with most contemporary PC-based media players.

4) 'The Visualisation of Polarimetric Radar Data'

A copy of this thesis is included under the 'Thesis' folder in .pdf format. This can be opened with the free Acrobat Reader application (see www.adobe.com for more details).

Appendix B: The Polarimetric Data Viewer – User Guide

Included on the CD rom is a zip file containing the Polarimetric Data Viewer. This is a set of IDL routines which are linked in by a single project file.

IDL version 5.6 or above is required to run this application. The version contained on this CD represents a beta distribution, which has undergone no external testing and is designed for research purposes only. For this reason, it is suggested that the routines contained in the zip file are extracted to a separate directory, to avoid damaging other files. The author takes no responsibility for any problems associated with the running of this application.

A sample dataset is included on the enclosed CD, which consists of L-band data taken over a region of boreal-type forest near Siggefora as part of the NOPEX field experiment (see Woodhouse and Hoekman, 2000, for further details). This dataset is formatted according to the requirements of the software application, and thus consists of 6 files representing the unique elements of the covariance matrix. The purpose of this datasets is to provide the reader with a means of assessing the Polarimetric Data Viewer as a research tool.

Below is a series of step-by-step instructions which describe both the installation of the viewer, and how to load the test dataset.

Installation:

The CD-ROM contains a file called viewer.zip. This should be extracted to a directory, which should contain xx files. To run the viewer, run IDL (version 5.6 or above) and open A_viewer.prj using 'File.. Open Project'. Compile the project, ignoring any error messages, and run. The user will subsequently be presented with a data selection screen, from where the sample data can be loaded.

Examining the Sample Data:

Included on the CD-ROM is a sample dataset, under the folder 'Data'. In this folder, there is a text file named sigg_l.hdr. This is required by the data viewer in order to find the datafiles, and is formatted accordingly:

E:/data/pm027_sigg_l	- location and prefix for datafiles
cov.sub	- suffix for datafiles
400	- data size (x)
400	- data size (y)
1	- is data formatted (1) or unformatted (0)?

0 - is data in XDR format (1) or not (0)?

Note that that path given assumes that the CD drive is mounted on drive E. Where this is not the case, the header file should be copied to a local directory, and rewritten to point to the correct drive letter. Note also that on UNIX systems, it is advisable to copy the whole directory to a local drive, and to reformat the paths accordingly. At no point, however, should the data files be altered.

Once the header file is reformatted, the user should be ale to load the data parameters into the polarimetric data viewer using the 'file open' icon. Subsequently, pressing 'OK' will load the dataset, and present the different visualisation options.

Examining other Data Sets

The polarimetric data viewer is capable of analysing polarimetric datasets in covariance matrix format. In order for the viewer to recognise a complete dataset, six files are required. These represent the six unique elements of the covariance matrix. Three of these files (namely hhhh, hvhv and vvvv) should be composed of single-precision real numbers, whilst the remainder (hhvv, hhhv and hvvv) consist of complex values.

To open a dataset within the viewer, a header file similar to the file described in the previous section is required. It is also required that each of the datafiles follows a predictable naming convention, outlined below:

(file prefix)+(name)+(file suffix)

Where 'name' is 'hhhh', 'hvhv', 'vvvv', 'hhvv', 'hhhv' or 'hvvv', respectively, and the file prefix includes the full path to the location of the dataset.

In order to help in the formatting of datasets, an application is provided within the data viewer, which accepts single-look complex data, and outputs viewer-compatible covariance matrix data alongside a working header file. This application, however, has only been tested on a small number of data types, and thus no guarantee is provided as to its effectiveness.

Section C: Code Examples

Below are a series of IDL routines which were used to develop the new visualisation strategies. Some of these routines perform basic functions, such as deriving the Stokes' matrix, and are provided as a resource for other polarimetry novices. Other routines, such as ellipse_vis.pro, can be used to replicate the visualisation strategies detailed in chapter 5 to 7.

In each case, the routines require some form of input, the format of which is detailed in the comments in the first few lines.

If the first line of a routine starts with the word 'function', then it is designed to be used as subroutine of a larger program. In this case it can be called from the main routine as follows (using the function 'stokes.pro' as an example).

Res = stokes(data)

Where 'stokes' is the name of the function (found in the first line), 'K' is the variable (or variables) required by the function to operate, and 'res' is the returned variable.

In each case, variables may be scalar values, complex numbers or matrices.

Ellipse_vis.pro – Routine to visualise values derived form the entropy/α decomposition using coloured ellipses, as detailed in chapter 5. This routine requires five equal-sized arrays as input, defining the span, alpha angle, entropy, beta angle and anisotropy, respectively.

```
pro ellipse_vis, span, alp, ent, bbeta, ani

; This routine requires five equal-sized arrays as input, defining the span, alpha
; angle, entropy, beta angle and anisotropy, respectively.

; get size of array
siz = siz(span, /dimensions)
dimx = siz(0)
dimy = siz(1)
; multiplier value for size of output image
im_mult = 4

; normalise and rescale values
tp = bytscl(span)/255.
alp = !radeg*((!pi/2.)-alp)*2.6667

; convert hue (alpha), saturation (entropy) and value (span) to rgb values
color_convert, alp, 1-ent, tp, r,g,b, /hsv_rgb

; create index array from ordered entropy values
; n.b. any of the input variables can be used in place of entropy, if required
ran = reverse(sort(ent))

dimarr = size(ran, /dimensions)
dimarr = dimarr(0)

device, decomposed= 1

window,7,xsize = dimx*im_mult, ysize = dimy*im_mult, /pixmap
plot, [0,0], [0,0], xrange = [0, dimx], yrange = [0,dimy], xstyle = 5, ystyle = 5, position =
[0,0,1,1], color = 0, background = 0

; use total power as blue 'underpainting'
tv, congrid((tp/2.)*255, 2800,3000), channel = 3

device, decomposed= 0
tvlct,0,0,0,0
tvlct,255,255,255,1

; loop through indexed array
; use a step value of four until the final 10% of value, where the step vale becomes one.

for kfc = 0, 9 do begin
if kfc lt 9 then step = 4 else step = 1
print, kfc
for j = (dimarr/10.)*kfc, ((dimarr/10.)*(kfc+1))-1, step do begin
```

```
i = ran(j)

; define ellipse
aa = findgen(36)*10*!dtor
a = fltarr(2, 36)
a(0,*) = sin(aa)

; use anisotropy value to set minor axis of ellipse
a(1,*) = cos(aa)*(0.1+((1-ani(i))*0.9))

; rotate ellipse (stored as 'a') using beta value
ang = bbeta(i)
rt = [[cos(ang), -sin(ang)], [sin(ang), cos(ang)]]*0.5
a = a##rt

;set size of ellipses, and colour of outline
siz = im_mult
cl = tp(i)*255.
tvlct, cl, cl, cl,2

usersym, (a(0,*)*(im_mult*tp(i)))*siz, (a(1,*)*(im_mult*tp(i)))*siz, /fill

;draw line ellipse in position specified by index file
plots,i-(fix(i/dimx)*dimx), fix(i/dimx), psym = 8, color = 2

siz = im_mult*0.9
usersym, a(0,*)*(im_mult*tp(i))*siz, a(1,*)*(im_mult*(tp(i)))*siz, /fill

;Use RGB values defined at start of routine to colour ellipse.
tvlct, r(i), g(i), b(i), 6
;draw coloured ellipse in position specified by index file
plots,i-(fix(i/dimx)*dimx), fix(i/dimx), psym = 8, color = 6

endfor
endfor

end
```

Stokes.pro - Calculates the Stokes' (Kennaugh) Matrix from covariance matrix

```
function stokes, data

; the input variable 'data' is a six-element vector
; representing the unique values of the covariance matrix
; and is a standard data-transfer variable used throughout viewer.prj

shhhh = data(0,0,0)
shvhv = data(1,0,0)
svvvv = data(2,0,0)
shhvv = data(3,0,0)
shhhv = data(4,0,0)
shvvv = data(5,0,0)

W = [[shhhh, shhhv, conj(shhhv), shvhv],$
     [shhhv, shhvv, shvhv, shvvv],$
     [conj(shhhv), shvhv, conj(shhvv), conj(shvvv)],$
     [shvhv, shvvv, conj(shvvv), svvvv]]


R = complex([[1,0,0,1],[1,0,0,-1],[0,1,1,0],[0,0,0,0]])
R(1,3) = complex(0,1)
R(2,3) = complex(0,-1)
P = [[1,0,0,0],[0,0,1,0],[0,1,0,0],[0,0,0,1]]

K = 2*(transpose(invert(R)))##W##invert(R)
WW = P##W##P
K = float(K)
return, K

; the returned variable 'K' is a 4*4 matrix, which can be used for polarisation synthesis.

end
```

Pol_resp_g.pro - routine to generate the polarimetric response for a single Stokes' (Kennaugh) Matrix. This resulting matrix can then be used to generate a polarimetric response globe using the routine named 'prg_globe_format.pro'..

```
function pol_resp_g, K

dimchi = 10
dimori = 72
inc = !pi/36.
inchi = !pi/36.

chi = double(0)
ori = double(0)
SR = fltarr(4)
ST = fltarr(1,4)
SC = fltarr(4)

power = dblarr(2,dimori,dimchi)

; loop through orientation (ori) and ellipticity (chi) angles.

for p = 0, dimori -1 do begin
ori = (-.5*!pi)+inc*p ; START AT -90 (VERTICAL)

        for q = 0, dimchi -1  do begin
        if p lt dimori/2 then chi =  float(-1)*inchi*q else chi = inchi*q

                iii = [!radeg*chi, !radeg*ori]

                ; Set Stokes' vector (received)
                SR(0) = 1
                SR(1) = cos(2*ori)*cos(2*chi)
                SR(2) = sin(2*ori)*cos(2*chi)
                SR(3) = sin(2*chi)

                n = where(abs(SR) lt 0.000000001)
                if n(0) gt -1 then SR(n) = 0.

                ; Set Stokes' vector (transmit – cross-pol)
                cpori = ori+!pi/2
                cpchi = -1*chi
                SC(0) = 1
                SC(1) = cos(2*cpori)*cos(2*cpchi)
                SC(2) = sin(2*cpori)*cos(2*cpchi)
                SC(3) = sin(2*cpchi)

                n = where(abs(SC) lt 0.000000001)
                if n(0) gt -1 then SC(n) = 0.

                ; Set Stokes' vector (transmit – co-pol)
                ;  (transpose of received vector)
```

```
                ST = transpose(SR)

            ;Calculate backscatter values for co- and cross-pol cases
                power(0,p,q) = SR##K##ST
                power(1,p,q)= SC##K##ST

endfor
endfor


power = power/max(power)            ; normalise power

return, power
end
```

Pol_resp_t.pro - routine to generate the polarimetric response for a single Stokes' (Kennaugh) Matrix. This can subsequently be used to represent polarimetric response using the traditional isometric representation.

```
function pol_resp_t, K

; the input variable 'K' defines the Stokes' (Kennaugh) Matrix, used in the analysis of
; polarimetric response.

dimchi = 19.
dimori = 37.
inc = !PI/36.
incchi = !pi/36.
valuex = fltarr(dimori)
valuey = fltarr(dimchi)
M = dblarr(4,4)
SR = dblarr(4)
ST = dblarr(1,4)
SC = dblarr(4)
power = dblarr(2,dimori,dimchi)


, loop through orientation (ori) and ellipticity (chi) angles

for i = 0, dimori -1 do begin
ori = (-!pi/2)+inc*i

        for j = 0, dimchi -1  do begin
        chi =  (-!pi/4) + incchi*j

                ; Set Stokes' vector (received)
                SR(0) = 1
                SR(1) = cos(2*ori)*cos(2*chi)
                SR(2) = sin(2*ori)*cos(2*chi)
                SR(3) = sin(2*chi)

                ;Set Stokes' Vector (transmit - cross-pol)
                cpori = ori+!pi/2
                cpchi = -1*chi
                SC(0) = 1
                SC(1) = cos(2*cpori)*cos(2*cpchi)
                SC(2) = sin(2*cpori)*cos(2*cpchi)
                SC(3) = sin(2*cpchi)

                ;Set Stokes' vector (transmit - co-pol)
                ST = transpose(SR)

                ;Calculate single intensity value for co- and cross-pol response
                power(0,i,j) = SR##K##ST                ; co-pol
                power(1,i,j)= SC##K##ST                 ; cross-pol
```

```
endfor
endfor

power = power/max(power)                ; normalise power


; visualise response graphs using the traditional isometric projection

window,1,xsize = 600, ysize = 400
surface, power(0,*,*)
window,2,xsize = 600, ysize = 400
surface, power(1,*,*)

return, power

; the returned variable 'power' is a 2*19*37 3D matrix, containing both the co- and cross-pol
; response
; co-pol = power (0,*,*)
;cross-pol = power(1,*,*)

end
```

Prg_globe_format – This routine is used to create the polarimetric response globe, using the hue-based colour scale to represent the ratio of the co- and cross-pol power in relation to the total power (as detailed in chapter 6). The input variable ('power') contains the polarimetric response for the co- and cross-pol cases, which can be derived from 'pol_resp_g.pro'.

```
function prg_globe_format, power

; the variable 'power' contains the polarimetric response for the co- and cross-pol cases, and
; is derived from 'pol_resp_g.pro'

device, decomposed = 1

siz = 300
window,1, xsize = siz, ysize = siz

maplimit = [-14, 1, 90, 360] ; Define mapping parameters  for azimuthal projection
map_set, /azimuthal ,90, $
   position = [0, 0,1, 1],$
                  limit = maplimit, /grid

;separate co- and cross-pol powers, and create one total power matrix

power_co = power(0,*,*)
power_co = reform(power_co)
power_cross = power(1,*,*)
power_cross = reform(power_cross)
npower = power_co+power_cross
npower = npower/max(npower)

; create an array of saturation values, all set to 1.
sat = npower
sat(*,*) = 1.

; Ascribe ratio of co- to cross-pol power to a hue value.
phas = power_co/(power_co+power_cross+0.000001)
huearr = phas*120.

; increase density of data points (for plotting purposes only).
npower = congrid(npower, dimx*10, dimy*10)
sat = congrid(sat, dimx*10, dimy*10)
huearr = congrid(huearr, dimx*10, dimy*10)


; create azimuthal projections of the intensity (p), saturation(s) and hue (h) channels.

p = map_image(npower,$
        lonmin = 0, lonmax = 360., latmin = 0, latmax = 90.,$
        missing =spval)
```

```
s = map_image(sat,$
        lonmin = 0, lonmax = 360., latmin = 0, latmax = 90.,$
        missing =0.)

h = map_image(huearr,$
        lonmin = 0, lonmax = 360., latmin = 0, latmax = 90.,$
        missing =120.)

outimage = bytarr(siz, siz,3)

color_convert, h, s, p, r,g,b, /hsv_rgb

r = congrid(r, siz,siz)
g = congrid(g, siz,siz)
b = congrid(b, siz,siz)

tv, r, channel = 1
tv, g, channel = 2
tv, b, channel = 3
image = tvrd(true = 3)
outimage(*,*,(0:2)) = image

; the returned variable (outimage) contains the red, green and blue colour channels of the
; polarimetric response globe.

return, outimage
end
```

Section D: Survey Questionnaire

Presented below is a hard copy of the web-based questionnaire which was used as the basis for the assessment of the Polarimetric Response Globe as a visual icon. The original html document from which this hard copy was taken can be found on the enclosed CD-ROM.

POLARIMETRIC RESPONSE GRAPH QUESTIONNAIRE

Please scroll down the page, answering the questions attached to each image.

For each image, you are asked whether there is a pattern apparent in the arrangement of graphical symbols.

In each case, the pattern represented is either a circle, a star or a crown shape.

After selecting a symbol, you are also required to indicate how sure you are of your choice.

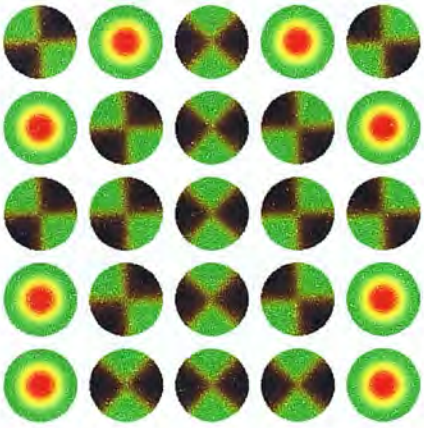

QUESTION 1 :Study the above image, and select the shape below which best corresponds to any pattern visible in the group of icons

☐ ☐ ☐

How confident are you in this choice?

Very Confident☐ Fairly Sure☐ Unsure☐

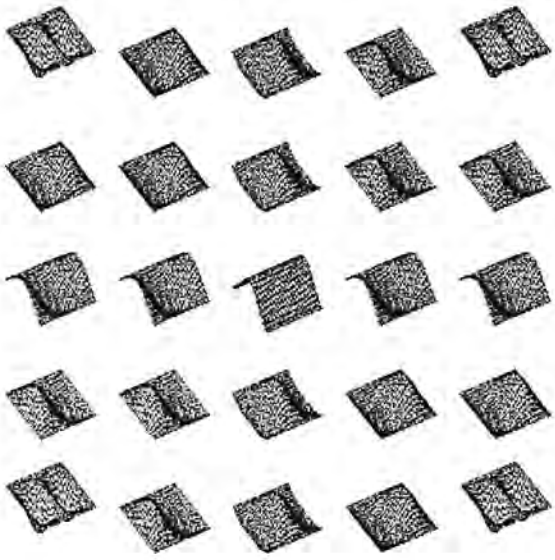

QUESTION 2 :Study the above image, and select the shape below which best corresponds to any pattern visible in the group of icons

How confident are you in this choice?

Very Confident☐ Fairly Sure☐ Unsure☐

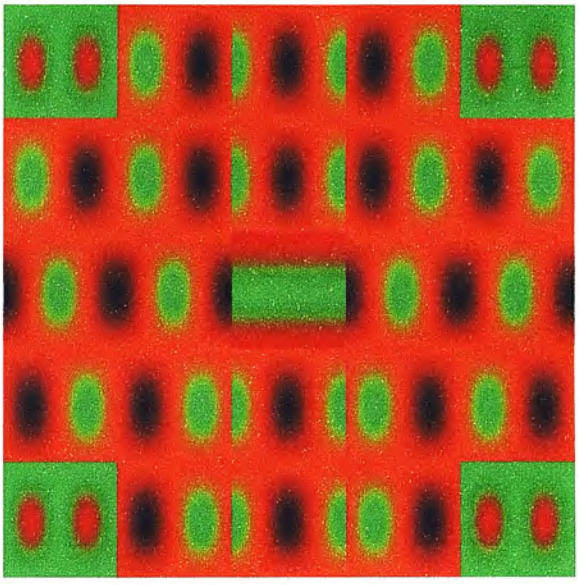

QUESTION 3 :Study the above image, and select the shape below which best corresponds to any pattern visible in the group of icons

How confident are you in this choice?

Very Confident☐ Fairly Sure☐ Unsure☐

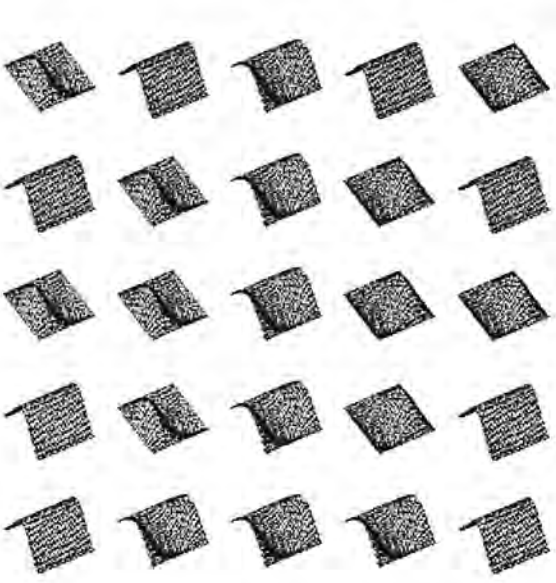

QUESTION 4 :Study the above image, and select the shape below which best corresponds to any pattern visible in the group of icons

How confident are you in this choice?

Very Confident☐ Fairly Sure☐ Unsure☐

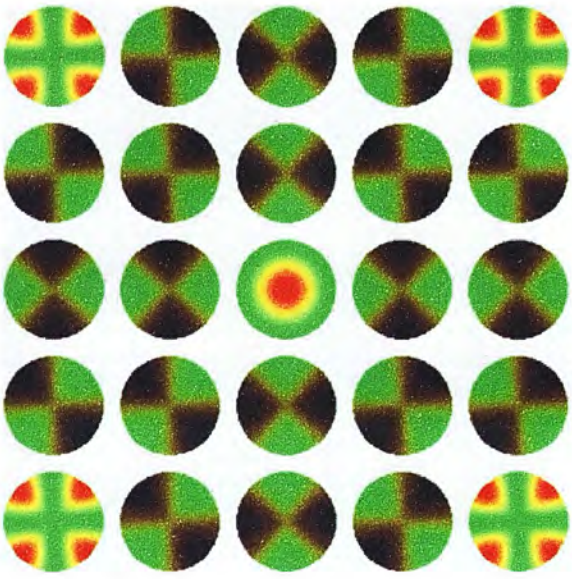

QUESTION 5 :Study the above image, and select the shape below which best corresponds to any pattern visible in the group of icons

How confident are you in this choice?

Very Confident☐ Fairly Sure☐ Unsure☐

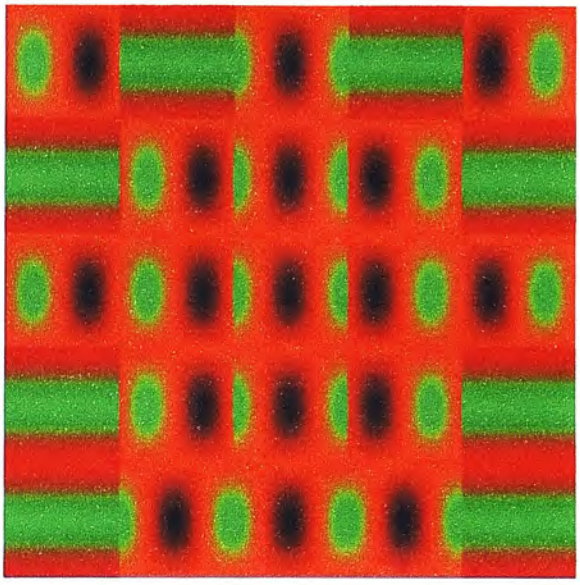

QUESTION 6 :Study the above image, and select the shape below which best corresponds to any pattern visible in the group of icons

How confident are you in this choice?

Very Confident☐ Fairly Sure☐ Unsure☐

Of the options presented, which do you feel were easiest to 'read'?

Circular Icons☐ 2D Graphs☐ 3D Graphs☐

Any other comments?

Thank you for your time